Random Lozenge Waterfall: Dimensional Collapse of Gibbs Measures

Alisa Knizel and Leonid Petrov

Abstract

We investigate the asymptotic behavior of the q-Racah probability measure on lozenge tilings of a hexagon whose side lengths scale linearly with a parameter $L \to \infty$, while the parameters $q \in (0,1)$ and $\kappa \in \mathbf{i}\mathbb{R}$ remain fixed. This regime differs fundamentally from the traditional case $q \sim e^{-c/L} \to 1$, in which random tilings are locally governed by two-dimensional translation-invariant ergodic Gibbs measures. In the fixed-q regime we uncover a new macroscopic phase, the *waterfall* (previously only observed experimentally), where the two-dimensional Gibbs structure collapses into a one-dimensional random stepped interface that we call a *barcode*.

We prove a law of large numbers and exponential concentration, showing that the random tilings converge to a deterministic waterfall profile. We further conjecture an explicit correlation kernel of the one-dimensional barcode process arising in the limit. Remarkably, the limit is invariant under shifts by $2\mathbb{Z}$ but not by $\mathbb{Z}$, exhibiting an emergent period-two structure absent from the original weights. Our conjectures are supported by extensive numerical evidence and perfect sampling simulations. The kernel is built from a family of functions orthogonal in both spaces $\ell^2(\mathbb{Z})$ and $\ell^2(\mathbb{Z}+\frac{1}{2})$, that may be of independent interest.

Our proofs adapt the spectral projection method of Borodin–Gorin–Rains (2009) to the regime with fixed q. The resulting asymptotic analysis is substantially more involved, and leads to non-self-adjoint operators. We overcome these challenges in the exponential concentration result by a separate argument based on sharp bounds for the ratios of probabilities under the q-Racah orthogonal polynomial ensemble.

1 Introduction

1.1 Overview

Random dimer coverings of graphs — most notably, random tilings of planar regions — form an exactly solvable setup for understanding phase transitions and emergent large-scale behavior in two-dimensional statistical mechanics. A prototypical example is uniformly random lozenge tilings of the hexagon (see Figure 1). When the side lengths of the hexagonal region grow proportionally to a large parameter L, several universal regimes emerge: **(i)** a deterministic limit shape with Gaussian Free Field fluctuations [CKP01], [Ken08], [Pet15], [BG18], [BNR24]; **(ii)** edge statistics governed by Random-Matrix and Pearcey-type kernels [OR06], [GP15], [OR07], [AG22], [HYZ24]; **(iii)** Kardar-Parisi-Zhang class behavior near arctic boundaries [BKMM07], [Pet14], [Hua24], [AH25]; and **(iv)** bulk lattice limits described by translation-invariant ergodic Gibbs measures [OR03], [She05], [KOS06], [Gor08], [Agg23]. For a broader survey, see [Gor21].

As the extensive list of references demonstrates, a diverse toolkit has emerged for studying uniformly random lozenge tilings of the hexagon, including the variational principle, orthogonal polynomial methods (Riemann–Hilbert or spectral projection approaches), determinantal formulas and their asymptotics, loop (Nekrasov) equations, and discrete complex analysis. Many of these methods survive once the uniform measure is tilted by weights, provided the weights preserve the underlying orthogonal polynomial structure. We study the most general family of weights of this kind, namely the *q-Racah weights* introduced in [BGR10]; they correspond to a terminal node of the q-Askey scheme [KS96]. (Other deformations, for example the doubly-periodic weights that necessitate matrix-valued orthogonal polynomials [Cha20], lie outside our scope.)

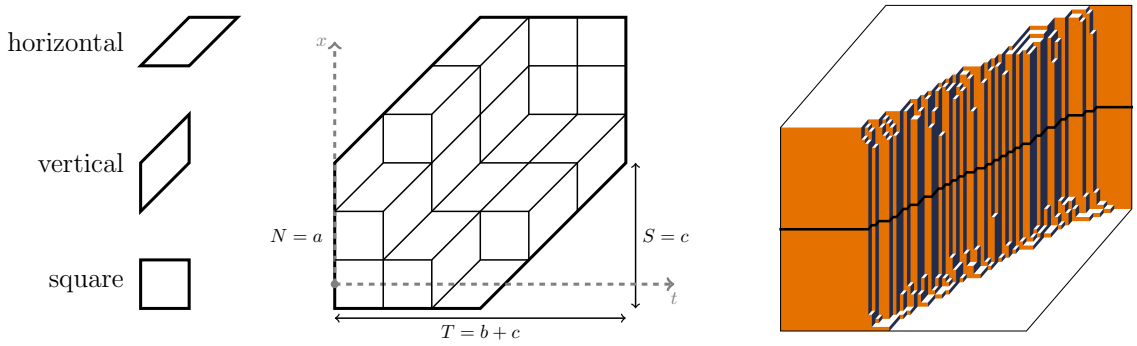

Figure 1: Left: the three types of lozenges. Center: an example of a lozenge tiling of a hexagon whose side lengths are all equal to 3. Observe that the plane can be affine transformed so that all lozenges become congruent; however, it is convenient throughout the paper to use the equivalent representation shown here. The sides of the hexagon are denoted by a, b, c, a, b, c, but throughout the paper we use the parameters $N = a$, $T = b + c$, and $S = c$. Right: a perfect sample of the q-Racah random tiling with $N = 50$, $T = 100$, $S = 30$, $q = 0.7$, and $\kappa = 3\mathbf{i}$ obtained by our `Python` port of the original algorithm from [BGR10] (provided as an ancillary file to the arXiv version of the paper). The cross-section of the 3D surface across the middle represents the barcode process.

The q-Racah probability measure on lozenge tilings of a hexagon is defined by assigning the probability

$$\frac{1}{Z} \prod_{\substack{\text{horizontal} \\ \text{lozenges } u}} \mathsf{w}_{q,\kappa}\big(\text{height}(u)\big), \qquad \mathsf{w}_{q,\kappa}(j) := \kappa q^{j-(S+1)/2} - \frac{1}{\kappa q^{j-(S+1)/2}}, \tag{1.1}$$

to each tiling, where Z is the normalizing constant, $S = c$ is one of the sides of the hexagon, and the height of a horizontal lozenge is defined as the number of $1 \times 1 \times 1$ cubes under this lozenge in the representation of a tiling as a 3D stepped surface. The parameters are[1] $\kappa \in \mathbf{i}\mathbb{R}$ and $q > 0$. Note that all of the factors $\mathsf{w}_{q,\kappa}(j)$ are purely imaginary with positive imaginary part, and after the normalization, (1.1) defines an honest probability measure.

[1] That is, we consider the so-called *imaginary q-Racah case*. There are two other cases, *real* and *trigonometric*, introduced in [BGR10, Section 2.2]. Throughout the paper, we focus only on the imaginary case since it leads to the waterfall behavior.

Because the total number of horizontal lozenges is fixed at $S(T-S)$, the involution $(q,\kappa)\mapsto(q^{-1},\kappa^{-1})$ leaves it invariant. We therefore fix the convention $0<q<1$ throughout. The limits $\kappa\to 0$ or $\kappa\to \mathbf{i}\infty$ reduce the q-Racah measure to the volume-tilted measures q^{vol} and $q^{-\mathsf{vol}}$, respectively, where vol is the three-dimensional volume under the stepped surface. The further limit $q\to 1$ gives back the uniform measure.

Until now, asymptotic investigations of the q-Racah model in the regime where the side lengths of the hexagon grow linearly with a parameter $L\to\infty$ have focused exclusively on the *traditional* $q\to 1$ *window*, i.e. the scaling $q=e^{-c/L}\to 1$. Using the spectral projection framework developed in [BO07], [Ols08] (see also [Tao12, Chapter 3.3]), Borodin–Gorin–Rains [BGR10] identified the local (bulk) lattice limits in this window with the same translation-invariant ergodic Gibbs measures present in the uniform case. Subsequent works by Dimitrov–Knizel [DK19] and Gorin–Huang [GH24] established Gaussian Free Field fluctuations of the height function via two complementary loop-equation approaches, while Duits–Duse–Liu [DDL24] confirmed the same universal behavior through an analysis of the recurrence coefficients of the underlying orthogonal polynomials.

By contrast, in the *fixed-q regime* almost nothing is rigorously understood. Aside from the striking *waterfall* phase observed in simulations in [BGR10] (see Figure 1, right, for an illustration), the asymptotic behavior for fixed q and κ has so far escaped a mathematical description. (For the simpler $q^{\pm\mathrm{vol}}$ measures, the limiting objects were connected in [KO07] to tropical curves, but those results do not extend to the q-Racah setting.) Describing the fixed-q regime and the waterfall phase is the central aim of the present work.

Our **main results** are as follows.

- We prove that, in the fixed-q regime, the q-Racah random tiling converges (with exponential bounds) to a deterministic *waterfall profile*. In the waterfall region $\mathcal{W}$ (a part of this profile in which locally one sees two types of lozenges), the two-dimensional lattice behavior *collapses* into a one-dimensional random stepped interface (which we call a *barcode*; this is the central broken line in the tiling in Figure 1, right).

- Extending the spectral projection framework to the fixed-q regime, we obtain (coefficient-wise) limits of the relevant difference operators at every macroscopic location. Away from the center of the waterfall region, i.e. when $x\not\sim\frac{1}{2}(S+t)$, the limiting operators are no longer self-adjoint. A systematic study of these non-self-adjoint operators is left for future work.

- By matching nonrigorous computations with numerical and perfect sampling data, we propose a determinantal correlation kernel for the one-dimensional *barcode process*. The conjectural kernel exhibits a surprising $2\mathbb{Z}$-periodicity, breaking the original lattice homogeneity.

Remark 1.1. Most tiling models feature degenerate regions where the two-dimensional Gibbs structure disappears. The familiar examples are the *frozen facets* outside an arctic boundary, in which the 3D stepped surface is parallel to one of the coordinate planes, and exhibits no fluctuations. Certain boundary conditions or periodic weights can also give rise to *semi-frozen* zones [Mkr14], [Mkr21], [BB23], in which locally only two types of lozenges appear, producing a barcode-type configuration that is, however, fully deterministic and periodic.

The waterfall phase we uncover is fundamentally different. Here, the bulk two-dimensional Gibbs structure *collapses* onto a single random stepped interface (the barcode), while the complementary regions remain fully frozen. To our knowledge, no prior tiling model with nonrandom weights exhibits a macroscopic facet that is simultaneously random and one-dimensional.

We remark that an effectively one-dimensional random phase, in which two types of lozenges are arranged as steps of a random walk, is expected to occur in domino tilings of the Aztec diamond with the *random* edge weights introduced in [BPZ25]. The randomness of the weights is essential for this effect, whereas in our model the barcode phase appears under a completely deterministic choice of weights.

Remark 1.2. The waterfall phase in our model represents a strong form of dimensional reduction: outside the waterfall region, all fluctuations are frozen, and only the one-dimensional barcode interface survives in the waterfall region. This can be contrasted with other known instances of dimensional reduction in statistical mechanics, such as in the scaling limit of the two-dimensional critical Ising model [WMTB76]. In the Ising case, while the correlation functions are famously described by lower-dimensional mathematical structures, the underlying two-dimensional field continues to exhibit non-trivial fluctuations in both spatial dimensions.

In the remainder of the Introduction, we provide a detailed discussion of our methods and their limitations.

1.2 Spectral projection approach and its limitations

Let $X = \{(t_i, x_i)\} \subset \mathbb{Z}^2$ be the random point configuration marking the positions of the vertical and square lozenges in a tiling of the hexagon (where t and x are the lattice coordinates defined as in Figure 1, center). For pairwise distinct $(s_1, x_1), \dots, (s_n, x_n)$, define the n-point correlation function

$$\rho_m\big((s_1, x_1), \dots, (s_m, x_m)\big) := \mathbb{P}\big\{(s_i, x_i) \in X,\ i = 1, \dots, m\big\},$$

where $\mathbb{P}$ is the q-Racah probability measure. Because this measure is equivalent to a dimer model on the bipartite hexagonal graph, the resulting correlation functions are determinantal; see the lecture notes [Ken09] for a general exposition. That is, there exists a kernel $K(s, x; t, y)$ such that

$$\rho_m\big((s_1, x_1), \dots, (s_m, x_m)\big) = \det\big[K(s_i, x_i; s_j, x_j)\big]_{i,j=1}^{m}, \qquad m \geq 1.$$

As shown in [BGR10], the kernel is given in terms of the q-Racah orthogonal polynomials:

$$K(s, x; t, y) = \begin{cases} \displaystyle\sum_{n=0}^{N-1} (C_n^t C_n^{t+1} \dots C_n^{s-1})^{-1} f_n^s(x) f_n^t(y), & s \geq t; \\ \displaystyle -\sum_{n \geq N} (C_n^s C_n^{s+1} \dots C_n^{t-1}) f_n^s(x) f_n^t(y), & s < t, \end{cases} \tag{1.2}$$

where the constants C_n^t are explicit, and the functions $f_n^t(x)$ form an orthonormal basis of the space ℓ^2 on the t-th vertical slice. The functions $f_n^t(x)$ are obtained from the relevant q-Racah orthogonal polynomials (with parameters depending on q, κ, t, and the side lengths of the hexagon) by multiplying by the square root of the q-Racah weight function, and then normalising. Complete formulas are given in Sections 2 and 6.

On each fixed vertical slice t, the kernel $K_t(x,y) \coloneqq K(t,x;t,y) = \sum_{n=0}^{N-1} f_n^t(x) f_n^t(y)$ can be interpreted as the *orthogonal spectral projection* onto the positive part of the spectrum of a certain difference operator with explicit product-form coefficients, see (4.1) and (2.8). We take the limits of these coefficients for fixed q and κ as $T = \lfloor L\mathsf{T} \rfloor$, $S = \lfloor L\mathsf{S} \rfloor$, and $N = \lfloor L\mathsf{N} \rfloor$ and around a macroscopic location (t, x), where $t = \lfloor L\mathsf{t} \rfloor$ and $x = \lfloor L\mathsf{x} \rfloor + \Delta x$. The waterfall phase arises only when $\mathsf{N} < \mathsf{T}$, and we assume this condition throughout the rest of the Introduction. Depending on the scaled location (t, x) on a slice t intersecting the waterfall region $\mathcal{W}$, we obtain various limiting symmetric Jacobi (tridiagonal) operators which act in the local shift Δx:

$$\big(Tg\big)(\Delta x) = d(\Delta x + 1)\, g(\Delta x + 1) + a(\Delta x)\, g(\Delta x) + d(\Delta x)\, g(\Delta x - 1), \tag{1.3}$$

Their coefficients are given in the following proposition.

Proposition 1.3 (Lemmas 4.1 and 4.3)**.** • *If (t, x) is above or below $\mathcal{W}$, we have $d(\Delta x) = 0$ and $a(\Delta x) = -1$, that is, the limiting difference operator is the negative identity $(-Id)$;*

- *If (t, x) lies on the upper boundary of $\mathcal{W}$, then*

$$d(\Delta x) = -\kappa^2 q^{2\Delta x + 1/2}, \qquad a(\Delta x) = -1 - \kappa^2 (1+q) q^{2\Delta x + 1}.$$

On the lower boundary of $\mathcal{W}$, one has to replace the powers of (q, κ) with those of (q^{-1}, κ^{-1}), while the factor $1 + q$ is kept the same.

- *Inside $\mathcal{W}$ but away from its center line $\lfloor L\mathsf{x} \rfloor = \frac{1}{2}(S + t)$, the coefficients in the upper half are*

$$d(\Delta x) = -\kappa^2 q^{2\Delta x + 1/2}, \qquad a(\Delta x) = -\kappa^2 (1+q) q^{2\Delta x + 1}.$$

The formulas for the lower part are obtained from these by the same symmetry as in the preceding item.

- *On the center line, we get*

$$d(\Delta x) = \frac{-\kappa^2 (1 - \kappa^2 q^{2\Delta x})^{-1} q^{2\Delta x + 1/2}}{\sqrt{(1 - \kappa^2 q^{2\Delta x - 1})(1 - \kappa^2 q^{2\Delta x + 1})}}, \qquad a(\Delta x) = \frac{-\kappa^2 (1+q)\, q^{2\Delta x + 1}}{(1 - \kappa^2 q^{2\Delta x})(1 - \kappa^2 q^{2\Delta x + 2})}. \tag{1.4}$$

If the scaled point (t, x) is either outside the waterfall region $\mathcal{W}$ or sits on the center line, the pre-limit difference operator converges to a *bounded, self-adjoint* limit — either $(-Id)$, or the operator given by (1.3)–(1.4). Then, by the spectral projection method based on the strong resolvent convergence (developed in [BO07], [Ols08]; we recall the main statement in Theorem 4.7), the correlation kernel K_t converges to zero outside $\mathcal{W}$ and to the identity operator on the center line. This result essentially parallels the spectral approach that proved successful in the traditional regime $q = e^{-c/L} \to 1$ in [BGR10], where it yielded the limiting kernel at *all* macroscopic points inside the hexagon.

However, for fixed q, on the boundary of $\mathcal{W}$ and inside of $\mathcal{W}$ but not on the center line, the coefficients of (1.3) grow rapidly at positive or negative infinity, so the limiting difference operator is no longer self-adjoint and in fact has von Neumann deficiency indices $(1, 1)$. The non-uniqueness of self-adjoint extensions of prevents us from singling out a canonical spectral projection. The most intriguing case is the boundary of $\mathcal{W}$, where one can see a nontrivial random configuration

with all three types of lozenges — thus, the spectral projection there should yield a new correlation kernel that is not zero nor the identity operator. We leave the full functional-analytic treatment of these non-self-adjoint operators for future work.

Although the spectral projection approach breaks down inside the waterfall region away from the center line, we bridge this gap by performing direct estimates for the q-Racah orthogonal polynomial ensemble (see Section 1.4 below). These estimates strengthen the kernel convergence along the center line to an exponential concentration statement, which is the main result of the present paper.

Theorem 1.4 (Combination of Proposition 4.8, Theorem 5.11, and Corollary 5.12)**.** *Assume that the side lengths of the hexagon, a, b, c, scale proportionally with a parameter $L \to +\infty$, while the q-Racah parameters κ and q remain fixed. Then the fixed-slice correlation kernel converges either to zero or the identity operator, depending on the scaled location (t, x):*[2]

$$\lim_{L\to+\infty} K_{\lfloor L\mathsf{t}\rfloor}(\lfloor L\mathsf{x}\rfloor + \Delta x, \lfloor L\mathsf{x}\rfloor + \Delta y) = \begin{cases} \mathbf{1}_{\Delta x=\Delta y}, & \text{if } (\mathsf{t},\mathsf{x}) \in \mathcal{W}; \\ 0, & \text{otherwise,} \end{cases} \quad \text{for all fixed } \Delta x, \Delta y \in \mathbb{Z}.$$

Moreover, the probability of finding a horizontal lozenge inside $\mathcal{W}$ or a square or vertical lozenge outside $\mathcal{W}$ decays exponentially fast in L.

1.3 Inter-slice transitions and the conjectural barcode kernel

To access inter-slice correlations and the barcode process, one has to look at the full two-dimensional kernel $K(s, x; t, y)$. Thanks to the structure of the q-Racah orthogonal polynomials, the coefficients C_n^t in (1.2) can be incorporated into the action of two-diagonal inter-slice operators $\mathfrak{U}_t$:

$$\frac{\sqrt{\lambda(t)}}{\sqrt{\lambda(t+1)}} C_n^t f_n^{t+1}(x) = \big(\mathfrak{U}_t f_n^t\big)(x), \qquad \big(\mathfrak{U}_t g\big)(x) := u_1^t(x-1)\, g(x-1) + u_0^t(x)\, g(x), \tag{1.5}$$

where $\lambda(\cdot)$ is a nonvanishing explicit gauge factor (6.3) that does not change the determinantal process, and the coefficients $u_0^t(x)$ and $u_1^t(x)$ have explicit product-form expressions, see Section 6.2 for details.

We represent the q-Racah correlation kernel (1.2) as

$$\frac{\sqrt{\lambda(s)}}{\sqrt{\lambda(t)}} K(s, x; t, y) = \begin{cases} \big(\mathfrak{U}_t^{-1}\mathfrak{U}_{t+1}^{-1}\dots\mathfrak{U}_{s-1}^{-1}\big)_y\, K_s(x, y), & s > t; \\ K_t(x, y), & s = t; \\ \big(\mathfrak{U}_{t-1}\dots\mathfrak{U}_{s+1}\mathfrak{U}_s\big)_y \left(-\mathbf{1}_{x=y} + K_s(x, y)\right), & s < t. \end{cases} \tag{1.6}$$

where the operators $\mathfrak{U}_\bullet$ act in the variable y.

Fixed-q limits of the coefficients $u_0^t(x)$ and $u_1^t(x)$ of the inter-slice operators $\mathfrak{U}_t$ (1.5) are immediately accessible. Taking the limit in the operators $\mathfrak{U}_t$ (together with rescaling and shifting to the required macroscopic location), we arrive at the operator

$$\big(\mathfrak{U}_t^{\text{barcode}} f\big)(x) := \mathfrak{a}(x - \tfrac{t}{2})\, f(x-1) + \mathfrak{a}(x - \tfrac{t}{2} + \tfrac{1}{2})\, f(x), \qquad \mathfrak{a}(x) := \sqrt{\frac{-\kappa^2 q^{2x-1}}{(1-\kappa^2 q^{2x})(1-\kappa^2 q^{2x-1})}},$$

[2]Here and throughout the paper, $\mathbf{1}_A$ stands for the indicator of an event or condition A.

where x belongs to $\mathbb{Z}$ or $\mathbb{Z}+\frac{1}{2}$. Due to the rapid decay of the coefficients $\mathfrak{a}(x)$ at $x \to \pm\infty$, the inverse of the operator $\mathfrak{U}_t^{\mathrm{barcode}}$ is not well-defined. Therefore, directly taking the fixed-q limit of the kernel (1.6) is not possible.

However, the bounded operator $\mathfrak{U}_t^{\mathrm{barcode}}$ itself admits a family of functions $\mathcal{F}_n^t(x)$, $n \in \frac{1}{2}\mathbb{Z}_{\geq 0}$, orthogonal in both spaces $\ell^2(\mathbb{Z})$ and $\ell^2(\mathbb{Z}+\frac{1}{2})$, which satisfy an identity similar to (1.5):

$$-q^n \mathcal{F}_n^{t+1}(x) = \left(\mathfrak{U}_t^{\mathrm{barcode}} \mathcal{F}_n^t\right)(x).$$

We develop properties of these functions in Appendix A. In particular, they may be expressed through the continuous q^{-1}-Hermite polynomials [KS96, Chapter 3.26], [IM94].

Motivated by this structure, we first conjectured the following series representation for the density function of the barcode process:

$$\rho^{\mathrm{barcode}}(t) = \mathfrak{a}(1-\tfrac{t}{2}) \sum_{n \in \frac{1}{2}\mathbb{Z}_{\geq 0}} \frac{-q^{-n}\mathcal{F}_n^t(0)\mathcal{F}_n^{t-1}(0)}{\|\mathcal{F}_n\|^2_{\ell^2(\mathbb{Z})}}. \tag{1.7}$$

However, this series **does not converge**. Numerical experiments indicate that its divergence is rather *mild*: the tail behaves as $\ldots + c - c + c - c + \ldots$. Consequently, the series in (1.7) can be regarded as having "**two distinct sums**," depending on how one pairs adjacent terms. Further numerical calculations and simulation studies confirm that the barcode process is **two-periodic**, with the even- and odd-site densities arising from these two alternative summations of (1.7). This periodicity is unexpected but can be explained a posteriori, see Remark 1.6 below.

Turning to the full correlation kernel, one would get even more divergent series which need to be regularized. Based on further numerics, we conjecture the existence of a universal limiting *barcode kernel* governing the local statistics inside the waterfall region. This conjectural kernel is given for $s \geq t$ by

$$\begin{aligned}\mathcal{K}^{\mathrm{barcode}}(s,t) \coloneqq \lim_{M\to\infty} q^{(M+1)(s-t)} \times (-1)^{t-s} \sqrt{\frac{-\kappa^2 q^{1-s}}{(1-\kappa^2 q^{2-t})(1-\kappa^2 q^{1-s})}} \\ \times \sum_{n=0}^{M+1/2} \frac{\left(-q^n\right)^{t-1-s} \mathcal{F}_n^s(0)\mathcal{F}_n^{t-1}(0)}{\|\mathcal{F}_n\|^2_{\ell^2(\mathbb{Z})}},\end{aligned} \tag{1.8}$$

where $M \in \mathbb{Z}$, and the sum is over $n \in \frac{1}{2}\mathbb{Z}_{\geq 0}$. For $s < t$, the kernel is extended by symmetry.

Conjecture 1.5 (Combination of Conjectures 7.2, 7.6 and 7.7)**.** *Around any macroscopic point* (t,x) *in the waterfall region* $\mathcal{W}$*, the random configuration of square lozenges on a horizontal slice converges to a determinantal* ***barcode process*** *on* $\mathbb{Z}$ *with the symmetric correlation kernel* $\mathcal{K}^{\mathrm{barcode}}(s,t)$.[3] *The barcode process depends only on the parameters* q *and* κ*, but not on the geometry of the hexagon or the macroscopic location* (t,x) *inside* $\mathcal{W}$*, as long as the waterfall phase is present, i.e.,* $\mathsf{N} < \mathsf{T}$.

The limiting kernel is 2×2 *block Toeplitz, that is,*

$$\begin{pmatrix} \mathcal{K}^{\mathrm{barcode}}(s,t) & \mathcal{K}^{\mathrm{barcode}}(s,t+1) \\ \mathcal{K}^{\mathrm{barcode}}(s+1,t) & \mathcal{K}^{\mathrm{barcode}}(s+1,t+1) \end{pmatrix} = \begin{pmatrix} \mathcal{K}_{00}^{\mathrm{barcode}}(s-t) & \mathcal{K}_{01}^{\mathrm{barcode}}(s-t) \\ \mathcal{K}_{10}^{\mathrm{barcode}}(s-t) & \mathcal{K}_{11}^{\mathrm{barcode}}(s-t) \end{pmatrix}, \qquad s,t \in 2\mathbb{Z},$$

[3] In particular, we conjecture that the limit (1.8) exists for all integers $s \geq t$.

and satisfies $\mathcal{K}^{\mathrm{barcode}}(0,0) = 1 - \mathcal{K}^{\mathrm{barcode}}(1,1)$ *(the plot of this function in* q *and* κ *is given in Figure 10). Consequently, the barcode process has global density* $1/2$ *for every choice of* q *and* κ*, and it is invariant under even but not odd shifts.*

Remark 1.6. The period-two behaviour of the barcode process was not anticipated a priori, since the q-Racah weights $\mathsf{w}_{q,\kappa}$ (1.1) assigned to horizontal lozenges do not possess this periodicity. However, this property may be explained as follows. In every vertical slice the number of horizontal lozenges is determined by the geometry of the hexagon, and moving from slice t to slice $t+1$ changes this number by exactly one. This extra lozenge is created either above or below the waterfall region, which introduces an imbalance. The imbalance is rectified after two slices, i.e., after an even translation, which accounts for the invariance of the barcode process under even shifts but not under all integer shifts.

Sections 7.4 and 7.5 corroborate Conjecture 1.5 in two ways. First, we find a very strong numerical agreement between the conjectural barcode kernel $\mathcal{K}^{\mathrm{barcode}}$ and the pre-limit correlation kernel $K(s,x;t,y)$ for a large hexagon, regardless of its geometry and the macroscopic location (t,x) inside the waterfall region $\mathcal{W}$ around which the limit is taken. We also observe that the sequence (1.8) converges with the geometric rate q^M, and, moreover, the (suitably rescaled) pre-limit kernels $K(s,x;t,y)$ also converge to a limit with the geometric rate q^L. Second, we ported the perfect sampling algorithm from [BGR10] to `Python` to automatically collect large samples of the barcode process. We compare the sample even- and odd-site densities, as well as two-point correlations, with the predictions based on $\mathcal{K}^{\mathrm{barcode}}$, and find a very good agreement.

A rigorous derivation of $\mathcal{K}^{\mathrm{barcode}}$ and the proof of Conjecture 1.5 will likely require new tools for dealing with the inverse of the operator $\mathfrak{U}_t^{\mathrm{barcode}}$. We leave these analytic developments to future work.

1.4 Exponential concentration

Complementing the spectral projection approach, in Section 5 we also develop a concentration result on a given vertical slice by working directly with the q-Racah orthogonal polynomial ensemble:

$$\frac{1}{Z}\prod_{1\le i<j\le N}\big(\mu(x_i)-\mu(x_j)\big)^2\prod_{i=1}^{N}w(x_i),\qquad \mu(x)\coloneqq q^{-x}+\kappa^2 q^{x+1-S-t}, \tag{1.9}$$

where the "particles" $x_1,\dots,x_N$ are the positions of the non-horizontal lozenges, and $w(x)$ is the q-Racah weight function (under which the q-Racah polynomials are orthogonal).

The key idea is to compare the probabilities of two N-particle configurations that differ only by moving a single particle from (t,x) to (t,y). The ratio of these probabilities exposes a dominant factor $q^{\mathcal{E}(x,y)}$, where the exponent decomposes into a one-body term $\mathcal{W}(u)$ (integrated between x and y) and an interaction term $\mathcal{G}(x,y,z_i)$, where z_i are the positions of the other particles that are not moved. We show that the interaction is minimized when the other $N-1$ particles form a densely packed block around the center line.

After this minimisation, the exponent $\mathcal{E}(x,y)$ becomes a discrete integral of a piecewise linear function which has order $1/L$ inside the waterfall region. This allows us to show that moving a single particle closer to the center line is advantageous of order q^{-cL} close to the boundary of the waterfall region, and of order $q^{-c'L^2}$ when move is across the waterfall boundary. These estimates

translate into the exponential concentration of square and vertical lozenges inside the waterfall region, and of the horizontal lozenges outside the waterfall region. Together with the spectral projection results, this establishes Theorem 1.4 for the entire hexagon.

1.5 Outline of the paper

In Section 2 we collect the necessary definitions related to the q-Racah random lozenge tilings, their connection with q-Racah orthogonal polynomials, and the spectral projection interpretation of the fixed-slice correlation kernel. We mostly follow the notation of [BGR10]. In Section 3 we introduce the fixed-q scaling regime, and discuss how it differs from the traditional scaling $q \to 1$. We also outline the heuristics for the waterfall phenomenon which are made rigorous in the subsequent Sections 4 and 5. Namely, in Section 4 we employ the spectral projection method to get the limit of the correlation kernel at the center line and outside the waterfall region, and in Section 5 we complement the analysis by direct estimates in the q-Racah orthogonal polynomial ensemble, leading to the exponential concentration result. These sections complete the proof of our main result, Theorem 1.4.

In Section 6 we review the two-dimensional correlation structure of q-Racah random lozenge tilings and set the stage for a subsequent nonrigorous analysis of their asymptotic behavior that culminates in the conjectural barcode kernel. The presentation in this section is completely rigorous; in particular, we derive asymptotic formulas for the inter-slice transition kernel that yield the limiting operator $\mathfrak{U}_t^{\mathrm{barcode}}$. Section 7 then combines a heuristic derivation of the barcode kernel with numerical and probabilistic evidence. We first carry out an informal asymptotic analysis explaining the eventual form of the kernel, and afterwards corroborate the predictions by means of exact-formula numerics and perfect sampling data.

Appendix A collects several properties of the functions $\mathcal{F}_n^t(x)$ appearing in the barcode kernel, which may be of independent interest. Appendix B contains the `Mathematica` code used for the numerical analysis of the exact formulas performed in Section 7.4.

1.6 Acknowledgements

We are grateful to Vadim Gorin for valuable remarks and for sharing with us the original `Fortran` source code implementing the shuffling algorithm for q-Racah random lozenge tilings described in [BGR10, Section 6]. AK was partially supported by the NSF grant DMS-2348756. LP was partially supported by the NSF grant DMS-2153869 and the Simons Collaboration Grant for Mathematicians 709055. Part of this research was performed in Spring 2024 while LP was visiting the program "Geometry, Statistical Mechanics, and Integrability" at the Institute for Pure and Applied Mathematics (IPAM), which is supported by the NSF grant DMS-1925919.

2 Preliminaries on q-Racah random tilings

In this section, we recall the definition and properties of the (imaginary) q-Racah probability measure on the set of lozenge tilings of a hexagon. This measure was introduced and studied in [BGR10], and we mostly follow the notation of that paper.

2.1 Random lozenge tilings and nonintersecting paths

Consider a hexagon drawn on the triangular lattice with integer sides a, b, c, a, b, c. We are interested in tilings of this hexagon by three types of lozenges. We will always work with an affine transformed lattice, in which one of the lozenges looks like a unit square. The hexagon with $a = b = c = 3$ and an example of its lozenge tiling are given in Figure 2, left.

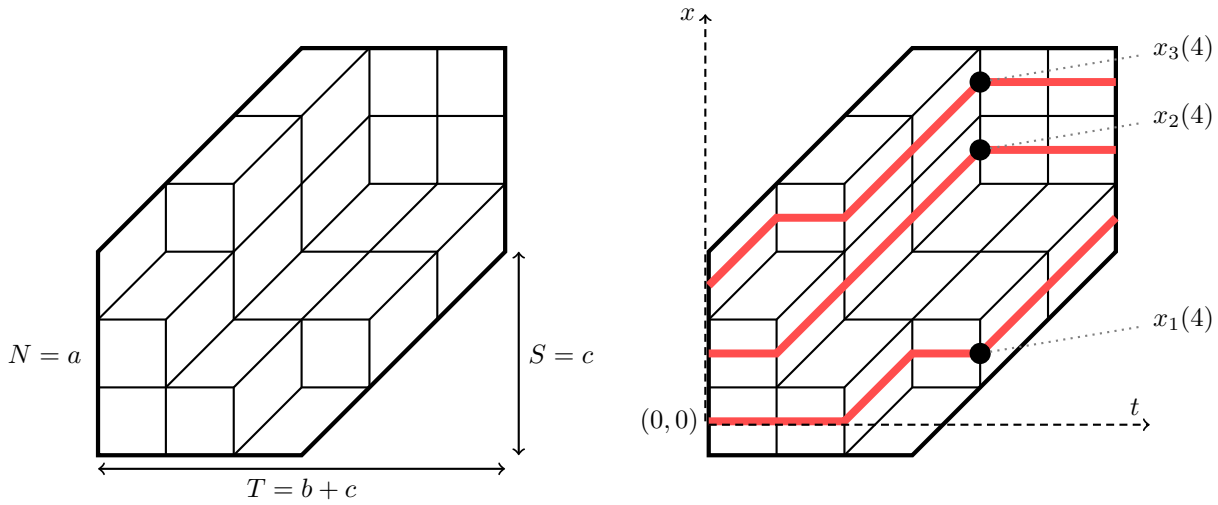

Figure 2: Left: An example of a lozenge tiling of a hexagon with sides $a = b = c = 3$. Right: The corresponding ensemble of $N = a$ nonintersecting paths.

We set $T := b + c$, $S := c$, and $N := a$, and use the parameters (T, S, N) throughout the paper. The lozenge tilings of our hexagon are in bijective correspondence with ensembles of N nonintersecting lattice paths that satisfy the following conditions:

- We view the horizontal axis as the "time" $t \in \{0, 1, \dots, T\}$. The paths start at locations $(0, 0), (0, 1), \dots, (0, N - 1)$ at time $t = 0$.
- The paths end at locations $(T, S), (T, S + 1), \dots, (T, S + N - 1)$ at time $t = T$.
- The paths make two types of steps:
  - horizontal, $(t, x) \to (t + 1, x)$,
  - and diagonal, $(t, x) \to (t + 1, x + 1)$.
- The paths do not intersect each other.

See Figure 2, right, for an example the path ensemble corresponding to a given lozenge tiling.

We denote by

$$X(t) := (x_1(t) < x_2(t) < \dots < x_N(t)) \tag{2.1}$$

the locations of the paths at time t. For example, in Figure 2, right, we have $X(4) = (1, 4, 5)$. These locations must satisfy

$$\max(0, t + S - T) \le x_i(t) \le \min(t + N - 1, S + N - 1), \qquad i = 1, \dots, N, \quad t = 0, \dots, T. \tag{2.2}$$

2.2 The q-Racah random lozenge tilings

Definition 2.1 (q-Racah measure on nonintersecting path ensembles)**.** We put a probability measure on the set of all nonintersecting path ensembles. The measure depends on the geometry of the hexagon (parametrized by (T, S, N)), and on two parameters $q > 0$ and $\kappa \in \mathbf{i}\mathbb{R}$. The probability weight of a nonintersecting path ensemble is proportional to

$$\prod_{\text{holes in the path ensemble}} \mathsf{w}_{q,\kappa}\bigl(x - \tfrac{t}{2} + 1\bigr), \qquad \mathsf{w}_{q,\kappa}(j) := \kappa q^{j-(S+1)/2} - \frac{1}{\kappa q^{j-(S+1)/2}}. \tag{2.3}$$

Here the holes are points (t, x) such that $x \notin X(t)$, but x satisfies the inequalities (2.2). In other words, holes are lozenges of the type $\diagup\!\!\square$. For example, in Figure 2, right, the holes are $(1,2), (2,1), (2,4), (3,0), (3,2), (3,5), (4,2), (4,3), (5,3)$. The probability weights are normalized so that the total probability of all path ensembles is 1. We call the resulting probability measure the *q-Racah measure* on nonintersecting path ensembles (equivalently, on lozenge tilings of the hexagon).

Remark 2.2. The number of holes in the path ensemble is a conserved quantity: it is equal to $S(T - S)$, which depends on the geometry of the hexagon but not on the path ensemble. This implies that the q-Racah measure is invariant under the transformation $(q, \kappa) \mapsto (1/q, 1/\kappa)$. Throughout the paper, we will assume that $q \in (0, 1)$, as this does not restrict the generality.

Proposition 2.3. *In terms of the coordinates $x_i(t)$, the probability weight of a path ensemble is equal to*

$$\prod_{t=0}^{T} \operatorname{const}(t, T, S, N) \prod_{i=1}^{N} \frac{q^{x_i(t)}}{1 - \kappa^2 q^{2x_i(t)-S-t+1}}. \tag{2.4}$$

Proof. This is essentially [BGR10, Proposition 3.3]. For the reader's convenience, we provide a brief proof here. To get (2.4) from (2.3), replace the product over the holes by the reciprocal of the product over the points in the path ensemble (this replacement contributes a constant factor independent of the path ensemble). Then, for $j = x - \frac{t}{2} + 1$, we have

$$\left(\kappa q^{j-(S+1)/2} - \frac{1}{\kappa q^{j-(S+1)/2}}\right)^{-1} = \frac{\kappa q^{\frac{1}{2}(S+t+2x+1)}}{\kappa^2 q^{2x+1} - q^{S+t}} = \operatorname{const}_0(t, T, S, N) \cdot \frac{q^x}{1 - \kappa^2 q^{2x-S-t+1}},$$

which completes the proof. □

From Proposition 2.3, one can readily notice the following degenerations of the q-Racah measure on nonintersecting path ensembles:

- As $\kappa \to 0$, the probability weight of a path ensemble becomes proportional to q^{vol}, where vol is the volume under the three-dimensional surface corresponding to the lozenge tiling.
- As $\kappa \to 0$ and further $q \to 1$, the probability measure becomes uniform.

Throughout the paper, we assume that $\kappa \neq 0$. Otherwise, the measure q^{vol} (studied in much more detail in the literature) does not display a dimensional collapse phenomenon. For definiteness in some formulas involving κ to the first power, we also assume that $\kappa \in \mathbf{i}\mathbb{R}_{>0}$.

2.3 q-Racah orthogonal polynomial ensemble

Under the q-Racah measure on nonintersecting path ensembles, the tuples $\{X(t)\}_{0\le t\le T}$ form a Markov chain, where t plays the role of time. For each fixed t, the distribution of $X(t)$ is connected to the *q-Racah orthogonal polynomial ensemble*. We refer to [Kön05] for a general survey of orthogonal polynomial ensembles.

In this subsection, we recall the q-Racah orthogonal polynomials and define the corresponding orthogonal polynomial ensemble. In the following Section 2.4, we will connect the orthogonal polynomial ensemble to the distribution of $X(t)$ coming from the nonintersecting paths. For the notation around the q-Racah polynomials, we follow [KS96, Chapter 3.2]. The connection of random nonintersecting paths of Definition 2.1 to q-Racah polynomials follows [BGR10, Theorem 4.1] (see also [DK19, Theorem 7.3.5] for a compact account of these results).

Throughout the paper, $(a;q)_k := (1-a)(1-aq)\dots(1-aq^{k-1})$ stands for the q-Pochhammer symbol.[4] The q-hypergeometric function ${}_4\phi_3$ is given by [GR04, (1.2.22)]:

$$ {}_4\phi_3\left(\begin{matrix}a,b,c,d\\ e,f,g\end{matrix}\,\middle|\,q;z\right) := \sum_{n=0}^{\infty}\frac{(a;q)_n(b;q)_n(c;q)_n(d;q)_n}{(e;q)_n(f;q)_n(g;q)_n(q;q)_n}z^n \tag{2.5}$$

Let $M\in\mathbb{Z}_{\ge 0}$ and $\alpha,\beta,\gamma,\delta\in\mathbb{R}$ be such that $\gamma q = q^{-M}$. Define the following *q-Racah weight function* on $\{0,1,\dots,M\}$:

$$ w^{qR}(x) := \frac{(\alpha q;q)_x(\beta\delta q;q)_x(\gamma q;q)_x(\gamma\delta q;q)_x}{(q;q)_x(\alpha^{-1}\gamma\delta q;q)_x(\beta^{-1}\gamma q;q)_x(\delta q;q)_x}\frac{\left(1-\gamma\delta q^{2x+1}\right)}{(\alpha\beta q)^x(1-\gamma\delta q)}, \qquad x\in\{0,1,\dots,M\}. \tag{2.6}$$

The weight w^{qR} is the orthogonality weight for the q-Racah polynomials which are defined as

$$ R_n(\mu(x);\alpha,\beta,\gamma,\delta\mid q) := {}_4\phi_3\left(\begin{matrix}q^{-n},\alpha\beta q^{n+1},q^{-x},\gamma\delta q^{x+1}\\ \alpha q,\beta\delta q,\gamma q\end{matrix}\,\middle|\,q;q\right), \qquad n=0,1,\dots,M. \tag{2.7}$$

These are polynomials of degree n in the variable $\mu(x)$ defined as

$$ \mu(x) := q^{-x}+\gamma\delta q^{x+1}. \tag{2.8}$$

The orthogonality means that

$$ \sum_{x=0}^{M} w^{qR}(x)\,R_m(\mu(x))R_n(\mu(x)) = \mathbf{1}_{m=n}\,h_n, \tag{2.9}$$

where the squared norms h_n have the form

$$ h_n = \frac{(\alpha\beta q^2;q)_M(\delta^{-1};q)_M}{(\alpha\delta^{-1}q;q)_M(\beta q;q)_M}\frac{(1-\alpha\beta q)(\delta q^{-M})^n}{(1-\alpha\beta q^{2n+1})}\frac{(q;q)_n(\alpha\beta q^{M+2};q)_n(\alpha\delta^{-1}q;q)_n(\beta q;q)_n}{(\alpha q;q)_n(\alpha\beta q;q)_n(\beta\delta q;q)_n(q^{-M};q)_n}. \tag{2.10}$$

The q-Racah polynomials R_n are eigenfunctions of a distinguished difference operator acting in x [KS96, (3.2.6)], that is, they satisfy

$$\begin{aligned} &q^{-n}(1-q^n)(1-\alpha\beta q^{n+1})R_n(\mu(x))\\ &\qquad = B(x)R_n(\mu(x+1)) - [B(x)+D(x)]R_n(\mu(x))(x) + D(x)R_n(\mu(x-1)), \end{aligned} \tag{2.11}$$

[4] Since $|q|<1$, the infinite q-Pochhammer symbol $(a;q)_\infty = \prod_{k=0}^{\infty}(1-aq^k)$ is also well-defined.

where

$$B(x) := \frac{(1-\alpha q^{x+1})(1-\beta\delta q^{x+1})(1-\gamma q^{x+1})(1-\gamma\delta q^{x+1})}{(1-\gamma\delta q^{2x+1})(1-\gamma\delta q^{2x+2})};$$
$$D(x) := \frac{q(1-q^x)(1-\delta q^x)(\beta-\gamma q^x)(\alpha-\gamma\delta q^x)}{(1-\gamma\delta q^{2x})(1-\gamma\delta q^{2x+1})}. \tag{2.12}$$

In (2.11), we have $x = 0, 1, \ldots, M$. Indeed, $B(M) = D(0) = 0$, so the values of $R_n(\mu(x))$ for $x = -1$ or $x = M+1$ do not enter the eigenrelation (2.11).

Remark 2.4. The q-Racah polynomials admit three parameter regimes $(\alpha, \beta, \gamma, \delta)$ that ensure the weight function vanishes for $x > M$. These regimes are specified by $\alpha q = q^{-M}$, $\beta\delta q = q^{-M}$, or $\gamma q = q^{-M}$. Accordingly, the norms h_n take different forms in each regime. For random tilings, it suffices to consider only the third regime $\gamma q = q^{-M}$, in which case h_n is given by (2.10).

Let us now describe the N-particle *q-Racah orthogonal polynomial ensemble* (abbreviated *q-Racah OPE*) on $\{0, 1, \ldots, M\}$ with parameters $\alpha, \beta, \gamma, \delta, M$ satisfying

$$M \geq N-1, \qquad q \in (0,1), \qquad \gamma q = q^{-M}, \qquad \alpha \geq \gamma, \qquad \beta \geq \gamma, \qquad \delta \leq 0. \tag{2.13}$$

With these restrictions on the parameters, one can check that the weights $w^{qR}(x)$ (2.6) are positive for all $x \in \{0, 1, \ldots, M\}$.

Definition 2.5. The q-Racah ensemble $\mathfrak{R}^{qR(N)}_{M,\alpha,\beta,\gamma,\delta}$ depending on the parameters satisfying (2.13), is a probability measure on N-tuples of particles $(x_1 < \ldots < x_N)$ in $\{0, 1, \ldots, M\}$, with probability weights given by

$$\mathfrak{R}^{qR(N)}_{M,\alpha,\beta,\gamma,\delta}(x_1, \ldots, x_N) = \frac{1}{Z(N, M, \alpha, \beta, \gamma, \delta)} \prod_{1 \leq i < j \leq N} (\mu(x_i) - \mu(x_j))^2 \prod_{i=1}^{N} w^{qR}(x_i). \tag{2.14}$$

Here $Z(N, M, \alpha, \beta, \gamma, \delta)$ is the normalization constant ensuring that the total probability is 1. The condition $M \geq N-1$ in (2.13) is required so that N particles can fit into $\{0, 1, \ldots, M\}$.

2.4 From orthogonal polynomials to lozenge tilings

Let us now connect the random nonintersecting path ensembles of Definition 2.1 to the q-Racah OPE. For this, we need to define four zones within the hexagon with sides a, b, c, a, b, c (recall that $T = b + c$, $S = c$, $N = a$), where the q-Racah parameters take different forms. These zones are determined by the value of the horizontal coordinate (time) t, and are defined as follows:

$$0 \leq t \leq \min(S-1, T-S-1) \quad \Rightarrow \quad \begin{matrix} M = t+N-1,\ \alpha = q^{-S-N}, \\ \beta = q^{S-T-N},\ \gamma = q^{-t-N},\ \delta = \kappa^2 q^{-S+N}; \end{matrix} \tag{2.15}$$

$$S \leq t \leq T-S-1 \quad \Rightarrow \quad \begin{matrix} M = S+N-1,\ \alpha = q^{-t-N}, \\ \beta = q^{t-T-N},\ \gamma = q^{-S-N},\ \delta = \kappa^2 q^{-t+N}; \end{matrix} \tag{2.16}$$

$$T-S \leq t \leq S-1 \quad \Rightarrow \quad \begin{matrix} M = T-S+N-1,\ \alpha = q^{-T-N+t}, \\ \beta = q^{-t-N},\ \gamma = q^{-T-N+S},\ \delta = \kappa^2 q^{-T+t+N}; \end{matrix} \tag{2.17}$$

$$\max(S, T-S) \le t \le T \quad \Rightarrow \quad \begin{matrix} M = T - t + N - 1,\ \alpha = q^{-T-N+S}, \\ \beta = q^{-S-N},\ \gamma = q^{-T-N+t},\ \delta = \kappa^2 q^{-T+S+N}; \end{matrix} \tag{2.18}$$

For each given hexagon, at most three of these zones are present, as conditions (2.16) and (2.17) are mutually exclusive. See Figure 3 for illustrations.

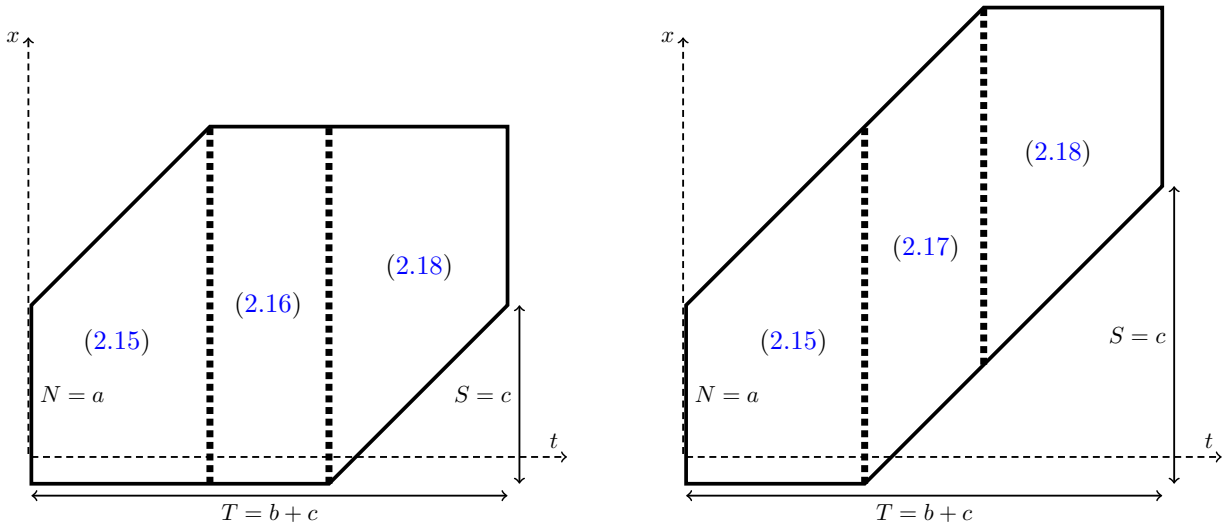

Figure 3: Zones inside the hexagon in which $X(t)$ (the path configuration at a slice $t = \text{const}$) has the q-Racah OPE distribution with different choices of parameters (see Theorem 2.6). For all T, S, N, the zones (2.15) and (2.18) are present inside the hexagon. The zone (2.16) is present if and only if $S \le T - S$, and otherwise we have the zone (2.17). On a border slice between two zones, the q-Racah parameters can be chosen in either of the two ways (for example, formulas in (2.15) and (2.16) coincide for $t = S$).

Theorem 2.6 ([BGR10, Theorem 4.1] and [DK19, Theorem 7.3.5]). *Fix T, S, N. In the zones (2.15) and (2.16), the distribution of $X(t)$ (2.1) under the q-Racah measure (Definition 2.1) is given by the N-particle q-Racah OPE on $\{0, 1, \dots, M\}$. In the zones (2.17) and (2.18), the distribution of the shifted configuration*

$$X(t) + T - t - S = (x_1(t) + T - t - S < x_2(t) + T - t - S < \ldots < x_N(t) + T - t - S) \tag{2.19}$$

is given by the N-particle q-Racah OPE on $\{0, 1, \dots, M\}$. In all cases, the parameters $M, \alpha, \beta, \gamma, \delta$ are given by the corresponding formulas in (2.15)–(2.18).

2.5 Determinantal correlation kernel and its operator interpretation

It is known [Kön05], [Bor11, Section 4] that orthogonal polynomial ensembles (in particular, the N-particle q-Racah OPE on $\{0, 1, \dots, M\}$) are determinantal point processes. Moreover, the two-dimensional random point configuration $\mathcal{X} := \{X(t)\}_{0 \le t \le T}$ forms a determinantal point process on $\mathbb{Z}^2$. The two-dimensional statement follows from the particular way of how the distributions of $X(t)$ on different slices are stitched together, and may be derived from [Bor11, Section 4].

Alternatively, the determinantal structure of $\mathfrak{X}$ follows from a dimer interpretation of the q-Racah random tiling model, cf. [Ken09, Corollary 3].

Let the space-time correlation functions be defined as

$$\rho_n(t_1, x_1; \dots; t_n, x_n) \coloneqq \mathbb{P}\left\{\text{the configuration } \mathfrak{X} \text{ contains all of } (t_1, x_1), \dots, (t_n, x_n)\right\},$$

where $(t_1, x_1), \dots, (t_n, x_n)$ are n pairwise distinct points. For any $n \geq 1$, these correlation functions are given by determinants

$$\rho_n(t_1, x_1; \dots; t_n, x_n) = \det[K(t_i, x_i; t_j, x_j)]_{i,j=1}^n, \tag{2.20}$$

coming from a single function of two points inside the hexagon. This function $K(t, x; s, y)$ is called the *correlation kernel*.

An explicit expression for $K(t, x; s, y)$ was obtained in [BGR10, Theorem 7.5] in terms of q-Racah polynomials. We now recall this result, together with an operator interpretation of the kernel

$$K_t(x, y) \coloneqq K(t, x; t, y) \tag{2.21}$$

on a fixed slice $t = \text{const}$, which also appears in [BGR10].

Consider a q-Racah OPE $\mathfrak{R}^{qR(N)}_{M,\alpha,\beta,\gamma,\delta}$ on $\{0, 1, \dots, M\}$ with parameters satisfying (2.13). Let us pass from the q-Racah polynomials (2.7) to the functions

$$f_n(x) = f_n(x; \alpha, \beta, \gamma, \delta \mid q) \coloneqq \frac{R_n(\mu(x))}{\sqrt{h_n}} \sqrt{w^{qR}(x)}, \qquad n = 0, 1, \dots, M, \tag{2.22}$$

which form an orthonormal basis in the Hilbert space $\ell^2(\{0, 1, \dots, M\})$. Thanks to (2.11), the $f_n(x)$'s are eigenfunctions of the difference operator

$$\left(\mathfrak{D}^{qR} g\right)(x) \coloneqq \sqrt{\frac{w^{qR}(x)}{w^{qR}(x+1)}} B(x)\, g(x+1) - [B(x) + D(x)]\, g(x) + \sqrt{\frac{w^{qR}(x)}{w^{qR}(x-1)}} D(x)\, g(x-1), \tag{2.23}$$

where $B(x)$ and $D(x)$ are given by (2.12). The eigenvalue of $f_n(x)$ is

$$\mathrm{ev}_n^{qR} \coloneqq q^{-n}(1 - q^n)(1 - \alpha\beta q^{n+1}). \tag{2.24}$$

In particular, $\mathrm{ev}_0^{qR} = 0$. Due to our assumptions on the parameters (2.13), the eigenvalues ev_n^{qR} are all nonpositive, and strictly decrease in n for $0 \leq n \leq M$.

Proposition 2.7 ([Meh04], [Kön05, Lemma 2.8]). *The correlation kernel of the N-particle q-Racah OPE on $\{0, 1, \dots, M\}$ is given by*

$$K^{qR}(x, y) = \sum_{n=0}^{N-1} f_n(x) f_n(y). \tag{2.25}$$

This is a kernel of the orthogonal projection operator onto $\operatorname{span}(f_0, f_1, \dots, f_{N-1})$ *in the Hilbert space* $\ell^2(\{0, 1, \dots, M\})$.

Following [BGR10, Section 8.2] which implements the operator approach pioneered in [BO07], [Ols08] (see also [Tao12, Chapter 3.3]), we view K^{qR} as the kernel of the orthogonal spectral projection onto the subspace of $\ell^2(\{0,1,\dots,M\})$ corresponding to the spectral interval

$$\left[-q^{-N+1}(1-q^{N-1})(\alpha\beta q^N-1),0\right] \tag{2.26}$$

of the operator $\mathfrak{D}^{qR}$ (2.23).

Let us now apply the spectral interpretation of K^{qR} to the correlation kernel $K_t(x,y)$ (2.21) on a fixed vertical slice inside the hexagon. Observe that in all four zones (2.15)–(2.18), we have $\alpha\beta q^N = q^{-T-N}$. Therefore, the spectral interval (2.26) stays the same throughout the hexagon. Denote

$$\tilde{x} := \begin{cases} x, & \text{if } t \text{ is in the zone (2.15) or (2.16);} \\ x+T-t-S, & \text{if } t \text{ is in the zone (2.17) or (2.18).} \end{cases} \tag{2.27}$$

One can check that the coefficients of the operator $\mathfrak{D}^{qR}$ (2.23) evaluated at $\tilde{x}$ are also the same in all four zones (2.15)–(2.18). More precisely, we have

$$\begin{aligned} B(\tilde{x}) &= \frac{q^{-2N-T}(q^T-\kappa^2q^{x+1})(q^{N+S}-q^{x+1})(q^{N+t}-q^{x+1})(q^{S+t}-\kappa^2q^{x+1})}{(q^{S+t}-\kappa^2q^{2x+1})(q^{S+t}-\kappa^2q^{2x+2})}, \\ D(\tilde{x}) &= \frac{(1-q^x)q^{-2N-T+1}(q^S-\kappa^2q^{N+x})(q^t-\kappa^2q^{N+x})(q^{S+t}-q^{T+x})}{(q^{S+t}-\kappa^2q^{2x})(q^{S+t}-\kappa^2q^{2x+1})}, \end{aligned} \tag{2.28}$$

and

$$\begin{aligned} \frac{w^{qR}(\tilde{x})}{w^{qR}(\tilde{x}+1)} &= \frac{q(1-q^{x+1})(q^S-\kappa^2q^{N+x+1})(q^t-\kappa^2q^{N+x+1})(q^{S+t}-\kappa^2q^{2x+1})(q^{S+t}-q^{T+x+1})}{(q^T-\kappa^2q^{x+1})(q^{N+S}-q^{x+1})(q^{N+t}-q^{x+1})(q^{S+t}-\kappa^2q^{x+1})(q^{S+t}-\kappa^2q^{2x+3})}; \\ \frac{w^{qR}(\tilde{x})}{w^{qR}(\tilde{x}-1)} &= \frac{(q^T-\kappa^2q^x)(q^{N+S}-q^x)(q^{N+t}-q^x)(q^{S+t}-\kappa^2q^x)(q^{S+t}-\kappa^2q^{2x+1})}{(q^x-1)(\kappa^2q^{N+x}-q^S)(\kappa^2q^{N+x}-q^t)(q^{S+t+1}-\kappa^2q^{2x})(q^{T+x}-q^{S+t})}. \end{aligned} \tag{2.29}$$

We conclude that the kernel $K_t(x,y)$ has the following spectral description, which is the same in all four zones (2.15)–(2.18):

Corollary 2.8. *The fixed-slice correlation kernel $K_t(x,y)$ (2.21) of the q-Racah nonintersecting path ensemble inside the hexagon with sides a,b,c,a,b,c (where $T=b+c$, $S=c$, $N=a$) is the kernel of the orthogonal spectral projection onto the subspace corresponding to the spectral interval*

$$\left[-q^{-N+1}(1-q^{N-1})(q^{-T-N}-1),0\right] \tag{2.30}$$

of the difference operator

$$\big(\mathfrak{D}g\big)(x) := \sqrt{\frac{w^{qR}(\tilde{x})}{w^{qR}(\tilde{x}+1)}}B(\tilde{x})\,g(x+1) - [B(\tilde{x})+D(\tilde{x})]\,g(x) + \sqrt{\frac{w^{qR}(\tilde{x})}{w^{qR}(\tilde{x}-1)}}D(\tilde{x})\,g(x-1). \tag{2.31}$$

This operator on functions of x acts in the (finite-dimensional) ℓ^2 space on the t-th vertical slice of the hexagon. Its coefficients are read off from (2.28) and (2.29).

Remark 2.9. One can check that

$$\sqrt{\frac{w^{qR}(\tilde{x}-1)}{w^{qR}(\tilde{x})}}B(\tilde{x}-1)=\sqrt{\frac{w^{qR}(\tilde{x})}{w^{qR}(\tilde{x}-1)}}D(\tilde{x}),$$

which means that the operator $\mathfrak{D}$ is self-adjoint with respect to the standard inner product in ℓ^2 on the t-th vertical slice.

3 Scaling regime

3.1 Traditional scaling of q-weighted lozenge tilings

We consider the asymptotic regime when the sides of the hexagon are scaled proportionally to some large parameter $L\to+\infty$. Typically, the parameter q (for the q^{vol} or the q-Racah measure on lozenge tilings) also goes to 1, at the rate $\exp(-c/L)$, where $c\in\mathbb{R}$ is fixed. In this regime, random tilings develop a so-called *liquid region*, in which local lattice distributions follow translation-invariant ergodic Gibbs measures (*pure states*, for short) on lozenge tilings of the whole plane $\mathbb{Z}^2$. Since in the limit the parameter q becomes 1, the limiting pure states (for both the q^{vol} and the q-Racah ensembles) satisfy the Gibbs property with respect to the *uniform resampling* of a tiling in any finite subregion, conditioned on the boundary of this subregion. Such Gibbs measures are uniquely determined by two parameters [She05], which in terms of nonintersecting paths may be taken as their vertical density and horizontal slope. These pure states universally arise as local lattice limits in uniformly random lozenge tilings of arbitrary polygons [Agg23].

The literature on this asymptotic regime of the measure q^{vol} is vast, and includes [NHB84], [CLP98], [CK01], [OR03], [FS03], [KOS06], [KO07], [BG13], [MP17], [DFG19], [PT23], [ARVP22]. Main results on the asymptotic behavior of the uniform and q^{vol} measures are summarized in [Ken09] and [Gor21]. Asymptotic behavior of the q-Racah measure as $q\to1$ was studied in [BGR10], [DK19], [GH24], [DDL24]. In these references, the limiting objects within the liquid region are two-dimensional, such as the pure Gibbs states at the lattice level, Gaussian Free Field describing global fluctuations, or the GUE corners process at points where the liquid region comes close to the boundary of the polygon.

The novelty of the present work is that we keep the parameter q fixed while scaling the sides of the hexagon to infinity. As was first observed in simulations in [BGR10], this leads to formation of a so-called *waterfall region* inside the hexagon. We describe this region in Section 3.2 below.

3.2 Waterfall scaling

We consider the limit behavior of the q-Racah nonintersecting path ensemble as the sides of the hexagon grow proportionally to infinity as $L\to+\infty$:

$$T=\lfloor L\mathsf{T}\rfloor,\ S=\lfloor L\mathsf{S}\rfloor,\ N=\lfloor L\mathsf{N}\rfloor,\ \mathsf{T}>\mathsf{S}>0,\ \mathsf{N}>0;\quad q\in(0,1),\ \kappa\in\mathbf{i}\mathbb{R}_{>0}\text{ fixed.}\tag{3.1}$$

In this regime, the q-Racah nonintersecting paths display a very different limit behavior from the traditional one (Section 3.1). Namely, for fixed q and κ, the two-dimensional lattice behavior *collapses* into a one-dimensional random stepped interface (which we call a *barcode*). One can

also think that this random interface satisfies (a degenerate version of) the q-deformed Gibbs property, which does not allow any changes under resampling.

Let us define the macroscopic *waterfall region* where this new behavior occurs.

Definition 3.1 (Waterfall region)**.** Fix the scaled dimensions $\mathsf{T}, \mathsf{S}, \mathsf{N}$ of the hexagon, and let (t, x) be the scaled coordinates. Denote by $\mathcal{H}$ the scaled hexagon, that is,

$$\mathcal{H} := \{(\mathsf{t}, \mathsf{x}) \colon 0 < \mathsf{t} < \mathsf{T},\ \max(0, \mathsf{t} - \mathsf{T} + \mathsf{S}) < \mathsf{x} < \min(\mathsf{S} + \mathsf{N}, \mathsf{t} + \mathsf{N})\}. \tag{3.2}$$

Let

$$\mathsf{t}_l := |\mathsf{N} - \mathsf{S}|, \qquad \mathsf{t}_r := \min(\mathsf{N} + \mathsf{S}, 2\mathsf{T} - \mathsf{N} - \mathsf{S}). \tag{3.3}$$

Denote the *waterfall region* by

$$\mathcal{W} := \{(\mathsf{t}, \mathsf{x}) \in \mathcal{H} \colon \mathsf{t}_l < \mathsf{t} < \mathsf{t}_r,\ |2\mathsf{x} - \mathsf{S} - \mathsf{t}| < \mathsf{N}\}. \tag{3.4}$$

Also, let the *center line* be the following line segment of slope $\frac{1}{2}$:

$$\mathcal{C} := \{(\mathsf{t}, \mathsf{x}) \in \mathcal{H} \colon \mathsf{t}_l < \mathsf{t} < \mathsf{t}_r,\ \mathsf{x} = \tfrac{1}{2}(\mathsf{t} + \mathsf{S})\} \subset \mathcal{W}. \tag{3.5}$$

See Figure 4 for illustrations of the waterfall region and the corresponding exact samples from the q-Racah measure generated by the shuffling algorithm of [BGR10].

Remark 3.2. Note that when $\mathsf{N} \geq \mathsf{T}$, we have $\mathsf{t}_l \geq \mathsf{t}_r$. This means that the waterfall region is nonempty only for $\mathsf{N} < \mathsf{T}$. In Section 5 below, we show that tor $\mathsf{N} > \mathsf{T}$, the nonintersecting paths can only have asymptotic slopes 0 or 1 (depending on the part of the hexagon), so the waterfall behavior does not occur. It would be interesting to probe the case of "thin waterfall" when $T/N \to 1$ while $T - N \gg 1$ (see Figure 5 for exact samples), but we do not address this question in the present work.

Definition 3.3. Denote by $\mathcal{W}^{\pm}$ the regions above and below the waterfall, that is,

$$\mathcal{W}^{+} := \begin{cases} \{(\mathsf{t}, \mathsf{x}) \in \mathcal{H} \colon \mathsf{x} > \mathsf{N} + (\mathsf{t} - \mathsf{T} + \mathsf{S})^{+}\}, & \text{if } \mathsf{N} > \mathsf{T}; \\ \{(\mathsf{t}, \mathsf{x}) \in \mathcal{H} \colon \mathsf{t}_l < \mathsf{t} < \mathsf{t}_r,\ \mathsf{x} > \frac{1}{2}(\mathsf{S} + \mathsf{t} + \mathsf{N})\} & \\ \quad \cup \{(\mathsf{t}, \mathsf{x}) \in \mathcal{H} \colon \mathsf{t} \leq \mathsf{t}_l,\ \mathsf{x} > \mathsf{N}\}\mathbf{1}_{\mathsf{N}>\mathsf{S}} & \\ \quad \cup \{(\mathsf{t}, \mathsf{x}) \in \mathcal{H} \colon \mathsf{t} \geq \mathsf{t}_r,\ \mathsf{x} > \mathsf{S} + \mathsf{N} + \mathsf{t} - \mathsf{T}\}\mathbf{1}_{\mathsf{S}+\mathsf{N}>\mathsf{T}}, & \text{if } \mathsf{N} < \mathsf{T}, \end{cases}$$

and

$$\mathcal{W}^{-} := \{(\mathsf{t}, \mathsf{x}) \in \mathcal{H} \colon \mathsf{t}_l < \mathsf{t} < \mathsf{t}_r,\ \mathsf{x} < \tfrac{1}{2}(\mathsf{S} + \mathsf{t} - \mathsf{N})\} \\ \cup \{(\mathsf{t}, \mathsf{x}) \in \mathcal{H} \colon \mathsf{t} \leq \mathsf{t}_l,\ \mathsf{x} < \mathsf{t}\}\mathbf{1}_{\mathsf{N}<\mathsf{S}} \cup \{(\mathsf{t}, \mathsf{x}) \in \mathcal{H} \colon \mathsf{t} \geq \mathsf{t}_r,\ \mathsf{x} < \mathsf{S}\}\mathbf{1}_{\mathsf{S}+\mathsf{N}<\mathsf{T}}.$$

Here the indicator $\mathbf{1}_{\mathsf{N}>\mathsf{S}}$ means that the subset in the union is present only if $\mathsf{N} > \mathsf{S}$, and similarly for all other indicators. In the samples in Figure 4, right, the regions $\mathcal{W}^{\pm}$ are the lighter-colored ones. They consist solely of the horizontal lozenges $\parallelogram$.[5]

Also denote $\mathcal{P} := \mathcal{H} \setminus (\mathcal{W}^{+} \cup \mathcal{W}^{-})$, this is the region inside the hexagon where we expect the nonintersecting paths to cluster together. We call $\mathcal{P}$ the *saturation band*. It has constant width N and includes the waterfall region.

[5]The below region $\mathcal{W}^{-}$ exists only if $\mathsf{N} < \mathsf{T}$. In Section 5 below, we show that for $\mathsf{N} > \mathsf{T}$, the nonintersecting paths stay as low as they can: First, they go straight with slope 0 until $\mathsf{t} = \mathsf{T} - \mathsf{S}$, and then continue diagonally with slope 1.

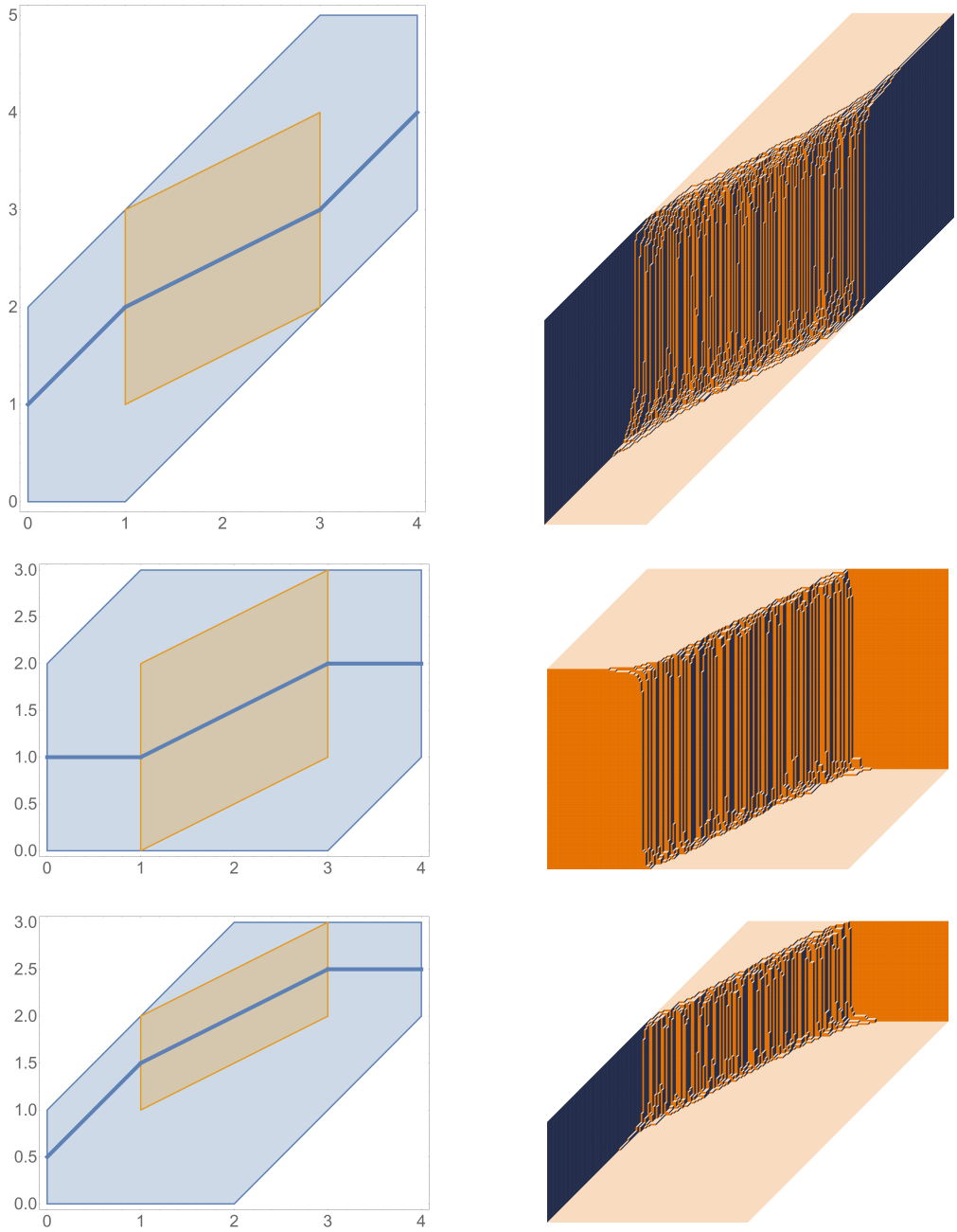

Figure 4: Examples of the waterfall region $\mathcal{W}$ inside the hexagon in the coordinate system $(\mathtt{t}, \mathtt{x})$, together with an exact sample produced by the shuffling algorithm from [BGR10]. On the left, we have displayed the large-scale limit of the trajectory of the nonintersecting path starting in the middle. Inside $\mathcal{W}$, this path stays close to the center line $\mathcal{C}$, and in particular, has asymptotic slope $1/2$. Outside $\mathcal{W}$, the slope is either 0 or 1, and the path proceeds right or right-up without fluctuations. Limit trajectories of all other nonintersecting paths are parallel translations of the center one. The parameters of the simulations are, from top to bottom: $(T, S, N, q) = (300, 225, 150, 0.9), (240, 60, 120, 0.8), (240, 120, 60, 0.8)$, and $\kappa = \mathbf{i}$ throughout. The horizontal lozenges (the lighter-colored ones) are exponentially (in L) rare in the waterfall region. This behavior corresponds to the asymptotic clustering of the paths.

Figure 5: Exact samples from the q-Racah measure generated by the shuffling algorithm of [BGR10] in the regime $N > T$. The parameters are $q = 0.85$, $\kappa = \mathbf{i}$, and $(N, T, S) = (180, 120, 80)$ (left) and $(N, T, S) = (100, 90, 60)$ (right). In the left-hand picture no waterfall behavior is present; presumably the limit shape at scales $\ll N$ coincides with that for q^{vol} random plane partitions without boundary studied in [CK01], [FS03], [OR03]. In the right-hand picture we observe a "thin waterfall," which appears when T/N is close to 1 (see also Remark 3.2).

3.3 Heuristics for the saturation band and the waterfall region

Heuristically, the appearance of the saturation band $\mathcal{P}$ where the nonintersecting paths cluster together with density 1 can be observed from the weights $\mathsf{w}_{q,\kappa}$ of the holes in the path ensemble, see (2.3). Indeed, we have

$$\mathsf{w}_{q,\kappa}(x - \tfrac{t}{2} + 1) = \kappa q^{\frac{1}{2}+(x-\frac{t+S}{2})} - \left(\kappa q^{\frac{1}{2}+(x-\frac{t+S}{2})}\right)^{-1}. \tag{3.6}$$

Since $\kappa \in \mathbf{i}\mathbb{R}_{>0}$, both summands in (3.6) have the same sign. When (t, x) is close to the center line $\mathcal{C}$ (3.5), both summands are asymptotically of order 1. However, when (t, x) is far from $\mathcal{C}$, one of the summands dominates and goes to infinity exponentially in L. Therefore, all holes in the path ensemble are encouraged to stay as far from the center line as possible. There are two possibilities, depending on whether $\mathsf{t}_l < \mathsf{t} < \mathsf{t}_r$:

- If $\mathsf{t}_l < \mathsf{t} < \mathsf{t}_r$, there is enough room inside the hexagon $\mathcal{H}$ for the holes to stay away from $\mathcal{C}$ symmetrically. This leads to the formation of the waterfall region $\mathcal{W}$: It is a band of width N centered around $\mathcal{C}$. Since the two summands in (3.6) are symmetric with respect to $\mathcal{C}$, the waterfall region $\mathcal{W}$ indeed must inherit this symmetry.
- When $\mathsf{t} \notin [\mathsf{t}_l, \mathsf{t}_r]$ or $\mathsf{N} > \mathsf{T}$, there is no room inside $\mathcal{H}$ to fit a symmetric band of width N around $\mathcal{C}$. Then the holes live only on one side of $\mathcal{C}$, and the nonintersecting paths are frozen and have slope 0 or 1.

In Section 5 below, we engage in a detailed analysis of the q-Racah orthogonal polynomial ensemble probability weights (2.14) to make this heuristic rigorous, and prove our main result (Theorem 1.4).

4 Asymptotic behavior on a vertical slice via spectral projections

In this section, we consider the asymptotic behavior of the fixed-slice correlation kernel $K_t(x,y)$ (2.21) in the regime described in Section 3.2. We employ the spectral description of K_t via the difference operator $\mathfrak{D}$ given by (2.31). It turns out that the spectral approach, which successfully worked throughout the whole hexagon in the traditional scaling regime $q \to 1$, can only describe the asymptotic behavior on the center line $\mathcal{C}$ when q is fixed.

4.1 Limit of the coefficients

Recall the limit regime (3.1). We consider a fixed vertical slice at $t = \lfloor L\mathsf{t} \rfloor$ inside the hexagon (where t is the scaled position of the slice). We aim to find the limit of the (suitably shifted and scaled) difference operator $\mathfrak{D}$ (2.31):

$$\big(\mathfrak{D}^{\mathrm{scaled}} g\big)(x) := \underbrace{q^{N+T+(N-|2\lfloor L\mathsf{x}\rfloor - S - t|)^+}}_{=:C_{\mathsf{x}}} \Big[\big(\mathfrak{D} g\big)(x) + q^{-N+1}(1-q^{N-1})(q^{-T-N}-1)\, g(x) \Big]. \tag{4.1}$$

Here and throughout the paper, we use the notation

$$a^+ := \max(a,0), \quad a^- := \min(a,0), \qquad a \in \mathbb{R}. \tag{4.2}$$

We will also abbreviate $C_{\mathsf{x}} := q^{N+T+(N-|2\lfloor L\mathsf{x}\rfloor - S - t|)^+}$, which is the scaling prefactor in (4.1).

The operator $\mathfrak{D}^{\mathrm{scaled}}$ is symmetric with respect to the standard inner product in $\ell^2(\mathbb{Z})$ (see Remark 2.9). Its coefficients have compact support in x, so $\mathfrak{D}^{\mathrm{scaled}}$ is bounded and thus self-adjoint. The subspace $\ell^2_0(\mathbb{Z})$ consisting of finite linear combinations of the standard basis vectors $e_x(y) := \mathbf{1}_{y=x}$ is an *essential domain*[6] for $\mathfrak{D}^{\mathrm{scaled}}$. Due to the shift in (4.1), the fixed-slice correlation kernel K_t (2.21) is the kernel of the orthogonal projection operator in $\ell^2(\mathbb{Z})$ onto the spectral interval $[0,+\infty)$ of the operator $\mathfrak{D}^{\mathrm{scaled}}$.

Assume that in (3.1) we have $\mathsf{N} < \mathsf{T}$, which guarantees the existence of the waterfall region. Let $x = \lfloor L\mathsf{x} \rfloor + \Delta x$ and $t = \lfloor L\mathsf{t} \rfloor$, where $\Delta x \in \mathbb{Z}$ is fixed. We also assume that $\mathsf{t}_l < \mathsf{t} < \mathsf{t}_r$. Throughout the rest of this subsection, we consider the asymptotic behavior of the coefficients of $\mathfrak{D}^{\mathrm{scaled}}$ one by one, depending on the position of (t,x) inside the hexagon.

Lemma 4.1 (Diagonal coefficient)**.** *Let $\mathsf{t}_l < \mathsf{t} < \mathsf{t}_r$, and the point (t,x) be inside the scaled hexagon $\mathcal{H}$ (3.2). Under the scaling described before the lemma, the diagonal coefficient of the operator $\mathfrak{D}^{\mathrm{scaled}}$ (4.1) has the following limit:*

$$\begin{aligned}
&\lim_{L\to+\infty} C_{\mathsf{x}} \cdot \big(q^{-N+1}(1-q^{N-1})(q^{-T-N}-1) - B(\tilde{x}) - D(\tilde{x}) \big) \\
&\quad = \begin{cases}
-1, & \mathsf{x} < \frac{1}{2}(\mathsf{S}+\mathsf{t}-\mathsf{N}); \\
-1-\kappa^{-2}(1+q)\,q^{-1-2\Delta x}, & \mathsf{x} = \frac{1}{2}(\mathsf{S}+\mathsf{t}-\mathsf{N}),\ \lfloor L\mathsf{x}\rfloor = \frac{1}{2}(S+t-N); \\
-\kappa^{-2}(1+q)\,q^{-1-2\Delta x}, & \frac{1}{2}(\mathsf{S}+\mathsf{t}-\mathsf{N}) < \mathsf{x} < \frac{1}{2}(\mathsf{S}+\mathsf{t}); \\
\dfrac{-\kappa^2(1+q)\,q^{2\Delta x+1}}{(1-\kappa^2 q^{2\Delta x})(1-\kappa^2 q^{2\Delta x+2})}, & \mathsf{x} = \frac{1}{2}(\mathsf{S}+\mathsf{t}),\ \lfloor L\mathsf{x}\rfloor = \frac{1}{2}(S+t); \\
-\kappa^2(1+q)\,q^{2\Delta x+1}, & \frac{1}{2}(\mathsf{S}+\mathsf{t}) < \mathsf{x} < \frac{1}{2}(\mathsf{S}+\mathsf{t}+\mathsf{N}); \\
-1-\kappa^2(1+q)\,q^{2\Delta x+1}, & \mathsf{x} = \frac{1}{2}(\mathsf{S}+\mathsf{t}+\mathsf{N}),\ \lfloor L\mathsf{x}\rfloor = \frac{1}{2}(S+t+N); \\
-1, & \mathsf{x} > \frac{1}{2}(\mathsf{S}+\mathsf{t}+\mathsf{N}).
\end{cases}
\end{aligned} \tag{4.3}$$

[6] This subspace is also sometimes called the *core* of an operator.

Note that depending on the geometry of the hexagon (determined by $\mathsf{T},\mathsf{S},\mathsf{N}$), not all of the above cases may be present.

Remark 4.2. In the three border cases (when x is not in an interval), we need to make more precise discrete assumptions about the parameters to fix the shift of the x-coordinate around the border. We also assume that the integers multiplied by $\frac{1}{2}$ are even. The latter can always be achieved by replacing S with $S \pm 1$. This shift does not affect the generality of the asymptotic analysis because the limiting quantity S can still be an arbitrary real number within a suitable interval.

Proof of Lemma 4.1. Combining all the terms in $q^{-N+1}(1-q^{N-1})(q^{-T-N}-1) - B(\tilde{x}) - D(\tilde{x})$, we have

$$\begin{aligned}
&C_{\mathsf{x}} \cdot \big(q^{-N+1}(1-q^{N-1})(q^{-T-N}-1) - B(\tilde{x}) - D(\tilde{x})\big) \\
&\quad = \frac{q^{(N-|2\lfloor L\mathsf{x}\rfloor - S - t|)^+}}{(q^{S+t}-\kappa^2 q^{2x})(q^{S+t}-\kappa^2 q^{2x+2})} \Big(\big[q^{2S+t+T+x+1} + q^{S+2t+T+x+1} - q^{2S+2t+T+1} \\
&\qquad\qquad - q^{2S+2t} + q^{-N+S+t+T+x+1} - q^{-N+S+t+T+2x+1} \\
&\qquad\qquad - q^{-N+S+t+T+2x+2} + q^{-N+2S+2t+x+1} \big] \\
&\qquad - \kappa^2 \big[-q^{N+S+t+T+x+1} - q^{S+t+T+2x+1} - q^{S+t+T+2x+3} + q^{N+S+t+T+2x+1} \\
&\qquad\qquad + q^{N+S+t+T+2x+2} - q^{2S+t+x+1} - q^{S+2t+x+1} - q^{N+2S+2t+x+1} \\
&\qquad\qquad - q^{S+t+2x} - q^{S+t+2x+2} + q^{2S+t+2x+1} + q^{2S+t+2x+2} \\
&\qquad\qquad + q^{S+2t+2x+1} + q^{S+2t+2x+2} + q^{S+T+2x+1} + q^{S+T+2x+2} \\
&\qquad\qquad - q^{S+T+3x+2} + q^{t+T+2x+1} + q^{t+T+2x+2} - q^{t+T+3x+2} \\
&\qquad\qquad + q^{-N+S+t+2x+1} + q^{-N+S+t+2x+2} - q^{-N+S+t+3x+2} - q^{-N+T+3x+2} \big] \\
&\qquad + \kappa^4 \big[-q^{N+S+t+2x+1} - q^{N+S+t+2x+2} + q^{N+S+t+3x+2} + q^{S+3x+2} \\
&\qquad\qquad + q^{t+3x+2} + q^{N+T+3x+2} - q^{T+4x+3} - q^{4x+2} \big] \Big).
\end{aligned} \tag{4.4}$$

Let us now consider the cases in (4.3) one by one.

Case $\mathsf{x} < (\mathsf{S}+\mathsf{t}-\mathsf{N})/2$. We have $(N - |2\lfloor L\mathsf{x}\rfloor - S - t|)^+ = 0$. The dominant contribution from the denominator in (4.4) is $\kappa^{-4}q^{-4x-2}$. Combining this power with all the powers in the long sum in the numerator, one can directly check that all terms except for $\kappa^{-4}q^{-4x-2}\cdot(-\kappa^4 q^{4x+2}) = -1$ vanish. This yields the first case of (4.3).

Case $\mathsf{x} = (\mathsf{S}+\mathsf{t}-\mathsf{N})/2$. Here, we still have $(N - |2\lfloor L\mathsf{x}\rfloor - S - t|)^+ = 0$, and the dominant contribution from the denominator is the same as in the previous case. Plugging $x = \Delta x + \frac{1}{2}(S+t-N)$ into (4.4), one can directly check that there are three surviving terms in the limit as $L \to +\infty$. One term is (-1), as in the previous case. The other two terms arise from the coefficient by $-\kappa^2$, and after multiplication by the contribution of the denominator, they have the form

$$-\kappa^{-2}(1+q)\,q^{-N+S+t-2x-1} = -\kappa^{-2}(1+q)\,q^{-2\Delta x-1}. \tag{4.5}$$

This yields the second case of (4.3).

Case $(\mathsf{S}+\mathsf{t}-\mathsf{N})/2 < \mathsf{x} < (\mathsf{S}+\mathsf{t})/2$**.** Here the extra factor $q^{(N-|2\lfloor L\mathsf{x}\rfloor - S - t|)^+} = q^{N-S-t+2\lfloor L\mathsf{x}\rfloor}$ is not 1 anymore, while the contribution from the denominator stays the same as in the previous two cases. One can check that with this extra factor, there are no new surviving terms in the limit. The summand (-1) multiplied by $q^{N-S-t+2\lfloor L\mathsf{x}\rfloor}$ vanishes in the limit. The two remaining terms become the same as in (4.5):

$$-\kappa^{-2} q^{N-S-t+2\lfloor L\mathsf{x}\rfloor}(1+q)\, q^{-N+S+t-2x-1} = -\kappa^{-2}(1+q)\, q^{-2\Delta x-1}.$$

This establishes the third case of (4.3).

Case $\mathsf{x} = (\mathsf{S}+\mathsf{t})/2$**.** In the denominator in (4.4), the contribution comes from all terms:

$$(q^{S+t} - \kappa^2 q^{2x})(q^{S+t} - \kappa^2 q^{2x+2}) = q^{2S+2t}(1-\kappa^2 q^{2\Delta x})(1-\kappa^2 q^{2\Delta x+2}).$$

The combined prefactor in front of the numerator is thus $q^{(N-|2\lfloor L\mathsf{x}\rfloor - S - t|)^+ - 2S - 2t} = q^{N-2S-2t}$. One can check that with this prefactor, all terms in the long sum in (4.4) except two vanish in the limit. These two terms come from the same summands as in (4.5):

$$-\kappa^2 q^{N-2S-2t}(1+q)\, q^{-N+S+t+2x+1} = -\kappa^2(1+q)\, q^{2\Delta x+1}.$$

This establishes the fourth case of (4.3).

Remaining cases $\mathsf{x} > (\mathsf{S}+\mathsf{t})/2$**.** The remaining three cases in (4.3) are symmetric with the first three cases. In all of them, the dominant contribution from the denominator in (4.4) is q^{-2S-2t}, and the rest of their computation is very similar to the first three cases. We omit the details. □

Lemma 4.3 (Off-diagonal coefficients)**.** *Let* $\mathsf{t}_l < \mathsf{t} < \mathsf{t}_r$*, and the point* (t,x) *is inside the scaled hexagon* $\mathcal{H}$ (3.2)*. Under the scaling described before Lemma 4.1, the off-diagonal coefficients of the operator* $\mathfrak{D}^{\mathrm{scaled}}$ (4.1) *have the following limits (cf. Remark 4.2 for a discussion of assumptions in the border cases):*

$$\lim_{L\to+\infty} C_{\mathsf{x}} \cdot \sqrt{\frac{w^{qR}(\tilde{x}-1)}{w^{qR}(\tilde{x})}} B(\tilde{x}-1) = \lim_{L\to+\infty} C_{\mathsf{x}} \cdot \sqrt{\frac{w^{qR}(\tilde{x})}{w^{qR}(\tilde{x}-1)}} D(\tilde{x})$$

$$= \begin{cases} 0, & \mathsf{x} < \frac{1}{2}(\mathsf{S}+\mathsf{t}-\mathsf{N}); \\ -\kappa^{-2} q^{-2\Delta x+1/2}, & \mathsf{x} = \frac{1}{2}(\mathsf{S}+\mathsf{t}-\mathsf{N}),\ \lfloor L\mathsf{x}\rfloor = \frac{1}{2}(S+t-N); \\ -\kappa^{-2} q^{-2\Delta x+1/2}, & \frac{1}{2}(\mathsf{S}+\mathsf{t}-\mathsf{N}) < \mathsf{x} < \frac{1}{2}(\mathsf{S}+\mathsf{t}); \\ \dfrac{-\kappa^2 q^{2\Delta x+1/2}}{(1-\kappa^2 q^{2\Delta x})\sqrt{(1-\kappa^2 q^{2\Delta x-1})(1-\kappa^2 q^{2\Delta x+1})}}, & \mathsf{x} = \frac{1}{2}(\mathsf{S}+\mathsf{t}),\ \lfloor L\mathsf{x}\rfloor = \frac{1}{2}(S+t); \\ -\kappa^2 q^{2\Delta x+1/2}, & \frac{1}{2}(\mathsf{S}+\mathsf{t}) < \mathsf{x} < \frac{1}{2}(\mathsf{S}+\mathsf{t}+\mathsf{N}); \\ -\kappa^2 q^{2\Delta x+1/2}, & \mathsf{x} = \frac{1}{2}(\mathsf{S}+\mathsf{t}+\mathsf{N}),\ \lfloor L\mathsf{x}\rfloor = \frac{1}{2}(S+t+N); \\ 0, & \mathsf{x} > \frac{1}{2}(\mathsf{S}+\mathsf{t}+\mathsf{N}). \end{cases} \tag{4.6}$$

Proof. The equality between the two quantities in the first line in (4.6) holds before the limit,

see Remark 2.9. Thus, we can consider only the first one. We have using (2.28)–(2.29):

$$q^{N+T}\sqrt{\frac{w^{qR}(\tilde{x}-1)}{w^{qR}(\tilde{x})}}B(\tilde{x}-1)=\frac{q^{-N+1/2}}{(q^{S+t}-\kappa^2q^{2x})\sqrt{(q^{S+t}-\kappa^2q^{2x-1})(q^{S+t}-\kappa^2q^{2x+1})}}$$
$$\times\Big((1-q^x)(q^{S+t}-q^{T+x})(q^{N+S}-q^x)(q^{N+t}-q^x)$$
$$\times(q^S-\kappa^2q^{N+x})(q^t-\kappa^2q^{N+x})(q^T-\kappa^2q^x)(q^{S+t}-\kappa^2q^x)\Big)^{\frac{1}{2}}. \tag{4.7}$$

We have for all seven cases in (4.6):

$$1-q^x\sim 1,\qquad q^{S+t}-q^{T+x}\sim q^{S+t},\qquad q^{N+S}-q^x\sim -q^x,\qquad q^{N+t}-q^x\sim -q^x.$$

Thus, it remains to address the product of the four other factors that contain κ. When $\mathsf{x}<\frac{1}{2}(\mathsf{S}+\mathsf{t})$, the dominant contribution coming from the denominator in (4.7) is $\kappa^{-4}q^{-4x}$. Let us expand:

$$\Big[\kappa^{-4}q^{-4x-N+1/2}\sqrt{q^{S+t+2x}(q^S-\kappa^2q^{N+x})(q^t-\kappa^2q^{N+x})(q^T-\kappa^2q^x)(q^{S+t}-\kappa^2q^x)}\Big]^2$$
$$=\kappa^{-8}q^{-6x-2N+S+t+1}\Big[q^{2S+2t+T}-\kappa^2q^{S+t+x}\left(q^{N+S+T}+q^{N+t+T}+q^{S+t}+q^T\right)$$
$$+\kappa^4q^{2x}\left(q^{2N+S+t+T}+q^{N+2S+t}+q^{N+S+2t}+q^{N+S+T}+q^{N+t+T}+q^{S+t}\right)$$
$$-\kappa^6q^{N+3x}\left(q^{N+S+t}+q^{N+T}+q^t+q^S\right)+\kappa^8q^{2N+4x}\Big]. \tag{4.8}$$

We consider the limits of (4.8) in the first three cases in (4.6), namely, when $\mathsf{x}<\frac{1}{2}(\mathsf{S}+\mathsf{t})$.

Case $\mathsf{x}<(\mathsf{S}+\mathsf{t}-\mathsf{N})/2$. One can readily check that the limit of each individual power of q in (4.8) is 0. This establishes the first case in (4.6).

Case $\mathsf{x}=(\mathsf{S}+\mathsf{t}-\mathsf{N})/2$. Setting $\lfloor L\mathsf{x}\rfloor=\frac{1}{2}(S+t-N)$ and $x=\Delta x+\frac{1}{2}(S+t-N)$, we see that the only surviving term in the limit in (4.8) is $\kappa^{-4}q^{-2N+2S+2t-4x+1}=\kappa^{-4}q^{-4\Delta x+1}$. Taking the square root, we get the second case in (4.6).

Case $(\mathsf{S}+\mathsf{t}-\mathsf{N})/2<\mathsf{x}<(\mathsf{S}+\mathsf{t})/2$. In this case, the expansion (4.8) gets an additional factor $q^{N-S-t+2\lfloor L\mathsf{x}\rfloor}$ coming from C_{x}. This factor keeps the only surviving term in the expansion (4.8) to be the same as in the previous case:

$$\kappa^{-4}q^{-2N+2S+2t-4x+1}q^{2(N-S-t+2\lfloor L\mathsf{x}\rfloor)}=\kappa^{-4}q^{4\lfloor L\mathsf{x}\rfloor-4x+1}=\kappa^{-4}q^{-4\Delta x+1}.$$

This establishes the third case in (4.6).

Case $\mathsf{x}=(\mathsf{S}+\mathsf{t})/2$. In this case, all terms in the denominator in (4.7) are of the same order:

$$(q^{S+t}-\kappa^2q^{2x})\sqrt{(q^{S+t}-\kappa^2q^{2x-1})(q^{S+t}-\kappa^2q^{2x+1})}$$
$$=q^{2(S+t)}(1-\kappa^2q^{2\Delta x})\sqrt{(1-\kappa^2q^{2\Delta x-1})(1-\kappa^2q^{2\Delta x+1})}.$$

Combining the dominant power $q^{-2(S+t)}$ with the prefactor q^N coming from C_{x}, we see that the numerator in (4.7) behaves as

$$q^{\Delta x+1/2}\sqrt{(q^{\frac{1}{2}(S-t)}-\kappa^2 q^{N+\Delta x})(q^{\frac{1}{2}(t-S)}-\kappa^2 q^{N+\Delta x})(q^{T-\frac{1}{2}(S+t)}-\kappa^2 q^{\Delta x})(q^{\frac{1}{2}(S+t)}-\kappa^2 q^{\Delta x})}$$
$$\sim q^{\Delta x+1/2}\sqrt{\kappa^4 q^{2\Delta x}} = -\kappa^2 q^{2\Delta x+1/2}.$$

This yields the fourth case in (4.6).

Remaining cases $\mathsf{x} > (\mathsf{S}+\mathsf{t})/2$. When $\mathsf{x} > \frac{1}{2}(\mathsf{S}+\mathsf{t})$, the dominant contribution from the denominator is $q^{-2(S+t)}$, and the remaining limits in (4.7) are obtained in a symmetric manner. We omit the details. □

Lemmas 4.1 and 4.3 complete the proof of Proposition 1.3 from the Introduction. There, we assumed that $\mathsf{N} < \mathsf{T}$ and $\mathsf{t}_l < \mathsf{t} < \mathsf{t}_r$. Let us record the limits in all the other cases when (t,x) belongs to a region with asymptotically no nonintersecting paths. These are the lighter-colored regions inside the hexagons in the exact samples in Figures 4 and 5. Recall the notation $\mathcal{W}^{\pm}$ (Definition 3.3).

Lemma 4.4. *Assume that $\mathsf{t} \notin (\mathsf{t}_l, \mathsf{t}_r)$ and $(\mathsf{t},\mathsf{x}) \in \mathcal{W}^+ \cup \mathcal{W}^-$. Then $C_{\mathsf{x}} = q^{N+T}$, and the limits as in the two previous lemmas take the form*

$$\begin{aligned}&\lim_{L\to+\infty} q^{N+T}\bigl(q^{-N+1}(1-q^{N-1})(q^{-T-N}-1) - B(\tilde{x}) - D(\tilde{x})\bigr) = -1,\\ &\lim_{L\to+\infty} q^{N+T}\sqrt{\frac{w^{qR}(\tilde{x}-1)}{w^{qR}(\tilde{x})}}B(\tilde{x}-1) = \lim_{L\to+\infty} q^{N+T}\sqrt{\frac{w^{qR}(\tilde{x})}{w^{qR}(\tilde{x}-1)}}D(\tilde{x}) = 0.\end{aligned} \tag{4.9}$$

Proof. The proof is very similar to the cases in the proofs of Lemmas 4.1 and 4.3 when (t,x) is outside the waterfall region, so we omit it. □

4.2 Diagonalization on the center line

We can explicitly diagonalize the operator that emerges in the limit along the center line. Define

$$\bigl(\mathfrak{T}^{\mathrm{ctr}} g\bigr)(x) := d^{\mathrm{ctr}}(x+1)\,g(x+1) + a^{\mathrm{ctr}}(x)\,g(x) + d^{\mathrm{ctr}}(x)\,g(x-1), \tag{4.10}$$

where

$$d^{\mathrm{ctr}}(x) := \frac{-\kappa^2 q^{2x+1/2}}{(1-\kappa^2 q^{2x})\sqrt{(1-\kappa^2 q^{2x-1})(1-\kappa^2 q^{2x+1})}}, \quad a^{\mathrm{ctr}}(x) := \frac{-\kappa^2(1+q)\,q^{2x+1}}{(1-\kappa^2 q^{2x})(1-\kappa^2 q^{2x+2})},$$

and we used the variable $x \in \mathbb{Z}$ instead of Δx to simplify the notation. Thanks to the exponential decay of the coefficients as $x \to \pm\infty$, the symmetric operator (4.10) is bounded in $\ell^2(\mathbb{Z})$, hence self-adjoint.

Consider the functions

$$g_n(x) := q^{x(x+1)}(-\kappa^2)^x\sqrt{q^{-x}-\kappa^2 q^{x+1}}\sum_{i=0}^{n}\kappa^{2i}q^{(2i-n)x-i(n-i-1)}\,\frac{(q;q)_n}{(q;q)_i(q;q)_{n-i}}, \tag{4.11}$$

where $n = 0, 1, 2, \ldots$ and $x \in \mathbb{Z}$.

Proposition 4.5. *The functions $g_n(x)$, $x \in \mathbb{Z}$, $n = 0, 1, 2, \ldots$, given by (4.11) form an orthogonal basis in $\ell^2(\mathbb{Z})$ and are eigenfunctions of the operator $\mathfrak{T}^{\mathrm{ctr}}$. The eigenvalue of $g_n(x)$ is q^{n+1}, $n = 0, 1, 2, \ldots$.*

Proof. Define

$$w^{\mathrm{ctr}}(x) := q^{2x(x+1)}(-\kappa^2)^{2x}(q^{-x} - \kappa^2 q^{x+1}), \qquad \tilde{g}_n(x) := \frac{g_n(x)}{\sqrt{w^{\mathrm{ctr}}(x)}}. \tag{4.12}$$

For each $n \in \mathbb{Z}_{\geq 0}$, $\tilde{g}_n(x)$ is a Laurent polynomial in q^x which contains powers $q^{(2n-i)x}$, $i = 0, \ldots, n$. These Laurent polynomials must be eigenfunctions of the modified operator

$$\big(\widetilde{\mathfrak{T}}^{\mathrm{ctr}}\tilde{g}\big)(x) := B^{\mathrm{ctr}}(x)\,\tilde{g}(x+1) + a^{\mathrm{ctr}}(x)\,\tilde{g}(x) + d^{\mathrm{ctr}}(x)\,\tilde{g}(x-1),$$

where

$$B^{\mathrm{ctr}}(x) := d^{\mathrm{ctr}}(x+1)\sqrt{\frac{w^{\mathrm{ctr}}(x+1)}{w^{\mathrm{ctr}}(x)}} = \frac{q^{4(x+1)}\kappa^4}{(1-\kappa^2 q^{2x+1})(1-\kappa^2 q^{2x+2})},$$
$$d^{\mathrm{ctr}}(x) := d^{\mathrm{ctr}}(x)\sqrt{\frac{w^{\mathrm{ctr}}(x-1)}{w^{\mathrm{ctr}}(x)}} = \frac{q}{(1-\kappa^2 q^{2x+1})(1-\kappa^2 q^{2x})}.$$

The eigenrelation $\big(\widetilde{\mathfrak{T}}^{\mathrm{ctr}}\tilde{g}_n\big)(x) = q^{n+1}\tilde{g}_n(x)$, $n = 0, 1, \ldots$, is equivalent to an identity of Laurent polynomials in q^x. The latter identity is verified in a straightforward manner using their explicit coefficients.

The functions $g_n(x)$ belong to $\ell^2(\mathbb{Z})$ thanks to the rapid decay of the power $q^{x(x+1)}$ at $x \to \pm\infty$. Since they are eigenfunctions of $\mathfrak{T}^{\mathrm{ctr}}$, they are orthogonal in $\ell^2(\mathbb{Z})$.

Each normalized function $\tilde{g}_n(x) \in \ell^2(\mathbb{Z}, w^{\mathrm{ctr}})$ is a polynomial in $(q^{-x} + \kappa^2 q^{x+1})$ of degree n. This follows by combining the opposite powers $q^{(2i-n)x}$ and $q^{(n-2i)x}$ with the same q-binomial coefficients in front. The powers $(q^{-x} + \kappa^2 q^{x+1})^m$, $m \in \mathbb{Z}_{\geq 0}$, span the weighted space $\ell^2(\mathbb{Z}, w^{\mathrm{ctr}})$. This implies that the $g_n(x)$'s span $\ell^2(\mathbb{Z})$, and completes the proof. □

Proposition 4.5 implies that the operator $\mathfrak{T}^{\mathrm{ctr}}$ has positive spectrum. Note that the orthogonal spectral projection onto the nonnegative part of the spectrum of $\mathfrak{T}^{\mathrm{ctr}}$ is the identity operator Id in $\ell^2(\mathbb{Z})$, which has the kernel $\mathbf{1}_{x=y}$, $x, y \in \mathbb{Z}$.

Remark 4.6. The Laurent polynomials $\tilde{g}_n$ (4.12) are the *Stieltjes-Wigert orthogonal polynomials* $S_n(y; q)$ (e.g., see [KS96, Chapter 3.27]), up to normalization and change of variable:

$$\tilde{g}_n(x) = q^{-nx}(q;q)_n\, S_n\left(-\kappa^2 q^{2x-(n-1)^+}; q\right), \qquad S_n(y;q) := \frac{1}{(q;q)_n}\,{}_1\phi_1\left(\begin{matrix} q^{-n} \\ 0 \end{matrix}\,\middle|\, q; -q^{n+1}y\right).$$

The Stieltjes-Wigert polynomials are at the same level of the q-Askey scheme as the q-Hermite ones, and their orthogonality weight $w^{\mathrm{ctr}}(x)$ on $\mathbb{Z}$ (given by (4.12)) may be thought of as a q-analogue of the usual Gaussian distribution. However, due to this change of variable, the form of the difference equation for the $\tilde{g}_n$'s in the proof of Proposition 4.5 is very different from the one for the Stieltjes-Wigert polynomials [KS96, (3.27.5)]. We do not use the connection to the Stieltjes-Wigert polynomials in Proposition 4.5 or elsewhere in the paper.

4.3 Convergence of spectral projections

The limits of the difference operator $\mathfrak{D}^{\mathrm{scaled}}$ (4.1) on the center line and outside the waterfall region are bounded operators in $\ell^2(\mathbb{Z})$ (namely, $\mathfrak{T}^{\mathrm{ctr}}$ (4.10) and the negative identity $(-Id)$, respectively). This allows us to obtain the convergence of the correlation kernel K_t (2.21) on a slice in these parts of the hexagon. We employ the following general result:

Theorem 4.7 ([RS72, combination of Theorems VIII.24(b) and VIII.25(a)]). *Assume that A_N and A are self-adjoint operators on the same Hilbert space H, and they have a common essential domain $H_0 \subset H$. Assume that $A_N\varphi \to A\varphi$ as $N \to +\infty$ for all $\varphi \in H_0$.*[7] *Let $a, b \in \mathbb{R} \cup \{\pm\infty\}$, $a < b$, be such that a, b are not eigenvalues of A. Then*

$$P_{(a,b)}(A_N)\varphi \to P_{(a,b)}(A)\varphi \quad \text{as } N \to +\infty \quad \text{for all } \varphi \in H,$$

where $P_{(a,b)}(A_N)$ denotes the orthogonal spectral projection onto the interval (a, b) corresponding to the operator A_N, and similarly for $P_{(a,b)}(A)$.

Let us now recall the limit regime for the kernel. We assume that the sides of the hexagon T, S, N grow proportionally to $L \to +\infty$ as in (3.1), and the point (t, x) belongs to the scaled hexagon $\mathcal{H}$ (3.2). Recall the notation $\mathsf{t}_l, \mathsf{t}_r$ (3.3). We have the following convergence of the correlation kernel K_t on the center line and outside the waterfall region:

Proposition 4.8 (Convergence of the correlation kernel). *We have the following limits of the correlation kernel K_t on a slice. On the center line, that is $\mathsf{N} < \mathsf{T}$, $\mathsf{t}_l < \mathsf{t} < \mathsf{t}_r$, $\mathsf{x} = \frac{1}{2}(\mathsf{S} + \mathsf{t})$, and $\lfloor L\mathsf{x} \rfloor = \frac{1}{2}(S + t)$, we have*

$$\lim_{L\to+\infty} K_{\lfloor L\mathsf{t} \rfloor}(\lfloor L\mathsf{x} \rfloor + \Delta x, \lfloor L\mathsf{x} \rfloor + \Delta y) = \mathbf{1}_{\Delta x = \Delta y} \quad \text{for all } \Delta x, \Delta y \in \mathbb{Z}. \tag{4.13}$$

Outside the waterfall region, that is, for $(\mathsf{t}, \mathsf{x}) \in \mathcal{W}^+ \cup \mathcal{W}^-$, we have

$$\lim_{L\to+\infty} K_{\lfloor L\mathsf{t} \rfloor}(\lfloor L\mathsf{x} \rfloor + \Delta x, \lfloor L\mathsf{x} \rfloor + \Delta y) = 0 \quad \text{for all } \Delta x, \Delta y \in \mathbb{Z}. \tag{4.14}$$

Proof. The correlation kernel K_t is the kernel of the orthogonal projection operator in $\ell^2(\mathbb{Z})$ onto the spectral interval $[0, +\infty)$ of the operator $\mathfrak{D}^{\mathrm{scaled}}$ (4.1). By (2.24), the eigenvalues of $\mathfrak{D}^{\mathrm{scaled}}$ around 0 are equal to

$$\{\dots, -(1-q)(1-q^T), 0, q^{-1}(1-q)(1-q^{T+2}), \dots\} \sim \{\dots, -(1-q), 0, q^{-1}(1-q), \dots\},$$

so, for large L, the spectral projection onto the open interval $(-(1-q)/2, +\infty)$ yields the same operator K_t.

We now apply the general Theorem 4.7. The operator $\mathfrak{D}^{\mathrm{scaled}}$ and the limiting operators $(-Id)$ and $\mathfrak{T}^{\mathrm{ctr}}$ are bounded in $H = \ell^2(\mathbb{Z})$. Taking $H_0 = \ell^2_0(\mathbb{Z})$ (the space of finitely supported functions), we see that the convergence of the coefficients of $\mathfrak{D}^{\mathrm{scaled}}$ (Lemmas 4.1, 4.3 and 4.4) implies the required convergence on the common essential domain H_0. This completes the proof. □

[7] The convergence on the common essential domain implies that $A_N \to A$ in the strong resolvent sense.

Remark 4.9. Inside the waterfall region but not on the center line, the limiting operators arising from the coefficients of $\mathfrak{D}^{\text{scaled}}$ (Lemmas 4.1, 4.3 and 4.4) are not bounded. Moreover, they are symmetric, but *not self-adjoint*. One can check that each of these operators has von Neumann deficiency indices $(1, 1)$. Thus, these limiting operators each possess a one-parameter family of self-adjoint extensions. Therefore, the general Theorem 4.7 does not immediately apply in these regions. We do not address the spectral analysis of the limiting non-self-adjoint operators outside the center line further in this paper.

Proposition 4.8 implies that the probability to find a path at any given location outside the saturation band $\mathcal{P}$ goes to zero. In principle, it does not rule out the presence of individual random paths that roam in $\mathcal{H} \setminus \mathcal{P}$, nor the presence of holes between the paths in the saturation band. In Section 5 below, we address these questions using a different approach based on the heuristics discussed in Section 3.3.

5 Concentration in the q-Racah ensemble. Proof of Theorem 1.4

In this section we employ a method different from the one used in Section 4. Specifically, we work with the explicit probability weights of the q-Racah orthogonal polynomial ensemble (OPE) (2.14) to derive a concentration-type estimate for the probability that a hole $\parallelogram$ appears in the nonintersecting path ensemble inside the saturation band $\mathcal{P} \subset \mathcal{H}$ (see Definitions 3.1 and 3.3). This probability is expected to be small because, by Proposition 4.8, the nonintersecting paths do not typically wander outside the saturation band $\mathcal{P}$ as $L \to +\infty$. Our objective, however, is to obtain a uniform bound that applies to every location where paths might stray into $\mathcal{H} \setminus \mathcal{P}$, or holes might appear within $\mathcal{P}$. We establish an exponential upper bound for this probability by considering the ratio of q-Racah OPE probabilities of two N-particle configurations on the same slice that differ only by moving one particle from (t, x) to (t, y).

Our plan is as follows. In Section 5.1 we identify the exact leading power of q in this ratio of the q-Racah OPE probabilities. Then, in Sections 5.2 and 5.3, we bound this leading power in the asymptotic regime where the sides of the hexagon grow proportionally. These bounds yield the main result of the section, Theorem 5.11, and complete the proof of Theorem 1.4 from the Introduction.

5.1 Ratio of the q-Racah probabilities

Fix the dimensions of the hexagon (T, S, N) as in Section 2.1, and consider two points (t, x) and (t, y) on a given vertical slice. Let us move a particle from (t, x) to (t, y), and estimate the ratio of the corresponding q-Racah OPE probabilities (2.14). Let $\vec{z} = (z_1 < \ldots < z_{N-1})$ (with $z_i \neq x, y$ for all i) denote the configuration of the particles which do not move. Recall the q-Racah orthogonality measure w^{qR} (2.6) on the segment $\{0, 1, \ldots, M\}$, the four zones (2.15)–(2.18) inside the hexagon for the q-Racah parameters $(M, \alpha, \beta, \gamma, \delta)$, and the notation $\mu(x)$ (2.8) and $\tilde{x}$ (2.27). We have

$$\frac{\mathbb{P}\left(X(t) = \vec{z} \cup \{x\}\right)}{\mathbb{P}\left(X(t) = \vec{z} \cup \{y\}\right)} = \frac{w^{qR}(\tilde{x})}{w^{qR}(\tilde{y})} \prod_{i=1}^{N-1} \left(\frac{\mu(\tilde{x}) - \mu(\tilde{z}_i)}{\mu(\tilde{y}) - \mu(\tilde{z}_i)} \right)^2. \tag{5.1}$$

Our first objective is to extract the leading powers of q in this product. Denote

$$\mathbf{k} := \frac{\log(-\kappa^2)}{\log q} \in \mathbb{R}, \quad \text{so that } -\kappa^2 = q^{\mathbf{k}}. \tag{5.2}$$

Define the functions

$$\begin{aligned}\mathcal{W}_{\mathbf{k}}(x \mid T,S,N,t) &:= S+t-2x-1+\min(S,N+x+\mathbf{k}+1)\\ &+\min(t,N+x+\mathbf{k}+1)+\min(S+t,\mathbf{k}+2x+1)\\ &-\min(T,x+\mathbf{k}+1)-\min(S+t,x+\mathbf{k}+1)-\min(S+t,\mathbf{k}+2x+3),\end{aligned} \tag{5.3}$$

and

$$\mathcal{G}_{\mathbf{k}}(x,y,z \mid A) := (z-x)^- + (z-A+x+\mathbf{k}+1)^- - (z-y)^- - (z-A+y+\mathbf{k}+1)^-. \tag{5.4}$$

In (5.4), we used the notation (4.2). In the next two Lemmas 5.1 and 5.2 we obtain estimates (up to multiplicative constants) for the factors in the product in (5.1). These estimates are given in terms of the functions $\mathcal{W}_{\mathbf{k}}$ and $\mathcal{G}_{\mathbf{k}}$.

Lemma 5.1. *There exists an absolute constant $c_1 = c_1(q,\kappa) > 0$ not depending on the size of the hexagon, such that for all T,S,N,t and points x,y on the t-th vertical slice of the hexagon, we have*

$$c_1 < q^{\operatorname{sgn}(x-y)\sum_{u=\min(x,y)}^{\max(x,y)-1}\mathcal{W}_{\mathbf{k}}(u|T,S,N,t)} \cdot \frac{w^{qR}(\tilde{x})}{w^{qR}(\tilde{y})} < c_1^{-1}. \tag{5.5}$$

Proof. We use the first formula in (2.29) which provides a unified expression for the ratio $\frac{w^{qR}(\tilde{u})}{w^{qR}(\tilde{u}+1)}$ in all four zones in the hexagon. From each linear factor in this product, we extract q raised to the minimal power. In the factors not containing κ, the dominating term which we extract is always the same. For example, in $(q^{N+t}-q^{x+1})$, we always have $N+t \geq x+1$, so the dominating term is q^{x+1}. In factors containing κ, we write $-\kappa^2 = q^{\mathbf{k}}$, and include expressions involving $\mathbf{k}$ in the comparison. The combined power of q thus arising from $\frac{w^{qR}(\tilde{u})}{w^{qR}(\tilde{u}+1)}$ becomes equal to $\mathcal{W}_{\mathbf{k}}(u \mid T,S,N,t)$ (5.3). Representing $\frac{w^{qR}(\tilde{x})}{w^{qR}(\tilde{y})}$ as a telescoping product of consecutive ratios, we get the desired power of q in (5.5). Indeed, if $x<y$, then the compensating sum is from x to $y-1$ with the minus sign, and if $x>y$, then we write $\frac{w^{qR}(\tilde{x})}{w^{qR}(\tilde{y})} = \big(\frac{w^{qR}(\tilde{y})}{w^{qR}(\tilde{x})}\big)^{-1}$, and the compensating sum is from y to $x-1$, but with the plus sign.

There could be a multiplicative correction in extracting the power $q^{\mathcal{W}_{\mathbf{k}}(u|T,S,N,t)}$ from $\frac{w^{qR}(\tilde{u})}{w^{qR}(\tilde{u}+1)}$ if $u \in \mathbb{Z}$ is such that both terms in a given linear factor in (2.29) are comparable (for example, if $q^{S+t} \sim -\kappa^2 q^{2u+1}$). However, the product over all such values u is bounded, as one can see from the following computation:

$$\prod\nolimits_{u\in\mathbb{Z}} (q^A - \kappa^2 q^u) q^{-\min(A,u+\mathbf{k})} = (-q^{\{\mathbf{k}\}};q)_\infty (-q^{1-\{\mathbf{k}\}};q)_\infty, \tag{5.6}$$

where $\{\mathbf{k}\} = \mathbf{k} - \lfloor \mathbf{k} \rfloor$ is the fractional part of $\mathbf{k}$. The right-hand side of (5.6) is bounded away from 0 and $+\infty$ by an absolute constant depending only on q and κ. Combining these bounds for the six linear factors in (2.29) containing κ, we obtain the multiplicative bounds by c_1, c_1^{-1} in (5.5). This completes the proof. □

Lemma 5.2. *There exists an absolute constant $c_2 = c_2(q,\kappa) > 0$ not depending on the size of the hexagon, such that for any t, any configuration $\vec{z} = (z_1 < \ldots < z_{N-1})$, and any x, y on the t-th vertical slice of the hexagon (with $z_i \neq x, y$ for all i), we have*

$$c_2 < q^{-2\sum_{i=1}^{N-1} \mathcal{G}_{\mathbf{k}}(x,y,z_i|S+t)} \cdot \prod_{i=1}^{N-1} \left(\frac{\mu(\tilde{x}) - \mu(\tilde{z}_i)}{\mu(\tilde{y}) - \mu(\tilde{z}_i)} \right)^2 < c_2^{-1}. \tag{5.7}$$

Proof. For pairwise distinct x, y, z_i on the t-th vertical slice inside the hexagon, in all four zones (2.15)–(2.18), we have

$$\left(\frac{\mu(\tilde{x}) - \mu(\tilde{z}_i)}{\mu(\tilde{y}) - \mu(\tilde{z}_i)} \right)^2 = \left(\frac{1 - q^{z_i - x}}{1 - q^{z_i - y}} \frac{1 - \kappa^2 q^{z_i - S - t + x + 1}}{1 - \kappa^2 q^{z_i - S - t + y + 1}} \right)^2. \tag{5.8}$$

Extracting the smallest power of q from each linear factor in (5.8), exactly as in the proof of Lemma 5.1, we obtain the factor $q^{2\mathcal{G}_{\mathbf{k}}(x,y,z_i|S+t)}$ (see (5.4)). This provides the required power of q in (5.7). The multiplicative bounds by c_2 and c_2^{-1} follow in the same way as in Lemma 5.1. □

5.2 Minimizing over the $(N-1)$-point configurations

By Lemmas 5.1 and 5.2, to estimate the ratio (5.1) of the q-Racah OPE probabilities, it suffices to consider the exponent

$$\begin{aligned} \mathcal{E}_{\mathbf{k}}(x,y) &= \mathcal{E}_{\mathbf{k}}(x,y \mid T,S,N,t \mid \vec{z}) \\ &\coloneqq -\operatorname{sgn}(x-y) \sum_{u=\min(x,y)}^{\max(x,y)-1} \mathcal{W}_{\mathbf{k}}(u \mid T,S,N,t) + 2\sum_{i=1}^{N-1} \mathcal{G}_{\mathbf{k}}(x,y,z_i \mid S+t). \end{aligned} \tag{5.9}$$

We aim to find pairs (x,y) for which $\mathcal{E}_{\mathbf{k}}(x,y)$ is positive and grows with L. If this is the case, then it is advantageous (under the q-Racah OPE measure) to replace the configuration $\vec{z} \cup \{x\}$ by $\vec{z} \cup \{y\}$. For an integer A, denote

$$d_{\mathbf{k}}^A(x;y) \coloneqq \left| x - \tfrac{1}{2}(A - \mathbf{k} - 1) \right| - \left| y - \tfrac{1}{2}(A - \mathbf{k} - 1) \right|, \tag{5.10}$$

where $\mathbf{k}$ is given by (5.2). Let us begin to lower bound (5.9) by first picking a configuration $\vec{z}$ which minimizes the second sum:

Lemma 5.3. *Fix $A \in \mathbb{Z}$, and let $d_{\mathbf{k}}^A(x;y) > 0$. Then for any $(N-1)$-point configuration $\vec{z}$ in $\mathbb{Z}$, we have*

$$\sum_{i=1}^{N-1} \mathcal{G}_{\mathbf{k}}(x,y,z_i \mid A) \geq \min\Big\{ \sum_{i \in I} \mathcal{G}_{\mathbf{k}}(x,y,i \mid A), \sum_{i \in I'} \mathcal{G}_{\mathbf{k}}(x,y,i \mid A) \Big\}, \tag{5.11}$$

where I and I' are $(N-1)$-point intervals in $\mathbb{Z}$ defined as

$$\begin{aligned} I &\coloneqq \left[\lfloor \tfrac{1}{2}(A - \mathbf{k} - 1) \rfloor - \lfloor \tfrac{N-1}{2} \rfloor + 1, \lfloor \tfrac{1}{2}(A - \mathbf{k} - 1) \rfloor + \lfloor \tfrac{N}{2} \rfloor \right] \cap \mathbb{Z}, \\ I' &\coloneqq \left[\lfloor \tfrac{1}{2}(A - \mathbf{k} - 1) \rfloor - \lfloor \tfrac{N}{2} \rfloor + 1, \lfloor \tfrac{1}{2}(A - \mathbf{k} - 1) \rfloor + \lfloor \tfrac{N-1}{2} \rfloor \right] \cap \mathbb{Z}. \end{aligned} \tag{5.12}$$

See Remark 5.4 below for a discussion of the intervals I and I' (5.12).

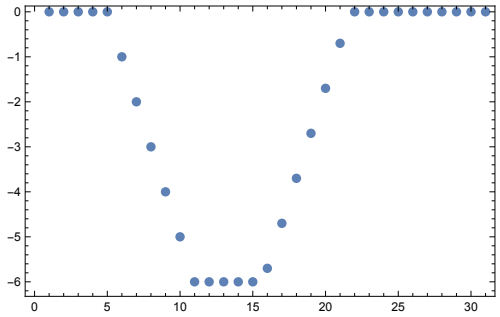

Figure 6: The plot of $\mathcal{G}_{\mathbf{k}}(x, y, z \mid A)$ as a function of z, where $x = 4$, $y = 10$, $A = 15$, and $\mathbf{k} = 4.3$.

Proof of Lemma 5.3. Under the assumptions on x, y, $\mathcal{G}_{\mathbf{k}}$ is nonpositive as a function of z. Moreover, it weakly decreases for $z \le \frac{1}{2}(A - \mathbf{k} - 1)$, weakly increases afterwards, and stays constant in an interval around $\frac{1}{2}(A - \mathbf{k} - 1)$. See Figure 6 for an illustration.

This behavior of $\mathcal{G}_{\mathbf{k}}$ implies that to minimize the sum (5.11), we should pick the $N-1$ points z_i to be as close as possible to the midpoint $\frac{1}{2}(A-\mathbf{k}-1)$. This is achieved by densely packing the z_i's together, symmetrically around the middle point $\frac{1}{2}(A - \mathbf{k} - 1)$. Therefore, the configuration $\vec{z}$ must fill the interval I or I' (5.12).

The intervals I and I' are the same for odd N. For even N, we need to account for the (possibly non-integer) shift in one of the strictly monotone parts of the plot in Figure 6 which arises because of the presence of $\mathbf{k}$. This completes the proof. □

Remark 5.4. The shift-by-one difference between the intervals I and I' in Lemma 5.3 matters only for even N. Then the two sums in the right-hand side of (5.11) differ by

$$\Big|\mathcal{G}_{\mathbf{k}}(x, y, \lfloor \tfrac{1}{2}(A - \mathbf{k} - 1)\rfloor + N/2 \mid A) - \mathcal{G}_{\mathbf{k}}(x, y, \lfloor \tfrac{1}{2}(A - \mathbf{k} - 1)\rfloor - N/2 + 1 \mid A)\Big|.$$

One can check that this expression is always ≤ 1, and thus the difference between I and I' will be inessential for our asymptotic estimates in Section 5.3 below.

Notice that in Lemma 5.3, we tacitly assumed that the minimizing configuration of the $N-1$ particles $\vec{z}$ fits in an interval around the middle point $\frac{1}{2}(A-\mathbf{k}-1) = \frac{1}{2}(S+t-\mathbf{k}-1)$. However, in $\mathcal{E}_{\mathbf{k}}(x, y)$ (5.9), depending on T, S, N, t, the middle point may be at a distance less than $\sim N/2$ from the boundary of the hexagon. In these cases, the minimizing configuration $\vec{z}$ must still be densely packed, but contained in an interval bordering the boundary of the hexagon. This corresponds to t being outside the waterfall bounds $\lfloor L\mathtt{t}_l\rfloor \le t \le \lfloor L\mathtt{t}_r\rfloor$. In more detail, we have:

Lemma 5.5. *Fix $A \in \mathbb{Z}$, and let $d^A_{\mathbf{k}}(x; y) > 0$. Assume that the configuration $\vec{z}$ is restricted to an interval $a \le z_1 < \ldots < z_N \le b$, and*

$$a \ge \lfloor \tfrac{1}{2}(A - \mathbf{k} - 1)\rfloor - \lfloor \tfrac{N-1}{2}\rfloor + 1 \qquad \text{or} \qquad b \le \lfloor \tfrac{1}{2}(A - \mathbf{k} - 1)\rfloor + \lfloor \tfrac{N-1}{2}\rfloor. \tag{5.13}$$

Then for any such restricted $(N-1)$-point configuration $\vec{z}$, we have in the two cases in (5.13), respectively:

$$\sum\nolimits_{i=1}^{N-1} \mathcal{G}_{\mathbf{k}}(x, y, z_i \mid A) \ge \sum\nolimits_{i=a}^{a+N-2} \mathcal{G}_{\mathbf{k}}(x, y, i \mid A) \qquad \text{or} \qquad \ge \sum\nolimits_{i=b-N+2}^{b} \mathcal{G}_{\mathbf{k}}(x, y, i \mid A).$$

Proof. This is established similarly to the proof of Lemma 5.3. □

Lemmas 5.3 and 5.5 establish a lower bound for the second sum in the leading q-power $\mathcal{E}_{\mathbf{k}}(x,y)$ (5.9) over all configurations $\vec{z}$. The minimizing configuration $\vec{z}$ is always densely packed. For uniformity of notation, we denote it by $\vec{z}_* = \{z_0, z_0+1, \dots, z_0+N-2\}$.

In our estimates, the point y (into which we move the particle from x) is in the saturation band. This allows us to strengthen (increase) the lower bounds of Lemmas 5.3 and 5.5 by recalling that the configuration $\vec{z}$ must satisfy $y \neq z_i$ for all i. Thus, instead of y, the minimizing configuration $\vec{z}$ must include one of the particles at distance 1 from the boundary of $\vec{z}_*$. The next statement, which formalizes this observation, is straightforward.

Lemma 5.6. *In the setting of Lemma 5.3 or 5.5, assume that $y \in \vec{z}_*$, where $\vec{z}_*$ is the densely packed configuration defined above. Then for any $(N-1)$-point configuration $\vec{z}$ in $\mathbb{Z}$ satisfying $z_i \neq x, y$ for all i (and additional restrictions of Lemma 5.5, if applicable), we have*

$$\begin{aligned}\sum_{i=1}^{N-1} \mathcal{G}_{\mathbf{k}}(x,y,z_i \mid A) \geq \sum_{i=z_0}^{z_0+N-2} \mathcal{G}_{\mathbf{k}}(x,y,i \mid A) \\ - \mathcal{G}_{\mathbf{k}}(x,y,y \mid A) + \min\bigl\{\mathcal{G}_{\mathbf{k}}(x,y,z_0-1 \mid A), \mathcal{G}_{\mathbf{k}}(x,y,z_0+N-1 \mid A)\bigr\}.\end{aligned} \tag{5.14}$$

The first line of (5.14) coincides with the bound established in Lemmas 5.3 and 5.5. In the proof of Lemma 5.10 below, we will show that the terms appearing in the second line are non-negative; hence, the lower bound in (5.14) is indeed stronger.

5.3 Estimates of the leading power and the probability of a hole

If the configuration $\vec{z} = \vec{z}_* = \{z_0, z_0+1, \dots, z_0+N-2\}$ is densely packed, then we can rewrite the leading q-power $\mathcal{E}_{\mathbf{k}}(x,y \mid T,S,N,t \mid \vec{z}_*)$ (5.9) as a discrete integral between x and y:

Lemma 5.7. *With the above notation, we have*

$$\mathcal{E}_{\mathbf{k}}(x,y \mid T,S,N,t \mid \vec{z}_*) = \operatorname{sgn}(y-x) \sum\nolimits_{u=\min(x,y)}^{\max(x,y)-1} \mathcal{H}_{\mathbf{k}}(u,z_0 \mid T,S,N,t), \tag{5.15}$$

where

$$\begin{aligned}\mathcal{H}_{\mathbf{k}}(u,z_0 \mid T,S,N,t) \coloneqq \mathcal{W}_{\mathbf{k}}(u \mid T,S,N,t) + 2\bigl[(z_0-S-t+u+\mathbf{k}+1)^- - (z_0-u-1)^- \\ - (z_0-S-t+u+N+\mathbf{k})^- + (z_0-u+N-2)^-\bigr].\end{aligned} \tag{5.16}$$

Proof. This follows by two telescopings. First, observe that

$$\mathcal{G}_{\mathbf{k}}(x,y,z \mid A) = \operatorname{sgn}(y-x) \sum\nolimits_{u=\min(x,y)}^{\max(x,y)-1} g_{\mathbf{k}}(u,z \mid A),$$

where

$$g_{\mathbf{k}}(x,z \mid A) = (z-x)^- + (z-A+x+\mathbf{k}+1)^- - \bigl((z-x-1)^- + (z-A+x+1+\mathbf{k}+1)^-\bigr).$$

Then, the sum of $\mathcal{G}_{\mathbf{k}}(x,y,i \mid A)$ over $i \in \vec{z} = \vec{z}_*$ becomes

$$2\operatorname{sgn}(y-x) \sum\nolimits_{u=\min(x,y)}^{\max(x,y)-1} \sum\nolimits_{z=z_0}^{z_0+N-2} g_{\mathbf{k}}(u,z \mid S+t).$$

The inner sum telescopes to the last four terms in (5.16), and we are done. □

Let us interpret $\mathcal{H}_{\mathbf{k}}$ (5.16) viewed as a function of u through cumulative distribution functions (cdfs) of Lebesgue measures on certain segments of $\mathbb{R}$. Denote the cdf of the density 1 Lebesgue measure on $[A,B]$ by $F_{A,B}(u)$. The next statement is checked directly:

Lemma 5.8. *We have*

$$\begin{aligned}\mathcal{H}_{\mathbf{k}}(u,z_0 \mid T,S,N,t) &= S+t-2u-1-F_{S-N-\mathbf{k}-1,T-\mathbf{k}-1}(u)-F_{t-N-\mathbf{k}-1,t+S-\mathbf{k}-1}(u)\\ &+2F_{z_0-1,z_0+N-2}(u)+2F_{S+t-N-\mathbf{k}-z_0,S+t-1-\mathbf{k}-z_0}(u)+2F_{\frac12(S+t-\mathbf{k}-1)-1,\frac12(S+t-\mathbf{k}-1)}(u).\end{aligned} \tag{5.17}$$

Recall that our limit regime (3.1) is $T=\lfloor L\mathsf{T}\rfloor$, $S=\lfloor L\mathsf{S}\rfloor$, $N=\lfloor L\mathsf{N}\rfloor$, $t=\lfloor L\mathsf{t}\rfloor$, and $L\to+\infty$. We are interested in the regime when $\mathsf{T}>\mathsf{N}$ and $\mathsf{t}_l<\mathsf{t}<\mathsf{t}_r$ (see (3.3) for the notation), that is, when there is waterfall behavior at the t-th vertical slice of $\mathcal{H}$. In the other cases when there is no waterfall on the t-th vertical slice (either $\mathsf{N}<\mathsf{T}$ and $\mathsf{t}\notin[\mathsf{t}_l,\mathsf{t}_r]$, or $\mathsf{N}>\mathsf{T}$), one can use Lemmas 5.3 and 5.5 to 5.8 to obtain exponential estimates similarly to Lemmas 5.9 and 5.10 below. They will imply that the nonintersecting paths are clustered when they have slope 0 or 1, which corresponds to the frozen behavior of the paths. We do not explicitly formulate these similar estimates here, as they are not needed for the waterfall region.

We begin with a simpler exponential estimate of order L^2, which illustrates our approach when the point y is inside the saturation band while x is outside.

Lemma 5.9. *Let* $\mathsf{t}_l<\mathsf{t}<\mathsf{t}_r$,

$$\bigl|\mathsf{y}-\tfrac{\mathsf{S}+\mathsf{t}}{2}\bigr|\le\tfrac12\mathsf{N},\qquad \bigl|\mathsf{x}-\tfrac{\mathsf{S}+\mathsf{t}}{2}\bigr|>\tfrac12\mathsf{N},$$

such that the points (t,x) *and* (t,y) *are inside* $\mathcal{H}$. *There exists a constant* $c>0$ *depending on* $\mathsf{T},\mathsf{S},\mathsf{N},\mathsf{t},\mathbf{k},\bigl|\mathsf{x}-\frac{\mathsf{S}+\mathsf{t}}{2}\bigr|-\frac12\mathsf{N}$, *such that for any* $\vec z$ *with* $x,y\neq z_i$ *for all* i, *any fixed* $\Delta x,\Delta y\in\mathbb{Z}$, *and any* L *large enough, we have*

$$\mathcal{E}_{\mathbf{k}}(x,y\mid T,S,N,t\mid\vec z)>cL^2,\qquad x=\lfloor L\mathsf{x}\rfloor+\Delta x,\quad y=\lfloor L\mathsf{y}\rfloor+\Delta y.$$

Proof. We can use the estimate of Lemma 5.3, since the condition $d_{\mathbf{k}}^{S+t}(x;y)>0$ (5.10) holds for large enough L. Let us lower bound the expression $\mathcal{E}_{\mathbf{k}}(x,y\mid T,S,N,t\mid\vec z_*)$ given by (5.15) and (5.17). Since our slice contains the waterfall region, we have $L^{-1}z_0\to\frac12(\mathsf{S}+\mathsf{t}-\mathsf{N})$ as $L\to+\infty$. The function $\mathcal{H}_{\mathbf{k}}$ grows proportionally to L:

$$\begin{aligned}&\mathcal{H}_{\mathbf{k}}\bigl(\lfloor L\mathsf{u}\rfloor,z_0\mid T,S,N,t\bigr)\\ &\quad=\underbrace{L\bigl(\mathsf{S}+\mathsf{t}-2\mathsf{u}-F_{\mathsf{S}-\mathsf{N},\mathsf{T}}(\mathsf{u})-F_{\mathsf{t}-\mathsf{N},\mathsf{t}+\mathsf{S}}(\mathsf{u})+4F_{\frac12(\mathsf{S}+\mathsf{t}-\mathsf{N}),\frac12(\mathsf{S}+\mathsf{t}+\mathsf{N})}(\mathsf{u})\bigr)}_{=:\mathsf{H}(\mathsf{u})}+O(1).\end{aligned} \tag{5.18}$$

To see that the error terms are indeed of order $O(1)$, observe that

$$\begin{aligned}\bigl|F_{\lfloor L\mathsf{a}\rfloor+\Delta a,\lfloor L\mathsf{b}\rfloor+\Delta b}(\lfloor L\mathsf{u}\rfloor)-LF_{\mathsf{a},\mathsf{b}}(\mathsf{u})\bigr|&=L\bigl|F_{L^{-1}\lfloor L\mathsf{a}\rfloor+L^{-1}\Delta a,L^{-1}\lfloor L\mathsf{b}\rfloor+L^{-1}\Delta b}(L^{-1}\lfloor L\mathsf{u}\rfloor)-F_{\mathsf{a},\mathsf{b}}(\mathsf{u})\bigr|\\ &\le|\Delta a|+|\Delta b|+3,\end{aligned}$$

uniformly in u.

The last cdf in (5.17) corresponds to a distribution supported on an interval of length 1, and so it is of order $O(1)$ and can be incorporated into the error term. Let us deal with the other four cdf terms in (5.17).

The discrete integral (5.15) of $\mathcal{H}_{\mathbf{k}}$ is the Riemann sum of a continuous integral from x to y, which provides one more power of L in the asymptotics. Namely, we have

$$\mathcal{E}_{\mathbf{k}}(x, y \mid T, S, N, t \mid \vec{z}) \geq L^2 \int_{\mathsf{x}}^{\mathsf{y}} \mathsf{H}(\mathsf{u})\, d\mathsf{u} + O(L).$$

The integrand $\mathsf{H}(\mathsf{u})$ defined in (5.18) is a piecewise linear function. One readily sees that

$$\begin{cases} \mathsf{H}(\mathsf{u}) = 0, & \mathsf{u} \in \left[\frac{1}{2}(\mathsf{S}+\mathsf{t}-\mathsf{N}), \frac{1}{2}(\mathsf{S}+\mathsf{t}+\mathsf{N})\right], \\ \mathsf{H}(\mathsf{u}) > 0, & \mathsf{u} < \frac{1}{2}(\mathsf{S}+\mathsf{t}-\mathsf{N}), \\ \mathsf{H}(\mathsf{u}) < 0, & \mathsf{u} > \frac{1}{2}(\mathsf{S}+\mathsf{t}+\mathsf{N}), \end{cases}$$

see Figure 7, right, for an illustration. Under our assumptions on x, y, the integral from x to y is always positive, which produces the desired estimate. □

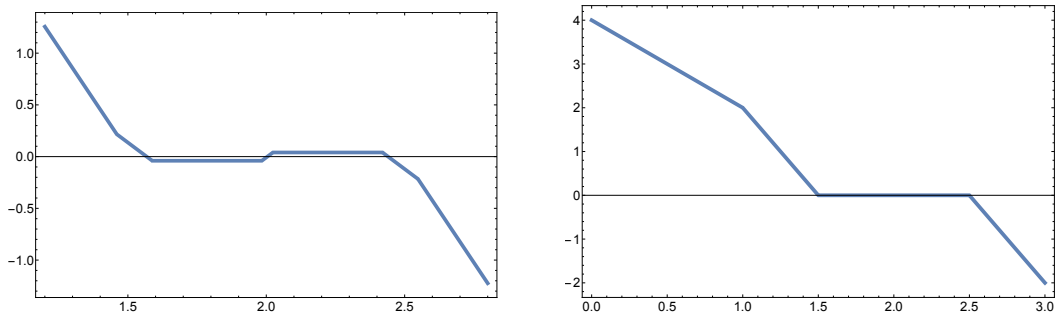

Figure 7: Left: The plot of $L^{-1}\mathcal{H}_{\mathbf{k}}(\lfloor L\mathsf{u}\rfloor, z_0 \mid T, S, N, t)$ as a function of u. Right: The plot of its continuous analogue $\mathsf{H}(\mathsf{u})$ on a larger interval. The parameters are $(\mathsf{T}, \mathsf{S}, \mathsf{N}) = (4, 2, 1)$, $\mathsf{t} = 2$, $\mathbf{k} = -2.2$, and $L = 25$, and the saturation band is $(1.5, 2.5)$. In the left plot, the values close to zero are equal to $\pm L^{-1}$.

When x can be close to the boundary of the saturation band, we need a more delicate estimate.

Lemma 5.10. *Assume that $\mathsf{t}_l < \mathsf{t} < \mathsf{t}_r$ and $y = \lfloor L\mathsf{y}\rfloor + \Delta y$, where y is in the saturation band, that is, $\left|\mathsf{y} - \frac{\mathsf{S}+\mathsf{t}}{2}\right| \leq \frac{1}{2}\mathsf{N}$. Let x be such that $d_{\mathbf{k}}^{S+t}(x; y) > K$. For any $\delta > 0$, sufficiently large fixed $K > 0$, all L large enough, and any configuration $\vec{z}$ with $x, y \neq z_i$ for all i, we have*

$$\mathcal{E}_{\mathbf{k}}(x, y \mid T, S, N, t \mid \vec{z}) > \min\left\{\tfrac{1}{8} d_{\mathbf{k}}^{S+t}(x; y), \delta L\right\}. \tag{5.19}$$

In Lemma 5.10 we assume that the parameters T, S, N, t scale with L in the usual way, and that y, lying inside the saturation band, also scales with L. For x we require that it stay at distance at least K from both y and the point $S + t - \mathbf{k} - 1 - y$ (the mirror image of y with respect to the midpoint of the saturation band), that is, $d_{\mathbf{k}}^{S+t}(x; y) > K$ (recall the notation (5.10)). The constant K may depend on $\mathsf{T}, \mathsf{S}, \mathsf{N}, \mathsf{t}, \mathbf{k}, \delta$ but not on L. This allows x to be close to the boundary of the saturation band, and even go inside the band.

Note that if $x/L \to \mathsf{x}$ and $\mathsf{x} \notin \{\mathsf{y}, \mathsf{S}+\mathsf{t}-\mathsf{y}\}$, then the right-hand side of (5.19) grows as $O(L)$, which produces an upper bound $\exp(-\text{const} \cdot L)$ for the ratio of the q-Racah probabilities (5.1).

Proof of Lemma 5.10. Throughout the proof, we assume that x is to the left of the midpoint of the saturation band $\frac{1}{2}(S+t-\mathbf{k}-1)$. The other case is analogous.

Case 1. When $x < (S+t-N)/2 - \alpha\sqrt{L}$ for some sufficiently large constant $\alpha > 0$ (independent of L), an argument analogous to the proof of Lemma 5.9 immediately yields a lower bound of order δL. Indeed, consider the discrete integral of $\mathcal{H}_{\mathbf{k}}$ in (5.15) taken from $(S+t-N)/2-\alpha_2\sqrt{L}$ to $(S+t-N)/2-\alpha_1\sqrt{L}$ with $\alpha_2 > \alpha_1 > 0$. Because $\mathcal{H}_{\mathbf{k}}$ is linearly decreasing on this interval with slope at most -1, this integral is of magnitude βL. By choosing α_1 large enough (still independent of L) we can make the constant β arbitrarily large. The resulting positive contribution βL offsets the discrete integral of $\mathcal{H}_{\mathbf{k}}(u) = \pm 1$ over u inside the saturation band, which can be negative and is of order $O(L)$. We analyze this negative contribution in the next case.

Case 2. It remains to consider the case when $x > (S+t-N)/2 - \alpha\sqrt{L}$ for some $\alpha > 0$. We use Lemma 5.6, and lower bound the right-hand side of (5.14). As in Lemmas 5.7 and 5.8, we can rewrite the first sum over $i = z_0, z_0+1, \dots, z_0+N-2$ (this is the sum over $\vec{z}_*$) as a discrete integral of $\mathcal{H}_{\mathbf{k}}$ between x and y. Under our hypotheses, this discrete integral may be negative. However, we can lower bound it for large L as

$$\operatorname{sgn}(y-x) \sum_{u=\min(x,y)}^{\max(x,y)-1} \mathcal{H}_{\mathbf{k}}(u, z_0 \mid T, S, N, t) > -d_{\mathbf{k}}^{S+t}(x;y) - C(K,\mathbf{k}), \qquad C(K,\mathbf{k}) > 0. \tag{5.20}$$

Indeed, $-d_{\mathbf{k}}^{S+t}(x;y)$ is (up to an additive constant) equal to

$$\operatorname{sgn}(y-x) \sum_{u=\min(x,y)}^{\max(x,y)-1} \big(-\mathbf{1}_{u<(S+t-\mathbf{k}-1)/2} + \mathbf{1}_{u>(S+t-\mathbf{k}-1)/2}\big),$$

where the above summand mimics $\mathcal{H}_{\mathbf{k}}$ in the saturation band, see Figure 7, left. The additive constant $C(K,\mathbf{k})$ in (5.20) is independent of L. This constant accounts for discrete effects coming from the presence of $\mathbf{k}$, and these effects are negligible for large L. When x is in **Case 1**, the right-hand side of (5.20) can be lower bounded by $-\beta' L$ for fixed $\beta' > 0$. Thus, we obtain a bound of order δL in **Case 1**, which completes the proof of that case.

Continuing with **Case 2**, notice that for y in the saturation band, we have the extra second line in (5.14). This second line turns out to be nonnegative. More precisely, to complete the proof, it remains to show that for large L and for x, y satisfying our assumptions, we have

$$2\min\big\{\mathcal{G}_{\mathbf{k}}(x,y,z_0-1 \mid S+t), \mathcal{G}_{\mathbf{k}}(x,y,z_0+N-1 \mid S+t)\big\} - 2\mathcal{G}_{\mathbf{k}}(x,y,y \mid S+t) > \tfrac{5}{4} d_{\mathbf{k}}^{S+t}(x;y). \tag{5.21}$$

Let us derive the estimate (5.21) for large L from its limiting version. To obtain the latter, we replace (x,y,S,t,N) by $(\mathsf{x},\mathsf{y},\mathsf{S},\mathsf{t},\mathsf{N})$, and set $\mathbf{k} = -1$ (which eliminates the additive constants $\mathbf{k}+1$ in $\mathcal{G}_{\mathbf{k}}$ and $d_{\mathbf{k}}^{\mathsf{S}+\mathsf{t}}$). We also replace $z_0 - 1$ and $z_0 + N - 1$ by $\frac{1}{2}(S+t-\mathsf{N})$ and $\frac{1}{2}(S+t+\mathsf{N})$, respectively. Observe that then $\mathcal{G}_{-1}(\mathsf{x},\mathsf{y},\frac{1}{2}(S+t-\mathsf{N}) \mid \mathsf{S}+\mathsf{t}) = \mathcal{G}_{-1}(\mathsf{x},\mathsf{y},\frac{1}{2}(S+t+\mathsf{N}) \mid \mathsf{S}+\mathsf{t})$, so no minimum is required in (5.21).

The resulting difference of the two sides in the limiting version of (5.21) has the form

$$2\mathcal{G}_{-1}(\mathsf{x},\mathsf{y},\tfrac{1}{2}(S+t-\mathsf{N}) \mid \mathsf{S}+\mathsf{t}) - 2\mathcal{G}_{-1}(\mathsf{x},\mathsf{y},\mathsf{y} \mid \mathsf{S}+\mathsf{t}) - \tfrac{5}{4} d_{-1}^{\mathsf{S}+\mathsf{t}}(\mathsf{x};\mathsf{y}). \tag{5.22}$$

Observe that (5.22) is invariant under simultaneous shifts of x, y by B and $\mathsf{S}+\mathsf{t}$ by $-2B$, so we can assume that $\mathsf{S}+\mathsf{t}=0$. Moreover, (5.22) is homogeneous under the simultaneous rescaling of $\mathsf{x}, \mathsf{y}, \mathsf{N}$, so we can set $\mathsf{N}=1$. The resulting expression is an even function separately in x and y, so we can further assume that $\mathsf{x} \geq \mathsf{y} > 0$ (note that $d^0_{-1}(\mathsf{x};\mathsf{y}) = |\mathsf{x}| - |\mathsf{y}|$ must be nonnegative). Then, the resulting specialization of (5.22) has the form

$$\tfrac{3}{4}(\mathsf{x}-\mathsf{y}) + (1-2\mathsf{x})^- - (1-2\mathsf{y})^-. \tag{5.23}$$

This explicit function is positive for $0 < \mathsf{x} < \frac{4}{5}$ and $0 \leq \mathsf{y} \leq \min\{\mathsf{x}, \frac{4-5\mathsf{x}}{3}\}$, see Figure 8.

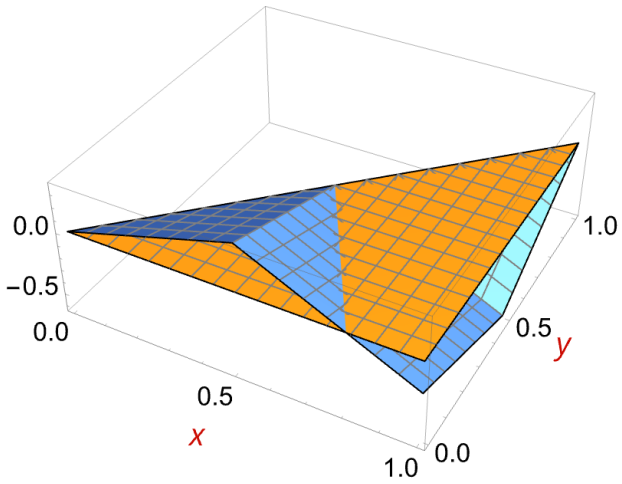

Figure 8: The plot of the function (5.23) for $\mathsf{x} \geq \mathsf{y} > 0$, and its horizontal cross-section at height zero. We see that the positive part of the function lies above the triangle with vertices $(0,0), (\frac{4}{5}, 0)$, and $(\frac{1}{2}, \frac{1}{2})$.

Since (5.23) is piecewise linear, we conclude that (5.21) holds for $x > (S+t-N)/2 - \gamma L$, where the constant $\gamma > 0$ depends only on the distance from y to the boundary of the saturation band. This range is larger than the assumption $x > (S+t-N)/2 - \alpha\sqrt{L}$, so we are done with **Case 2**. This completes the proof. □

We can now formulate and prove the main result of this section:

Theorem 5.11. *Let the parameters T, S, N, t grow proportionally to L as in (3.1). Fix their scaled values $\mathsf{T}, \mathsf{S}, \mathsf{N}, \mathsf{t}$. For any $\varepsilon > 0$, there exists $c > 0$ (depending on $\mathsf{T}, \mathsf{S}, \mathsf{N}, \mathsf{t}, \varepsilon$) such that*

$$\mathbb{P}\Big(\text{there exists a hole } \square \text{ in the nonintersecting path ensemble at some point } (t,y), \\ \text{where } \mathsf{t}_l + \varepsilon < \frac{t}{L} < \mathsf{t}_r - \varepsilon \text{ and } \Big|\frac{y}{L} - \frac{\mathsf{S}+\mathsf{t}}{2}\Big| < \frac{\mathsf{N}-\varepsilon}{2}\Big) < e^{-cL},$$

for all L large enough.

Proof. Fix (t,y) satisfying the hypotheses of the theorem. We need to upper bound $\sum_{\mathcal{C}\colon y \notin \mathcal{C}} \mathbb{P}[\mathcal{C}]$, where the sum is over all N-particle configurations on the t-th vertical slice of the hexagon. Due

to the assumption on y, for each such $\mathcal{C}$, there exists $x_{\mathcal{C}}$ such that, by Lemma 5.10, we have the bound

$$\mathbb{P}[\mathcal{C}] < q^{\varepsilon' L}\, \mathbb{P}[(\mathcal{C} \cup \{y\}) \setminus \{x_{\mathcal{C}}\}], \tag{5.24}$$

where $\varepsilon' > 0$ depends on ε. Indeed, since y is $(L\varepsilon/2)$-inside the waterfall region, we can pick a particle $x_{\mathcal{C}}$ with $d_{\mathbf{k}}^{S+t}(x_{\mathcal{C}}; y)$ positive and of order L. In other words, since not all particles can fit $(L\varepsilon/4)$-inside the waterfall region, we can pick a particle $x_{\mathcal{C}}$ which did not fit. Then, the estimate (5.19) from Lemma 5.10 immediately leads to the desired bound (5.24).

To bound the sum over $\mathcal{C}$, let us rewrite it as

$$\sum_{\mathcal{C}\colon y\notin\mathcal{C}} \mathbb{P}[\mathcal{C}] < q^{\varepsilon' L} \sum_{x} \sum_{\substack{\mathcal{C}\colon y\notin\mathcal{C} \\ x_{\mathcal{C}}=x}} \mathbb{P}[(\mathcal{C} \cup \{y\}) \setminus \{x_{\mathcal{C}}\}] < \text{const} \cdot L q^{\varepsilon' L} \sum_{\mathcal{C}} \mathbb{P}[\mathcal{C}] \le \text{const} \cdot L q^{\varepsilon' L},$$

where the sum over x on the t-th vertical slice produces a factor $O(L)$, and we bound the sum over some configurations by the sum over all configurations, which is at most 1.

Thus, we have obtained an exponential upper bound on the probability that a hole appears at (t, y). This bound is uniform over all (t, y) such that $\mathsf{t}_l + \varepsilon < t/L < \mathsf{t}_r - \varepsilon$ and $|y/L - (\mathsf{S}+\mathsf{t})/2| < (\mathsf{N} - \varepsilon)/2$. Applying a union bound over all such pairs (t, y) yields the desired result. □

Using Theorem 5.11, we can enlarge the region where the correlation kernel K_t converges to the identity to the whole slice inside the waterfall region:

Corollary 5.12. *Let* $\mathsf{N} < \mathsf{T}$, $\mathsf{t}_l < \mathsf{t} < \mathsf{t}_r$, *and* $\frac{1}{2}(\mathsf{S}+\mathsf{t}-\mathsf{N}) < \mathsf{x} < \frac{1}{2}(\mathsf{S}+\mathsf{t}+\mathsf{N})$. *Then*

$$\lim_{L\to+\infty} K_{\lfloor L\mathsf{t}\rfloor}(\lfloor L\mathsf{x}\rfloor + \Delta x, \lfloor L\mathsf{x}\rfloor + \Delta y) = \mathbf{1}_{\Delta x = \Delta y} \quad \text{for all } \Delta x, \Delta y \in \mathbb{Z}. \tag{5.25}$$

Corollary 5.12 complements Proposition 4.8 which dealt with the center line and the regions outside the waterfall.

Proof of Corollary 5.12. The clustering of the paths (Theorem 5.11) immediately implies that all local correlations (in the vertical direction) inside the waterfall region go to one. This means that all principal minors of $K_{\lfloor L\mathsf{t}\rfloor}$ converge to 1. Since the one-dimensional kernel $K_t(x, y)$ living on a slice is symmetric in (x, y), we conclude that all its off-diagonal elements converge to 0. This completes the proof. □

We have completed the proof of Theorem 1.4 from the Introduction.

6 Correlations across vertical slices

In this section, we recall the full two-dimensional correlation kernel $K(s, x; t, y)$ of the q-Racah nonintersecting paths ensemble from [BGR10, Section 7], together with the inverse Kasteleyn matrix for the q-Racah measure on lozenge tilings of the hexagon (equivalently, on dimer configurations on the underlying hexagonal grid). We also present the pre-limit correlation kernel of the barcode process, which is the one-dimensional random stepped interface appearing inside the waterfall region. In the last part (Section 6.5), we prove several partial asymptotic results that point toward the limiting barcode kernel, which will be discussed in Section 7 below.

Remark 6.1. We focus in this section and the next on the first parameter zone of the hexagon, see (2.15). Doing so streamlines the notation and simplifies several computations. The remaining three zones, (2.16)–(2.18), can be treated in exactly the same way, with only straightforward modifications.

6.1 Two-dimensional kernel and gauge transformations

Recall from Section 2.5 the two-dimensional correlation kernel $K(s,x;t,y)$ which encodes the distribution of the q-Racah nonintersecting path ensemble. Here, we present a representation of K in terms of the q-Racah orthogonal polynomials first obtained in [BGR10, Section 7.1]. This representation extends the kernel $K_t(x,y) = K(t,x;t,y)$ from Proposition 2.7. This extension is an instance of a general principle [Bor11, Section 4] for correlation kernels of measures given by products of determinants.

Recall the notation of the *orthonormal* q-Racah polynomials $f_n(x)$ (2.22), and let $f_n^t(x)$ denote the specialization of $f_n(x)$ onto the t-th vertical slice of the hexagon. That is, in $f_n^t(x)$, we have substituted the q-Racah parameters $(\alpha,\beta,\gamma,\delta)$ in terms of the hexagon parameters T,S,N,t, assuming that $t \le \min(S-1, T-S-1)$ since we work in the first zone (2.15). Similarly, denote by $w_t(x)$ the weight function $w^{qR}(x)$ (2.6) specialized to the t-th slice. From (2.6), we have in the first zone (2.15):

$$w_t(x) = \frac{q^{x(2N+T-1)}(q^{1-N-S};q)_x(q^{1-N-t};q)_x(q^{1-T}\kappa^2;q)_x(q^{1-S-t}\kappa^2;q)_x}{(q;q)_x(q^{1-S-t+T};q)_x(q^{N-S+1}\kappa^2;q)_x(q^{N-t+1}\kappa^2;q)_x}\frac{1-\kappa^2 q^{1-S-t+2x}}{1-\kappa^2 q^{1-S-t}}. \tag{6.1}$$

To connect to formulas from [BGR10], it is more convenient to renormalize the weight function w_t as in [BGR10, Theorem 4.1]. Indeed, while the functions $f_n^t(x)$ (orthonormal in the standard $\ell^2(\mathbb{R})$ space on the t-th slice) are defined canonically, the weight function $w_t(x)$ may be *gauge transformed* into $\widetilde{w}_t(x) = \lambda(t)\, w_t(x)$, where $\lambda(t)$ is any nonvanishing function of t which does not depend on x, but may depend on the hexagon parameters T,S,N. This gauge transformation does not affect the fixed-slice kernel $K_t(x,y)$, but modifies $K(s,x;t,y)$ into

$$\widetilde{K}(s,x;t,y) = K(s,x;t,y)\sqrt{\lambda(s)/\lambda(t)}. \tag{6.2}$$

Clearly, the determinants (2.20) of the new kernel $\widetilde{K}$ are the same as those of the original kernel, so this change does not affect the determinantal process.

Denote the normalization of the q-Racah weight in [BGR10, Theorem 4.1] by $\widetilde{w}_t(x)$. Let us pick the gauge factor $\lambda(t)$ to be

$$\begin{aligned}\lambda(t) \coloneqq (-1)^t\frac{\widetilde{w}_t(x)}{w_t(x)} = {}& \frac{(-1)^t q^{\frac{1}{2}t(2N+t-1)}(q^N\kappa^2;\tfrac{1}{q})_t(q^{T-S};\tfrac{1}{q})_t}{(q^N;q)_t(q^{1-S}\kappa^2;\tfrac{1}{q})_t}\\ &\times\frac{(-1)^S(1-\kappa^2 q^{1-S})}{(\frac{1}{q};\frac{1}{q})_{N-1}(\frac{1}{q};\frac{1}{q})_{N+S-1}(q;q)_{T-S}(q^{1-S}\kappa^2;q)_N(q^{1-T}\kappa^2;q)_{N+T}}.\end{aligned} \tag{6.3}$$

These these factors are independent of x. Note that the product in the second line in (6.3) is also independent of t, so it does not play a role in gauge transformations. We included it only for completeness.

Denote

$$a_0^t(x) \coloneqq (1-q^{x+T-t-S})\,\frac{1-\kappa^2 q^{x+N-t}}{1-\kappa^2 q^{2x-t-S+1}};$$
$$a_1^t(x) \coloneqq q^{T+N-1-t}(q^{x-S-N+1}-1)\,\frac{1-\kappa^2 q^{x-T+1}}{1-\kappa^2 q^{2x-t-S+1}}. \tag{6.4}$$

Define

$$\widetilde{\mathfrak{C}}_n^t \coloneqq \left((q^{n-t-N}-1)(1-q^{T+N-t-n-1})\right)^{\frac{1}{2}}. \tag{6.5}$$

By [BGR10, (24)], we have

$$\widetilde{\mathfrak{C}}_n^t f_n^{t+1}(x) = \sqrt{\frac{\widetilde{w}_t(x-1)}{\widetilde{w}_{t+1}(x)}}\, f_n^t(x-1)\, a_1^t(x-1) + \sqrt{\frac{\widetilde{w}_t(x)}{\widetilde{w}_{t+1}(x)}}\, f_n^t(x)\, a_0^t(x) \tag{6.6}$$

for all n and all x on the t-th vertical slice.

Remark 6.2. We have changed the signs of $a_0^t(x), a_1^t(x)$ (6.4) compared to the coefficients in [BGR10, (24)] (given by Lemma 7.4 in that paper), and also multiplied $\widetilde{\mathfrak{C}}_n^t$ by an extra factor $\mathbf{i}$ to make the expression under the square root in (6.5) positive. These sign changes are convenient in our case of imaginary κ, and come from the sign $(-1)^t$ in (6.3).

With the notation developed above in this subsection, we can now write down the two-dimensional correlation kernel:

Proposition 6.3 ([BGR10, Theorem 7.5])**.** *The two-dimensional correlation kernel $\widetilde{K}(s,x;t,y)$ of the q-Racah nonintersecting path ensemble is given by*

$$\widetilde{K}(s,x;t,y) = \begin{cases} \displaystyle\sum_{n=0}^{N-1} (\widetilde{\mathfrak{C}}_n^t \widetilde{\mathfrak{C}}_n^{t+1} \dots \widetilde{\mathfrak{C}}_n^{s-1})^{-1}\, f_n^s(x)\, f_n^t(y), & s \geq t; \\ \displaystyle -\sum_{n\geq N} (\widetilde{\mathfrak{C}}_n^s \widetilde{\mathfrak{C}}_n^{s+1} \dots \widetilde{\mathfrak{C}}_n^{t-1})\, f_n^s(x)\, f_n^t(y), & s < t. \end{cases} \tag{6.7}$$

Clearly, for $s=t$, expression (6.7) reduces to the fixed-slice kernel K_t (2.25).

6.2 Operator for transitions between vertical slices

Using (6.6), define the operator $\mathfrak{U}_t$ by

$$\big(\mathfrak{U}_t f\big)(x) \coloneqq \sqrt{\frac{\widetilde{w}_t(x-1)}{\widetilde{w}_{t+1}(x)}}\, a_1^t(x-1)\, f(x-1) + \sqrt{\frac{\widetilde{w}_t(x)}{\widetilde{w}_{t+1}(x)}}\, a_0^t(x)\, f(x), \tag{6.8}$$

where the coefficients $a_0^t(x), a_1^t(x)$ are given by (6.4). It is useful to view $\mathfrak{U}_t$ as an operator that maps functions on the t-th vertical slice to functions on the $(t+1)$-st slice. Recall that the t-th slice in the first zone (2.15) is $\{0,1,\dots,N+t-1\}$. In particular, identity (6.6) implies that

$$(\mathfrak{U}_t f_n^t)(y) = \widetilde{\mathfrak{C}}_n^t f_n^{t+1}(y), \qquad 0 \leq n \leq N+t-1, \quad 0 \leq y \leq N+t. \tag{6.9}$$

The $(t+1)$-st slice has one more point than the t-th slice. Let us define the (partial) inverse of $\mathfrak{U}_t$ as follows:

$$\mathfrak{U}_t^{-1} f_n^{t+1} = \begin{cases} (\widetilde{\mathfrak{C}}_n^t)^{-1} f_n^t, & 0 \le n \le N+t-1; \\ 0, & n = N+t. \end{cases} \tag{6.10}$$

Note also that $\widetilde{\mathfrak{C}}_{N+t}^t = 0$, while the formula for $f_{N+t}^t(y)$ (2.22) also yields zero for $0 \le y \le N+t$. The composition $\mathfrak{U}_t^{-1}\mathfrak{U}_t$ is the identity operator on the t-th slice, while the composition $\mathfrak{U}_t\mathfrak{U}_t^{-1}$ in the opposite order maps f_{N+t}^{t+1} to zero, and all the other basis functions f_n^{t+1}, $0 \le n \le N+t-1$, to themselves.

The operators (6.8) and (6.10) provide the following operator interpretation of the kernel:

Proposition 6.4 ([BGR10, Section 8])**.** *We have*

$$\widetilde{K}(s,x;t,y) = \begin{cases} \left(\mathfrak{U}_t^{-1}\mathfrak{U}_{t+1}^{-1}\dots\mathfrak{U}_{s-1}^{-1}\right)_y K_s(x,y), & s > t; \\ K_t(x,y), & s = t; \\ \left(\mathfrak{U}_{t-1}\dots\mathfrak{U}_{s+1}\mathfrak{U}_s\right)_y \left(-\mathbf{1}_{x=y} + K_s(x,y)\right), & s < t. \end{cases} \tag{6.11}$$

Here the subscript y indicates that the operators act on functions in the variable y.

Proof. We have for $s < t$:

$$\begin{aligned} \widetilde{K}(s,x;t,y) &= -\sum_{n\ge N} (\widetilde{\mathfrak{C}}_n^s \widetilde{\mathfrak{C}}_n^{s+1} \dots \widetilde{\mathfrak{C}}_n^{t-1})\, f_n^s(x)\, f_n^t(y) \\ &= -\left(\mathfrak{U}_{t-1}\dots\mathfrak{U}_{s+1}\mathfrak{U}_s\right)_y \sum_{n\ge N} f_n^s(x)\, f_n^s(y) \\ &= \left(\mathfrak{U}_{t-1}\dots\mathfrak{U}_{s+1}\mathfrak{U}_s\right)_y \left(-\mathbf{1}_{x=y} + K_s(x,y)\right), \end{aligned}$$

where we used the fact that the sum of $f_n^s(x) f_n^s(y)$ over all $n \ge 0$ produces the identity operator, since the functions $f_n^s(x)$ are orthonormal. Similarly, for $s > t$, we have:

$$\widetilde{K}(s,x;t,y) = \sum_{n=0}^{N-1} (\widetilde{\mathfrak{C}}_n^t \widetilde{\mathfrak{C}}_n^{t+1} \dots \widetilde{\mathfrak{C}}_n^{s-1})^{-1} f_n^s(x)\, f_n^t(y) = \left(\mathfrak{U}_t^{-1}\mathfrak{U}_{t+1}^{-1}\dots\mathfrak{U}_{s-1}^{-1}\right)_y K_s(x,y), \tag{6.12}$$

as desired. Note that the application of the inverse operators in (6.12) is valid since in the sum we have $n \le N-1 < N+t$. □

6.3 Inverse Kasteleyn matrix

The two-dimensional correlation kernel $\widetilde{K}(s,x;t,y)$ (6.7) describes the determinantal structure of the nonintersecting paths. As is evident from the correspondence between nonintersecting paths and lozenge tilings (see Figure 2), $\widetilde{K}$ lets us access only the non-horizontal lozenges □ and ▱, and it does not distinguish between these two types. These are precisely the lozenges that appear in the waterfall region (see Figures 4 and 9), and we would like to tell them apart. Therefore, we must upgrade the correlation kernel to the *inverse Kasteleyn matrix* which can access all three types of lozenges. For a general overview of Kasteleyn theory in the context of random dimer

coverings (and, in particular, lozenge tilings), see [Ken09, Chapter 3]. An expression for the inverse Kasteleyn matrix through the kernel $\widetilde{K}(s,x;t,y)$ is given in [BGR10, Section 7.2].

Represent each lozenge in a tiling as an occupied edge of a dimer covering of the underlying hexagonal lattice. It is useful to coordinatize this lattice as follows. Divide the two-dimensional triangular lattice (dual to the hexagonal lattice) into black and white triangles (the black triangles point left, and the white one point right), such that each lozenge is a union of two neighboring triangles as follows:

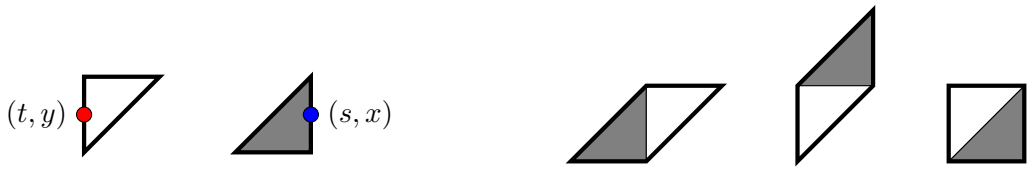

Let the lattice coordinates of a triangle be the coordinates of the midpoint of its vertical side. These triangles represent vertices in the hexagonal grid, and lozenges (unions of two neighboring triangles) correspond to edges included in a dimer covering. To each lozenge, we associate its white and black triangle's coordinates. The Kasteleyn matrix has rows and columns indexed by the white and black triangles, respectively, and is defined by

$$\operatorname{Kast}(t,y;s,x) := \begin{cases} \mathsf{w}_{q,\kappa}\big(y-\frac{t}{2}+1\big), & s=t,\ x=y; \\ 1, & s=t+1,\ x=y+1; \\ 1, & s=t+1,\ x=y; \\ 0, & \text{otherwise.} \end{cases} \tag{6.13}$$

where $\mathsf{w}_{q,\kappa}(\cdot)$ is the weight of a horizontal lozenge ▱ (2.3).

The role of the inverse of the matrix (6.13) is that for any (t_i,y_i) and (s_i,x_i), $i=1,\dots,m$, the probability that a random lozenge tiling contains all m lozenges $[(t_i,y_i);(s_i,x_i)]$ (the coordinates refer to the white and black triangles forming the lozenge) is given by [Ken09, Corollary 3]:

$$\prod_{i=1}^{m} \operatorname{Kast}(t_i,y_i;s_i,x_i)\cdot \det\left[\operatorname{Kast}^{-1}(s_i,x_i;t_j,y_j)\right]_{i,j=1}^{m}. \tag{6.14}$$

Proposition 6.5 ([BGR10, Theorem 7.6])**.** *The inverse Kasteleyn matrix is expressed through the two-dimensional correlation kernel $\widetilde{K}$ (6.7) as follows:*

$$\operatorname{Kast}^{-1}(s,x;t,y) = \frac{G(s,x)}{G(t,y)}\frac{\mathbf{1}_{s=t}\mathbf{1}_{x=y}-\widetilde{K}(s,x;t,y)}{\mathsf{w}_{q,\kappa}(x-\frac{s}{2}+1)}, \tag{6.15}$$

where (s,x) and (t,y) are the coordinates of a black (resp., white) triangle. The factor G is

$$G(t,x) := \frac{1}{\sqrt{\widetilde{w}_t(x)}}\frac{(-1)^x\kappa^{-t}q^{x(T+N-t-1)+t(S/2-1/2)+t(t+1)/4}\left(1-\kappa^2q^{2x-t-S+1}\right)}{(\frac{1}{q};\frac{1}{q})_{S+N-1-x}(q;q)_{T-S+x-t}(\kappa^2q^{x-T+1};q)_{T+N-t}}. \tag{6.16}$$

Remark 6.6. The function $G(t,x)$ (6.16) differs from the one in [BGR10, (25)] by the sign $(-1)^t$, which reflects the sign gauge in the definition of the correlation kernel, see Remark 6.2.

6.4 Pre-limit barcode kernel for a specific hexagon

Let us now focus on the waterfall region of the q-Racah random lozenge tiling ensemble, see Figure 9 for an illustration. The one-dimensional random stepped interface (the *barcode*) we see

Figure 9: Local structure of the one-dimensional random stepped interface in the waterfall region (see Figure 4 for the global picture). This barcode configuration is encoded as a sequence of particles (square lozenges, the lighter ones in the figure) and holes (vertical lozenges, the darker ones in the figure). The binary sequence (encoding particles and holes) for this barcode configuration is 11011010101011010110010110011010010101010110000110 1.

in the waterfall region can be represented as a random sequence of square and vertical lozenges, □ and ▯. Let us interpret each square lozenge $[(t-1,x);(t,x)]$ as a particle at $t\in\mathbb{Z}$. We may pick the vertical coordinate x arbitrarily so that (t,x) asymptotically lies in the waterfall region $\mathcal{W}$ (recall Definition 3.1). Indeed, this is possible thanks to the clustering of the nonintersecting paths in $\mathcal{W}$ (which is equivalent to the absence of the horizontal lozenges ▱ in $\mathcal{W}$), see Theorem 5.11. Thus, we arrive at the (pre-limit) *barcode point process* on $\mathbb{Z}$.

To access the (conjectural) barcode kernel in the limit, throughout the rest of the paper, we fix a hexagon with the specific scaled side lengths $T=8L$ and $N=S=4L$.[8] This leads to the following definition.

Definition 6.7 (Pre-limit barcode kernel)**.** Let L be a positive integer. Consider the hexagon with parameters $T=8L$, $N=S=4L$. Denote $T_0:=2L$, and $X_0:=3L$. The point (T_0,X_0) is in the first zone of the hexagon (2.15), and asymptotically lies on the center line $\mathsf{x}=\frac{1}{2}(\mathsf{t}+\mathsf{S})$ of the waterfall region. Let $s,t\in\mathbb{Z}$ be such that $|s|,|t|<L$. We define the *pre-limit barcode kernel* by

$$K_{(L)}^{\mathrm{barcode}}(s,t):=\mathrm{Kast}^{-1}\left(T_0+s,X_0;T_0+t-1,X_0\right), \tag{6.17}$$

where Kast^{-1} is the inverse Kasteleyn matrix for the q-Racah measure on lozenge tilings of our specific hexagon. In other words, the pre-limit barcode kernel describes the joint distribution of the square lozenges □ around the point (T_0,X_0) in the waterfall region.

Proposition 6.8. *For the hexagon with L-dependent sides as in Definition 6.7, for any m and any distinct $t_1,\dots,t_m\in\mathbb{Z}$, $|t_i|<L$, we have*

$$\mathbb{P}\big\{\text{there are square lozenges at } (t_i+T_0,X_0),\ i=1,\dots,m\big\}=\det\big[K_{(L)}^{\mathrm{barcode}}(t_i,t_j)\big]_{i,j=1}^{m}. \tag{6.18}$$

Proof. This follows from the general formula (6.14) for the probability of finding a given set of lozenges in a random tiling. Note that the prefactor involving the Kasteleyn matrix is equal to 1, since we are considering only square lozenges for which the edge weight is 1, see (6.13). □

[8] While we believe that the limiting barcode kernel is the same for any hexagon, a specific choice of side lengths simplifies many of the formulas in the remainder of this Section 6 and in the next Section 7. See also examples in Sections 7.4.2 and 7.5.2 below.

6.5 Asymptotics of inter-slice coefficients and some prefactors

In this subsection, we prove a number of lemmas on the asymptotic behavior of various components entering the pre-limit barcode kernel (6.17). Recall that for the rest of the paper we assume that the hexagon has the specific side lengths $T = 8L$ and $N = S = 4L$. Moreover, as in (6.17), we set $t = T_0 + t = 2L + t$ and $x = X_0 = 3L$.

First, we need the following preliminary result. We use the notation and properties of the Jacobi theta function $\theta_q(z)$ from Appendix A.1.

Lemma 6.9. *Let $\alpha, \beta > 0$ be fixed. Then*

$$\lim_{L\to\infty} \frac{(\alpha q^L; q)_\infty}{(\beta q^L; q)_\infty} = 1,$$

and

$$\lim_{L\to-\infty} \left(\frac{\beta}{\alpha}\right)^L \frac{(-\alpha q^{-L}; q)_\infty}{(-\beta q^{-L}; q)_\infty} = \frac{\theta_q(-\alpha)}{\theta_q(-\beta)}.$$

Proof. The first statement is evident, since both the numerator and the denominator rapidly approach 1 as $L \to \infty$. The second statement follows from standard properties of the q-Pochhammer symbols, for example, see [GR04, Exercise 1.1]. □

Let us denote

$$\mathfrak{a}(x) := \left[\frac{-\kappa^2 q^{2x-1}}{(1-\kappa^2 q^{2x})(1-\kappa^2 q^{2x-1})}\right]^{\frac{1}{2}}, \qquad x \in \tfrac{1}{2}\mathbb{Z}. \tag{6.19}$$

Note that this expression rapidly decays as $x \to \pm\infty$.

Lemma 6.10. *The coefficients of the operator $\mathfrak{U}_t$ (6.8) have the following asymptotic behavior at coordinates $(T_0 + t, X_0 + x)$, where $t, x \in \mathbb{Z}$ are fixed:*

$$\lim_{L\to\infty} q^{3L}\sqrt{\frac{\widetilde{w}_{T_0+t}(X_0+x-1)}{\widetilde{w}_{T_0+t+1}(X_0+x)}}\, a_1^{T_0+t}(X_0+x-1) = q^{-\frac{t}{2}}\,\mathfrak{a}(x-\tfrac{t}{2});$$

$$\lim_{L\to\infty} q^{3L}\sqrt{\frac{\widetilde{w}_{T_0+t}(X_0+x)}{\widetilde{w}_{T_0+t+1}(X_0+x)}}\, a_0^{T_0+t}(X_0+x) = q^{-\frac{t}{2}}\,\mathfrak{a}(x-\tfrac{t}{2}+\tfrac{1}{2}).$$

Proof. We have

$$\frac{\widetilde{w}_{T_0+t}(X_0+x-1)}{\widetilde{w}_{T_0+t+1}(X_0+x)} = \frac{q^{-11L}(1-q^{3L+x})(1-\kappa^2 q^{3L+x})(q^{t+1}-\kappa^2 q^{2x})(q^{1-5L+x}\kappa^2;q)_\infty}{(q^x-q^{5L})(q^t-\kappa^2 q^{2x})(q^{-5L+x}\kappa^2;q)_\infty};$$

$$\frac{\widetilde{w}_{T_0+t}(X_0+x)}{\widetilde{w}_{T_0+t+1}(X_0+x)} = \frac{(q^{-3L-t+x}-1)(q^t-q^{2x+1}\kappa^2)(q^{-3L-t+x}\kappa^2;q)_\infty}{(1-q^{5L-t+x})(q^t-q^{2x}\kappa^2)(1-q^{5L-t+x}\kappa^2)(q^{1-3L-t+x}\kappa^2;q)_\infty};$$

$$a_1^{T_0+t}(X_0+x-1) = \frac{(q^x-q^{5L})(q^{5L}-\kappa^2 q^x)}{q^{t+1}-\kappa^2 q^{2x}};$$

$$a_0^{T_0+t}(X_0+x) = \frac{(1-q^{5L-t+x})(1-\kappa^2 q^{5L-t+x})}{1-\kappa^2 q^{1-t+2x}}.$$

Using Lemma 6.9, we immediately get the desired limits. □

Lemma 6.11. *The ratio of the prefactors G (6.16) in the pre-limit barcode kernel has the following asymptotic behavior:*

$$\lim_{L\to\infty} q^{-3L(t-1-s)} \frac{G(T_0+s,X_0)}{G(T_0+t-1,X_0)\mathsf{w}_{q,\kappa}(X_0-\frac{T_0+s}{2}+1)} = -\mathbf{i}^{t-s} q^{\frac{1}{2}\binom{t-1}{2}-\frac{1}{2}\binom{s-1}{2}+1-s} \sqrt{\frac{-\kappa^2}{(1-\kappa^2q^{2-t})(1-\kappa^2q^{1-s})}}. \tag{6.20}$$

Proof. One can check that the ratio $\frac{G(T_0+s,X_0)}{G(T_0+t-1,X_0)\mathbf{i}^{t-1-s}}$ is positive for all s,t. Its square is given by

$$\left(\frac{G(T_0+s,X_0)}{G(T_0+t-1,X_0)\mathbf{i}^{t-1-s}}\right)^2 = \frac{(-1)^{t+s}(q^s-\kappa^2q)\kappa^{-2s+2t-2}q^{-3L(s-t+1)+t-s}}{\kappa^2q^2-q^t} \times \frac{(q^{5L-s+1};q)_\infty(q^{3L+t-1};q)_\infty(q^{-3L-s+1}\kappa^2;q)_\infty(q^{5L-s+1}\kappa^2;q)_\infty}{(q^{3L+s};q)_\infty(q^{5L-t+2};q)_\infty(q^{-3L-t+2}\kappa^2;q)_\infty(q^{5L-t+2}\kappa^2;q)_\infty}.$$

By Lemma 6.9, the expression in the second line behaves as $\sim \left(\frac{q^{1-s}\kappa^2}{q^{2-t}\kappa^2}\right)^{3L} \frac{\theta_q(q^{1-s}\kappa^2)}{\theta_q(q^{2-t}\kappa^2)}$. Using the quasi-periodicity of the theta function and simplifying, we arrive at the desired result. □

Remark 6.12. When the expression (6.20) appears inside the barcode kernel, certain factors on the right-hand side of (6.20) (specifically $\mathbf{i}^{t-s}q^{\frac{1}{2}\binom{t-1}{2}-\frac{1}{2}\binom{s-1}{2}}$) can be removed through a conjugation (gauge transformation) of the correlation kernel. In addition, the factor $q^{-3L(t-s)}$ on the left-hand side of (6.20) is likewise a conjugation factor applied before taking the limit. The latter factor is necessary for the convergence of the ratio of the G prefactors, but in the full barcode kernel, it can be adjusted (by a conjugation) to ensure the convergence of the kernel (see Conjecture 7.6 below).

7 Barcode kernel. Conjectures and numerical evidence

7.1 Obstacles posed by the limiting inter-slice operator

In Section 6 we expressed the *pre-limit* barcode kernel $K^{\mathrm{barcode}}_{(L)}(s,t)$ (encoding the one-dimensional random stepped interface that emerges in the waterfall region) in terms of the two-dimensional correlation kernel $\widetilde{K}(T_0+s,X_0;T_0+t-1,X_0)$ of the q-Racah nonintersecting path ensemble. Recall that we focus on the hexagon with the specific side lengths $T=8L$ and $N=S=4L$, and we set $T_0=2L$ and $X_0=3L$. Thanks to Proposition 6.4, $\widetilde{K}$ admits an operator representation via the family of linear operators $\mathfrak{U}_{T_0+t}$ given by (6.8). Recall that Lemma 6.11 provides additional explicit scaling and normalization for $\widetilde{K}$ to get to $K^{\mathrm{barcode}}_{(L)}$.

Along the center line of the waterfall region, the coefficients of $\mathfrak{U}_{T_0+t}$ converge to expressions involving the function $\mathfrak{a}(x)$ (6.19), see Lemma 6.10. This enables us to define the limiting linear operators:

$$\big(\mathfrak{U}^{\mathrm{barcode}}_t f\big)(x) \coloneqq \mathfrak{a}(x-\tfrac{t}{2})f(x-1)+\mathfrak{a}(x-\tfrac{t}{2}+\tfrac{1}{2})f(x), \qquad x\in\mathbb{Z} \text{ or } \mathbb{Z}+\tfrac{1}{2}, \tag{7.1}$$

so that

$$q^{3L+\frac{t}{2}}\big(\mathfrak{U}_{T_0+t}f\big)(X_0+x)\sim\big(\mathfrak{U}_t^{\mathrm{barcode}}f\big)(x),\qquad L\to\infty. \tag{7.2}$$

The functions $\mathcal{F}_n(x)$ defined by (A.2) in Appendix A play the same role for the limiting operators as the orthonormal q-Racah polynomials $f_n^t(x)$ do for the pre-limit ones. Namely, define

$$\mathcal{F}_n^t(x):=\mathcal{F}_n(x-\tfrac{t-1}{2}), \tag{7.3}$$

then by Proposition A.2, we have (compare with (6.9)):

$$\big(\mathfrak{U}_t^{\mathrm{barcode}}\mathcal{F}_n^t\big)(x)=-q^n\mathcal{F}_n^{t+1}(x),\qquad t,x\in\mathbb{Z},\quad n\in\tfrac{1}{2}\mathbb{Z}_{\ge0}. \tag{7.4}$$

A natural idea would be to replace $\mathfrak{U}_{T_0+t}$ with $\mathfrak{U}_t^{\mathrm{barcode}}$ in the operator representation of $\widetilde{K}$ and expect that the resulting expression (rewritten in terms of the $\mathcal{F}_n^t(x)$'s) yields the limit of $K_{(L)}^{\mathrm{barcode}}$. Let us explain why this seemingly straightforward step in fact requires a considerably more delicate analysis, which will be carried out in another work.

When $q\to1$ while q^L remains bounded (the regime analyzed in [BGR10, Section 8]), the operators $\mathfrak{U}_{T_0+t}$ converge to a bounded two-diagonal operator with constant coefficients. In Fourier space, both the limiting operator and its inverse act by multiplication by a function and its reciprocal, respectively. This makes it possible to obtain the limiting local lattice kernel simply by inverting the Fourier transform. The kernel in the limit as $q\to1$ is given by the same expressions as before the limit Proposition 6.4, In this way one recovers the celebrated *incomplete Beta kernel* [OR03], which describes correlations in the Gibbs pure phase (see Section 3.1 for further discussion and references). We see that for bounded lattice operators, the operator method (in particular, the results from [RS72] quoted in Theorem 4.7) provides a rigorous derivation of the local limiting kernel.

In our case of fixed q, the situation is dramatically different. While the two-diagonal operators $\mathfrak{U}_t^{\mathrm{barcode}}$ are bounded, their coefficients decay exponentially at $\pm\infty$. Therefore, their inverses are unbounded, and, for example, applying $\big(\mathfrak{U}_t^{\mathrm{barcode}}\big)^{-1}$ in the variable y to the limit of $K_s(x,y)$ (which is the delta function at $y=x$) does not yield a function in ℓ^2.

Throughout the remainder of this section we outline the main computations (which, in fact, reveal further obstacles to the operator approach based on the functions $\mathcal{F}_n^t$), derive the conjectural limiting density of the barcode process, and compare it with both the numerical pre-limit barcode kernel and with probabilistic simulations of the q-Racah ensemble. We also discuss a possible approach towards the full limiting barcode kernel. In computations in Sections 7.2 and 7.3, we will explicitly indicate nonrigorous steps.

7.2 Nonrigorous limit of the barcode kernel. Density

We first consider the diagonal elements of the pre-limit barcode kernel, which define the density function

$$\rho_{(L)}^{\mathrm{barcode}}(t):=K_{(L)}^{\mathrm{barcode}}(t,t),\qquad t\in\mathbb{Z}. \tag{7.5}$$

From (6.17) and Lemma 6.11, we have the asymptotic equivalence as $L\to\infty$:

$$\rho_{(L)}^{\mathrm{barcode}}(t)\sim q^{-3L-\frac{t-1}{2}}\widetilde{K}(T_0+t,X_0;T_0+t-1,X_0)\underbrace{\sqrt{\frac{-\kappa^2q^{1-t}}{(1-\kappa^2q^{2-t})(1-\kappa^2q^{1-t})}}}_{\mathfrak{a}(1-\frac{t}{2})}. \tag{7.6}$$

The "time" arguments in $\widetilde{K}$ are ordered as in the first case in (6.11). Thus, we need to compute the limit of

$$q^{-3L-\frac{t-1}{2}}\left(\mathfrak{U}^{-1}_{T_0+t-1}\right)_y K_{T_0+t}(X_0,X_0), \tag{7.7}$$

where we apply the inverse operator to the function $y\mapsto K_{T_0+t}(X_0,X_0+y)$, and then set $y=0$. Let us now replace this function in y by its limit $\mathbf{1}_{y=0}$ (that follows from Proposition 4.8), and also use the asymptotic equivalence (7.2) for the inverse operator $\mathfrak{U}^{-1}_{T_0+t-1}$, which reads

$$q^{-3L-\frac{t}{2}}\left(\mathfrak{U}^{-1}_{T_0+t}f\right)(X_0+x)\sim\left((\mathfrak{U}^{\mathrm{barcode}}_t)^{-1}f\right)(x),\qquad L\to\infty. \tag{7.8}$$

Therefore, we have

$$(7.7)\sim\left(\mathfrak{U}^{\mathrm{barcode}}_t\right)^{-1}\mathbf{1}_{y=0}\Big|_{y=0}, \tag{7.9}$$

where the operator acts on the variable y. Using the representation of the identity in Proposition A.8, we have

$$\rho^{\mathrm{barcode}}_{(L)}(t)\sim\mathfrak{a}(1-\tfrac{t}{2})\left(\mathfrak{U}^{\mathrm{barcode}}_t\right)^{-1}\sum_{n\in\frac12\mathbb{Z}_{\ge0}}\frac{\mathcal{F}^t_n(0)\mathcal{F}^t_n(y)}{\|\mathcal{F}_n\|^2_{\ell^2(\mathbb{Z})}}\Big|_{y=0}=\mathfrak{a}(1-\tfrac{t}{2})\sum_{n\in\frac12\mathbb{Z}_{\ge0}}\frac{-q^{-n}\mathcal{F}^t_n(0)\mathcal{F}^{t-1}_n(0)}{\|\mathcal{F}_n\|^2_{\ell^2(\mathbb{Z})}}. \tag{7.10}$$

Remark 7.1. Passing to the limit separately in K_{T_0+t} and $\mathfrak{U}^{-1}_{T_0+t-1}$ in (7.7) is nonrigorous. Moreover, we did not rigorously define $(\mathfrak{U}^{\mathrm{barcode}}_t)^{-1}$, either, so the right-hand side of (7.9) does not formally make sense.

Let us examine the final formula for the density more closely. First, numerically one can check that the series in n in the right-hand side of (7.10) **diverges** for any $t\in\mathbb{Z}$. However, this series diverges only "mildly", in the sense that the terms are approaching the same nonzero constant as $n\to\infty$, but they have alternating signs. Therefore, the series in (7.10) may be thought of as having "**two different sums**", coming from two possible ways of pairing the neighboring terms. We make a precise conjecture:

Conjecture 7.2. *The following limits*

$$\rho_0(t):=\lim_{M\to\infty}\mathfrak{a}(1-\tfrac{t}{2})\sum_{n=0}^{M+1/2}\frac{-q^{-n}\mathcal{F}^t_n(0)\mathcal{F}^{t-1}_n(0)}{\|\mathcal{F}_n\|^2_{\ell^2(\mathbb{Z})}},\quad \rho_1(t):=\lim_{M\to\infty}\mathfrak{a}(1-\tfrac{t}{2})\sum_{n=0}^{M}\frac{-q^{-n}\mathcal{F}^t_n(0)\mathcal{F}^{t-1}_n(0)}{\|\mathcal{F}_n\|^2_{\ell^2(\mathbb{Z})}}$$

exist for all $t\in\mathbb{Z}$, where $M\in\mathbb{Z}$, and the sums are over $n\in\frac12\mathbb{Z}_{\ge0}$. Moreover, they take only two different values, depending on the parity of t:

$$\rho^{\mathrm{barcode}}_{\mathrm{even}}:=\rho_0(2k)=\rho_1(2k+1),\qquad \rho^{\mathrm{barcode}}_{\mathrm{odd}}:=\rho_0(2k+1)=\rho_1(2k+2),$$

and $\rho^{\mathrm{barcode}}_{\mathrm{even}}+\rho^{\mathrm{barcode}}_{\mathrm{odd}}=1$.

The pre-limit barcode density has the following asymptotic behavior for all $t\in\mathbb{Z}$:

$$\lim_{L\to\infty}\rho^{\mathrm{barcode}}_{(L)}(t)=\begin{cases}\rho^{\mathrm{barcode}}_{\mathrm{even}}, & \text{if } t \text{ is even;}\\ \rho^{\mathrm{barcode}}_{\mathrm{odd}}, & \text{if } t \text{ is odd.}\end{cases}$$

Let us make a few comments on this conjecture. Recall that $\rho^{\mathrm{barcode}}_{(L)}(t)$ is the density of the square lozenges $\square$.

Remark 7.3. The conjectural limits $\rho_0(t)$ and $\rho_1(t)$ may be equivalently written as infinite sums, for example,

$$\rho_0(t) = -\mathfrak{a}(1-\tfrac{t}{2})\sum_{k=0}^{\infty}\left(\frac{q^{-k}\mathcal{F}_k^t(0)\mathcal{F}_k^{t-1}(0)}{\|\mathcal{F}_k\|^2_{\ell^2(\mathbb{Z})}}+\frac{q^{-(k+1/2)}\mathcal{F}_{k+1/2}^t(0)\mathcal{F}_{k+1/2}^{t-1}(0)}{\|\mathcal{F}_{k+1/2}\|^2_{\ell^2(\mathbb{Z})}}\right).$$

Here the sum is over integer k. A similar series representation can be written down for $\rho_1(t)$; in that case one first isolates the term corresponding to $k=0$ and then groups together the terms with indices $k-\frac{1}{2}$ and k for $k=1,2,\ldots$. The convergence of these infinite series is equivalent to the first part of Conjecture 7.2.

Remark 7.4. The conjectural limit of the barcode density becomes *periodic* in t with period two. This periodicity was not expected a priori, since the q-Racah measure on lozenge tilings of the hexagon did not have any such periodicity. A posteriori, this periodicity may be explained as follows.

The number of horizontal lozenges $\parallelogram$ in the t-th vertical slice of the hexagon is determined by the shape of the hexagon and grows linearly with t. Thus, increasing t by one adds exactly one horizontal lozenge to that slice. In the scaling limit, with probability exponentially close to one, these horizontal lozenges concentrate in the two regions $\mathcal{W}^{\pm}$ lying outside the waterfall region (see Definition 3.3). When t is incremented by one, the newly added horizontal lozenge can be placed only in one of the two regions, either $\mathcal{W}^+$ or $\mathcal{W}^-$. This asymmetry introduces an imbalance in the limiting density. By contrast, when t increases by an even amount, the additional horizontal lozenges can be evenly distributed between $\mathcal{W}^+$ and $\mathcal{W}^-$, which leads to the observed period-two translation invariance of the limiting density.

Remark 7.5. The fact that $\rho^{\mathrm{barcode}}_{\mathrm{even}}+\rho^{\mathrm{barcode}}_{\mathrm{odd}}=1$ means that on larger scales, the proportion of the square lozenges $\square$ (and similarly the vertical lozenges $\diagup\!\!\!\!\square$) tends to $\frac{1}{2}$. This is consistent with the fact that the waterfall region has slope $\frac{1}{2}$, see Figure 4 for illustrations.

7.3 Nonrigorous limit of the barcode kernel. General case

First, based on numerics (detailed in Section 7.4 below), we are able to conjecture the right gauge of the pre-limit barcode kernel which leads to a convergent expression.

Conjecture 7.6. *The following limit exists for all $t,s\in\mathbb{Z}$:*

$$\lim_{L\to\infty}\mathbf{i}^{t-s}q^{2L(s-t)}K^{\mathrm{barcode}}_{(L)}(s,t)=:\mathcal{K}^{\mathrm{barcode}}(s,t). \tag{7.11}$$

The limit kernel $\mathcal{K}^{\mathrm{barcode}}(s,t)$ is symmetric in s and t, and is 2×2 block Toeplitz:

$$\begin{pmatrix}\mathcal{K}^{\mathrm{barcode}}(s,t) & \mathcal{K}^{\mathrm{barcode}}(s,t+1)\\ \mathcal{K}^{\mathrm{barcode}}(s+1,t) & \mathcal{K}^{\mathrm{barcode}}(s+1,t+1)\end{pmatrix}=\begin{pmatrix}\mathcal{K}^{\mathrm{barcode}}_{00}(s-t) & \mathcal{K}^{\mathrm{barcode}}_{01}(s-t)\\ \mathcal{K}^{\mathrm{barcode}}_{10}(s-t) & \mathcal{K}^{\mathrm{barcode}}_{11}(s-t)\end{pmatrix},\qquad s,t\in 2\mathbb{Z}.$$

In particular, $\mathcal{K}^{\mathrm{barcode}}_{00}(0) = \rho^{\mathrm{barcode}}_{\mathrm{even}}$ and $\mathcal{K}^{\mathrm{barcode}}_{11}(0) = \rho^{\mathrm{barcode}}_{\mathrm{odd}}$.

We can express the limiting kernel $\mathcal{K}^{\mathrm{barcode}}(s,t)$ for $s \geq t$ in terms of the orthogonal functions $\mathcal{F}^t_n(x)$ (7.3). Since the kernel is conjecturally symmetric, specifying it for $s \geq t$ uniquely determines $\mathcal{K}^{\mathrm{barcode}}(s,t)$ for all $s,t \in \mathbb{Z}$.

To access $\mathcal{K}^{\mathrm{barcode}}(s,t)$ for $s \geq t$, we use the operator representation of the two-dimensional correlation kernel $\widetilde{K}(T_0+s, X_0; T_0+t-1, X_0)$, which involves the inverse operators $\mathfrak{U}^{-1}_{T_0+j}$; see Proposition 6.4. Arguing as in Section 7.2, we obtain an expression involving an infinite series of the form:

$$(-1)^{t-s}\sqrt{\frac{-\kappa^2 q^{1-s}}{(1-\kappa^2 q^{2-t})(1-\kappa^2 q^{1-s})}} \sum_{n\in\frac{1}{2}\mathbb{Z}_{\geq 0}} \frac{\left(-q^n\right)^{t-1-s}\mathcal{F}^s_n(0)\mathcal{F}^{t-1}_n(0)}{\|\mathcal{F}_n\|^2_{\ell^2(\mathbb{Z})}}. \tag{7.12}$$

As we discussed in Section 7.2, for $s=t$, the series in (7.12) diverges "mildly", as its tail behaves like $+c-c+c-c+\ldots$. For $s \geq t+1$, however, the presence of the negative powers of q^n (starting from q^{-2n}) in the summands make them rapidly growing, and so the series diverges "worse" than in the case $s=t$. However, it turns out that if we regularize the partial sums of the series, we get a well-defined limit which (numerically) coincides with the limit in Conjecture 7.6:

Conjecture 7.7. *The following limit exists for all $s,t \in \mathbb{Z}$, $s \geq t$:*

$$\lim_{M\to\infty} q^{(M+1)(s-t)} \times (-1)^{t-s}\sqrt{\frac{-\kappa^2 q^{1-s}}{(1-\kappa^2 q^{2-t})(1-\kappa^2 q^{1-s})}} \sum_{n=0}^{M+1/2} \frac{\left(-q^n\right)^{t-1-s}\mathcal{F}^s_n(0)\mathcal{F}^{t-1}_n(0)}{\|\mathcal{F}_n\|^2_{\ell^2(\mathbb{Z})}}, \tag{7.13}$$

where $M \in \mathbb{Z}$, and the sum is over $n \in \frac{1}{2}\mathbb{Z}_{\geq 0}$. The limit (7.13) coincides with $\mathcal{K}^{\mathrm{barcode}}(s,t)$.

Moreover, if we take the sum until M instead of $M+1/2$, and correspondingly replace the regularization factor $q^{(M+1)(s-t)}$ by $q^{(M+\frac{1}{2})(s-t)}$, then the limit also exists, and coincides with the shifted kernel $\mathcal{K}^{\mathrm{barcode}}(s+1,t+1)$.

7.4 Numerics

Here we present numerical evidence in support of our Conjectures 7.2, 7.6 and 7.7 on the asymptotic behavior of the barcode kernel. We use `Mathematica` for symbolic and precise numerical computations. The code defining all the functions and kernels is reproduced in Appendix B. Throughout the rest of this section, we denote by $\mathcal{K}^{\mathrm{barcode}}_{(M)}(s,t)$ the renormalized partial sum of the series in (7.13) up to $M+\frac{1}{2}$. We also set

$$\widehat{K}^{\mathrm{barcode}}_{(L)}(s,t) := \mathbf{i}^{t-s} q^{2L(s-t)} K^{\mathrm{barcode}}_{(L)}(s,t) \tag{7.14}$$

for the renormalized (conjugated) pre-limit kernel.

7.4.1 Rate of convergence

The pre-limit kernel $\widehat{K}^{\mathrm{barcode}}_{(L)}(s,t)$ and the partial sums $\mathcal{K}^{\mathrm{barcode}}_{(M)}(s,t)$ both converge at a geometric rate q in L and M, respectively, see Table 1.

L	$q=2/3$	ratios	$q=1/3$	ratios
10	0.46557005	0.69146	0.43591993	0.3333278
11	0.46659216	0.68248	0.43592101	0.3333315
12	0.46729892	0.67691	0.43592137	0.3333327
13	0.46778127	0.67336	0.43592149	0.3333331
14	0.46810778	0.67107	0.43592153	0.3333332
15	0.46832764	0.66958	0.43592154	0.3333333
16	0.46847518	0.66860	0.43592155	0.3333333
17	0.46857397	0.66795	0.43592155	0.3333333
18	0.46864002	0.66752	0.43592155	0.3333333
19	0.46868414		0.43592155	
20	0.46871359		0.43592155	

L	$q=2/3$	ratios	$q=1/3$	ratios
10	0.05154306	0.64841	0.01901038	0.3331699
11	0.05233498	0.65338	0.01901074	0.3332788
12	0.05284846	0.65728	0.01901086	0.3333152
13	0.05318396	0.66016	0.01901090	0.3333273
14	0.05340448	0.66222	0.01901091	0.3333313
15	0.05355006	0.66365	0.01901092	0.3333327
16	0.05364646	0.66463	0.01901092	0.3333331
17	0.05371044	0.66530	0.01901092	0.3333333
18	0.05375296	0.66575	0.01901092	0.3333333
19	0.05378125		0.01901092	
20	0.05380008		0.01901092	

Table 1: Convergence of the pre-limit barcode kernel for various q and for $\kappa = 2\mathbf{i}$. Left: density $\widehat{K}^{\mathrm{barcode}}_{(L)}(0,0)$. Right: elements $\widehat{K}^{\mathrm{barcode}}_{(L)}(6,1)$ of the kernel. Here and in Table 2, we take ratios of a sequence a_k defined as $(a_{k+1}-a_{k+2})/(a_k-a_{k+1})$. We see that the ratios become close to q.

M	$q=2/3$	ratios	$q=1/3$	ratios
12	0.46719254	0.66801	0.43592134	0.3333333
13	0.46771795	0.66757	0.43592148	0.3333333
14	0.46806893	0.66727	0.43592153	0.3333333
15	0.46830323	0.66707	0.43592154	0.3333333
16	0.46845957	0.66693	0.43592155	0.3333333
17	0.46856386	0.66684	0.43592155	0.3333333
18	0.46863342	0.66678	0.43592155	0.3333333
19	0.46867980	0.66675	0.43592155	0.3333333
20	0.46871072	0.66672	0.43592155	0.3333333
21	0.46873134		0.43592155	
22	0.46874509		0.43592155	

M	$q=2/3$	ratios	$q=1/3$	ratios
12	0.05141315	0.64925	0.01901026	0.3333306
13	0.05224775	0.65456	0.01901070	0.3333324
14	0.05278962	0.65836	0.01901085	0.3333330
15	0.05314430	0.66102	0.01901089	0.3333332
16	0.05337781	0.66286	0.01901091	0.3333333
17	0.05353216	0.66411	0.01901092	0.3333333
18	0.05363448	0.66495	0.01901092	0.3333333
19	0.05370242	0.66552	0.01901092	0.3333333
20	0.05374761	0.66590	0.01901092	0.3333333
21	0.05377768		0.01901092	
22	0.05379770		0.01901092	

Table 2: Convergence of the renormalized series $\mathcal{K}^{\mathrm{barcode}}_{(M)}(0,0)$ (left) and $\mathcal{K}^{\mathrm{barcode}}_{(M)}(6,1)$ (right) for various q and for $\kappa = 2\mathbf{i}$.

7.4.2 Density function

The diagonal values (i.e., the density function) of the pre-limit barcode kernel, together with those of its conjectural limit, are collected in Table 3. We chose smaller L in the former to show some dependence on t, while also took larger M in the latter to demonstrate that the limiting density depends on t only through its parity. In particular, the values $\mathcal{K}^{\mathrm{barcode}}_{(M)}(t,t)$ and $\mathcal{K}^{\mathrm{barcode}}_{(M)}(t+2,t+2)$ in Table 3 match up to ten decimal places. One can see that

$$\left|\mathcal{K}^{\mathrm{barcode}}_{(M)}(7,7) - \mathcal{K}^{\mathrm{barcode}}_{(M)}(-7,-7)\right| \approx 2.7\cdot 10^{-16}.$$

We can also evaluate the inverse Kasteleyn matrix at other macroscopic coordinates $(T_0, X_0) \neq (2L, 3L)$, to confirm that the limiting barcode kernel is independent of the global location, and depends only on the parameters (q,κ). For example, for $q=\frac{1}{7}$, $\kappa = 3\mathbf{i}$, $L=16$, and the global locations $(T_0,X_0) = (\frac{L}{2}, \frac{9L}{4})$ (on the center line) and $(T_0,X_0) = (\frac{L}{2}, 3L)$ (off the center line), we have the values given in Table 4.

In both Tables 3 and 4, we set $q=\frac{1}{7}$, a relatively small value chosen to accelerate convergence and get the limiting barcode kernel with higher precision.

We plot the density at $(0,0)$, i.e. the quantity $\rho^{\mathrm{barcode}}_{\mathrm{even}}$ from Conjecture 7.2, as a function of the parameters q and κ. The resulting surface, displayed in Figure 10, exhibits a striking system of

t	$\widehat{K}^{\mathrm{barcode}}_{(L)}(t,t)$	t	$\mathcal{K}^{\mathrm{barcode}}_{(M)}(t,t)$
-7	0.5523372977	-7	0.5611174103
-6	0.4387439934	-6	0.4388825896
-5	0.5598645425	-5	0.5611174103
-4	0.4388625943	-4	0.4388825896
-3	0.5609384574	-3	0.5611174103
-2	0.4388797292	-2	0.4388825896
-1	0.5610918461	-1	0.5611174103
0	0.4388821809	0	0.4388825896
1	0.5611137582	1	0.5611174103
2	0.4388825313	2	0.4388825896
3	0.5611168883	3	0.5611174103
4	0.4388825813	4	0.4388825896
5	0.5611173341	5	0.5611174103
6	0.4388825883	6	0.4388825896
7	0.5611173877	7	0.5611174103

Table 3: Diagonal values $\widehat{K}^{\mathrm{barcode}}_{(L)}(t,t)$ and $\mathcal{K}^{\mathrm{barcode}}_{(M)}(t,t)$ for $-7 \le t \le 7$. Parameters: $L = 6$, $M = 20$, $q = \frac{1}{7}$, $\kappa = 3\mathbf{i}$. All numbers are truncated to 10 decimal digits.

t	$\mathrm{Kast}^{-1}(\frac{L}{2}+t, \frac{9L}{4}; \frac{L}{2}+t-1, \frac{9L}{4})$	$\mathrm{Kast}^{-1}(\frac{L}{2}+t, 3L; \frac{L}{2}+t-1, 3L)$
-2	0.438744002701398029726330344950846261091117	0.438744002701397996700040430298460774145 93
-1	0.559864542689336428941964543890893079446439	0.559864542689336428425425841013168294080068
0	0.438862595645192998493904028142472069596241	0.438862595645192993780780403343843713850882
1	0.560938457463989285851404171643209418839516	0.560938457463989285776297216171385214228610
2	0.438879729391405022754197543436512517729097	0.438879729391405022081083055826078202044213

Table 4: Entries of the inverse Kasteleyn matrix at two different macroscopic locations, where $L = 16$, $q = \frac{1}{7}$, and $\kappa = 3\mathbf{i}$. We see that the values for the same $T_0 = L/2$ and different X_0 agree extremely closely, which reflects the exponential concentration established in Theorem 5.11. These values also agree with the ones in Table 3.

waves whose frequency increases as $q \to 1$ or as $\kappa/\mathbf{i} \to 0$. Several one-dimensional cross-sections of this surface are shown in Figure 11.

Remark 7.8. Figures 10 and 11 suggest the existence of a well-defined limit of $\rho^{\mathrm{barcode}}_{\mathrm{even}}$ as $q \to 0$. In this limit, many of our formulas should simplify, while the waterfall phenomenon in lozenge tilings persists for arbitrarily small q. We do not pursue this limit here.

7.4.3 Correlation decay

The covariance between the events to find a particle in the barcode process at 0 and t is given by

$$\mathrm{Cov}\left(\mathbf{1}_{\mathrm{barcode}}(0), \mathbf{1}_{\mathrm{barcode}}(t)\right) = -\mathcal{K}^{\mathrm{barcode}}_{(M)}(0,t)^2.$$

As for all determinantal point processes with a symmetric kernel, the covariance is negative, which indicates repulsion. The plot of the function

$$t \mapsto \frac{\log\left|\mathcal{K}^{\mathrm{barcode}}_{(M)}(0,t)\right|}{\log q}, \qquad t = 1, 2, \ldots, 24,$$

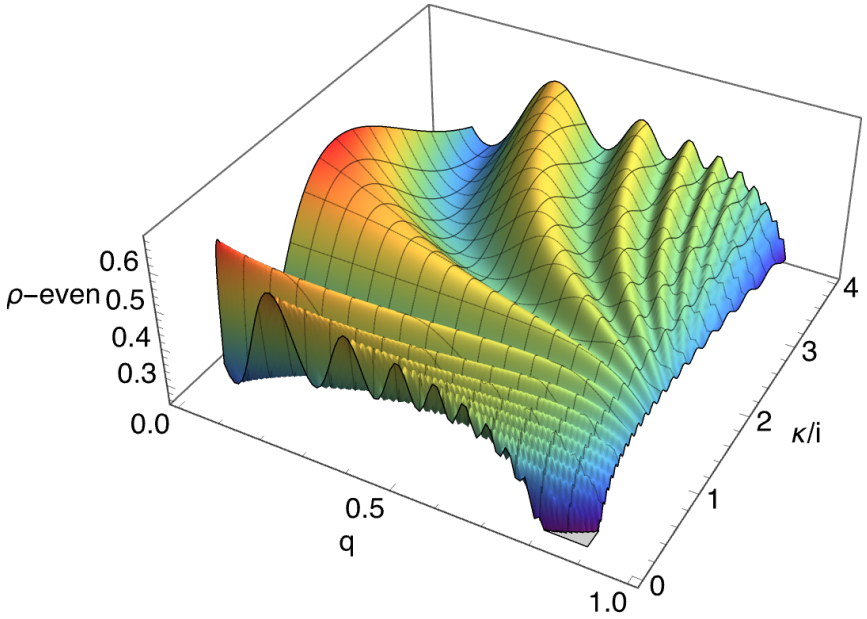

Figure 10: The even density function $\rho_{\text{even}}^{\text{barcode}} = \mathcal{K}_{(M)}^{\text{barcode}}(0,0)$ as a function of the parameters q and $\kappa/\mathbf{i}$. Here we take $M = 10$, $\frac{1}{10} \leq q \leq \frac{9}{10}$, $\frac{1}{13} \leq \kappa/\mathbf{i} \leq 4$, and the discretization in both parameters is $1/100$. Note that the theta functions in the denominator of (A.2) lead to singularities when q and $\kappa/\mathbf{i}$ are mutual inverses.

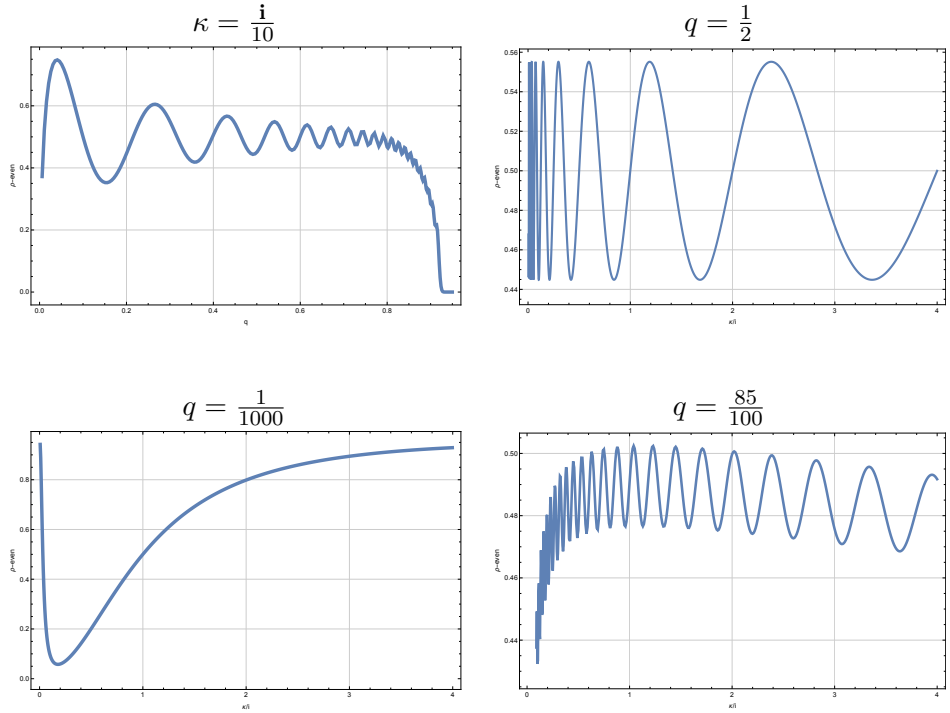

Figure 11: Cross-sections of the surface $\rho_{\text{even}}^{\text{barcode}}$ as one of the parameters q or $\kappa/\mathbf{i}$ is fixed.

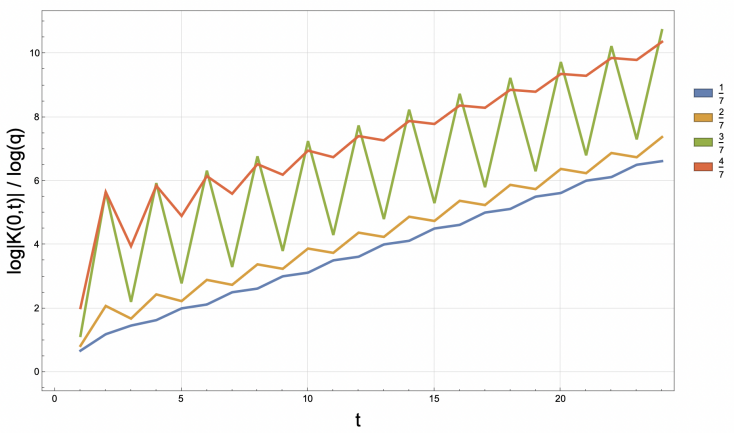

Figure 12: Two-point correlations in the barcode process as a function of t, for $q = \frac{1}{7}, \frac{2}{7}, \frac{3}{7}$, and $\frac{4}{7}$. The other parameters are $M = 20$ and $\kappa = \frac{3\mathbf{i}}{2}$. The two-periodicity in t is apparent, and the approximately linear growth corresponds to the hypothetical exponential decay of correlations.

for various values of q is shown in Figure 12. This plot suggests a conjecture that correlations decay exponentially in t.

The exponential decay of correlations stands in stark contrast to the polynomial decay exhibited under ergodic Gibbs measures on lozenge tilings with uniform resampling; see [KOS06] and the further references in Section 3.1 above. This numerical observation distinguishes the barcode process from the sine process (a cross-section of an ergodic Gibbs configuration), whose correlations also decay polynomially. For the continuous sine process this decay was already observed in [Dys62].

7.5 Probabilistic simulations

7.5.1 Porting the perfect sampling algorithm

Apart from numerics based on explicit formulas (Section 7.4), we can also test our Conjectures 7.2, 7.6 and 7.7 with the help of the exact sampling algorithm for the q-Racah random lozenge tilings [BGR10]. The key observation underlying the algorithm is that one can construct explicit Markov transition matrices on the space of lozenge tilings; these transitions transport the q-Racah measure for a hexagon with parameters (T, S, N) to the corresponding measures with parameters $(T, S+1, N)$ or $(T, S-1, N)$. For nearly twenty years, the only available implementation of this algorithm was Vadim Gorin's original `Compaq Visual Fortran` code, whose source he kindly shared with us. With the assistance of modern AI-based coding tools we have ported the relevant parts of this program to `Python`; the resulting script is provided as an ancillary file to the arXiv version of the paper. We have also created an interactive web-based simulator [Pet25]; the latter samples the measure q^{vol}, i.e. the specialization $\kappa = 0$, which does not display the waterfall phenomenon.

The new `Python` implementation is particularly well suited for batch generation of random lozenge tilings. As in [BGR10], the algorithm starts with the unique tiling of the hexagon with parameters $(T, 0, N)$ (that is, a parallelogram), and then performs the sequence of Markov moves

that increment S by one, thereby producing an exact sample from the q-Racah distribution with parameters (T, S, N). For the final tiling, we also record the barcode process, encoding it as a binary sequence. See Figure 13 for an example.[9] A key advantage of the script is that it can operate in a "head-less" mode: it need not render the tiling and thus can produce large collections of barcode process samples in a short time.

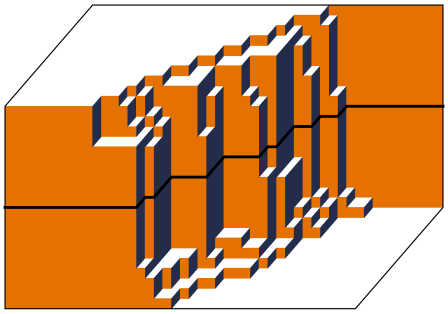

Figure 13: Graphical output of the `Python` script. Here $T = 50$, $S = 10$, $N = 20$, $q = \frac{7}{10}$, and $\kappa = 3\mathbf{i}$. The barcode process realization is 11111111111111101001110011110100110110111111111111.

In the rest of this subsection, we compare empirical pattern counts in the barcode process with the predictions of Conjectures 7.2 and 7.6, and also demonstrate fluctuations of the height function of the barcode process.

7.5.2 Density and correlations

In Table 5 we present empirical density counts for various choices of (T, S, N) (including the base case $(8L, 4L, 4L)$, but also with other choices of the size), with parameters $q = \frac{1}{7}$ and $\kappa = 4.3\mathbf{i}$. This particular value of κ is chosen since it induces a comparatively strong bias between the densities on even and odd sites, namely,

$$\mathcal{K}^{\text{barcode}}_{(M)}(0,0) = 0.345174\ldots, \qquad \mathcal{K}^{\text{barcode}}_{(M)}(1,1) = 0.654826\ldots, \qquad M = 20. \tag{7.15}$$

For Table 5, we compute the frequency of ones on even and odd sites, inside the waterfall region. Indeed, note that when the hexagon is not symmetric (i.e., outside the base case $(8L, 4L, 4L)$; see Figure 13 for an example), the barcode process may start and end with a frozen string of zeroes or ones, and we needed to cut these out.

Similarly, we can count the number of patterns of the form 11 (length 2) and $1\star1$ (length 3) in the realizations of the barcode process (where $\star$ is either 0 or 1), and confirm the two-periodicity of these correlations, as well as the agreement with the theoretical predictions

$$\det\begin{bmatrix} \mathcal{K}^{\text{barcode}}_{(M)}(t,t) & \mathcal{K}^{\text{barcode}}_{(M)}(t,t+1) \\ \mathcal{K}^{\text{barcode}}_{(M)}(t+1,t) & \mathcal{K}^{\text{barcode}}_{(M)}(t+1,t+1) \end{bmatrix} = 0.132142\ldots;$$

$$\det\begin{bmatrix} \mathcal{K}^{\text{barcode}}_{(M)}(t,t) & \mathcal{K}^{\text{barcode}}_{(M)}(t,t+2) \\ \mathcal{K}^{\text{barcode}}_{(M)}(t+2,t) & \mathcal{K}^{\text{barcode}}_{(M)}(t+2,t+2) \end{bmatrix} = \begin{cases} 0.108658\ldots, & \text{if } t \text{ is even;} \\ 0.418309\ldots, & \text{if } t \text{ is odd,} \end{cases}$$

[9] Examples in Figures 4 and 5 were generated by the original `Fortran` program.

T	S	N	Even 1's count	Odd 1's count	Normalization	Even frequency	Odd frequency
400	200	200	6,730	12,764	19,500	0.345128	0.654564
300	180	140	3,626	6,886	10,500	0.345333	0.65581
400	20	20	6,68	1,238	1,900	0.351579	0.651579
400	200	50	1,716	3,367	5,000	0.3432	0.6734

Table 5: Each row is based on 100 independently generated samples. For example, in the first row we have 100 realizations of a barcode sequence of length 400; removing five sites from each end to eliminate the boundary effects leaves 390 positions per sample. Thus the number of even (and, separately, odd) sites contributing to the empirical counts equals $390 \times 100/2 = 19{,}500$. The parameters are $q = \frac{1}{7}$ and $\kappa = 4.3, \mathbf{i}$. In all cases, we observe a strong agreement of the sample densities with the theoretical ones (7.15).

for $q = \frac{1}{7}$, $\kappa = 4.3\mathbf{i}$, and $M = 20$. Note that the first two-point correlation is fully translation-invariant. For the data used for the first line in Table 5, we observe the frequency 0.133933 of the pattern 11 (over *all* offsets, even or odd), and 0.10653 and 0.413419 for the patterns $1\star1$ with even and odd offsets, respectively.

7.5.3 Height function of the barcode process

Finally, let us consider fluctuations of the height function of the barcode process in the bulk of the waterfall region. For a barcode process realization $\vec{b} = (b_1, b_2, \dots, b_T)$, $b_j \in \{0, 1\}$, we define the height function by

$$h(t) := \sum\nolimits_{j=K}^{t} b_j,$$

where K is a fixed offset chosen to reduce the effect of the left boundary of the waterfall region. Since the density of particles in the barcode process is $\frac{1}{2}$, we consider the fluctuations $h(t) - \frac{t}{2}$. Plots of fluctuations are given in Figure 14. Based on them, we conjecture that the fluctuations of the height function grow slower than any power of L.

7.6 Conclusion

The nonrigorous analysis carried out in the present Section 7 paints the following conjectural picture. There exists a family of determinantal point processes on $\mathbb{Z}$ with the correlation kernels

$$\mathcal{K}^{\text{barcode}}(s, t \mid q, \kappa)$$

depending on the parameters $q \in (0, 1)$ and $\kappa \in \mathbf{i}\mathbb{R}_{>0}$. These processes governs the local statistics in the waterfall regime of the q-Racah random lozenge tilings of the hexagon. The limiting local process is universal — it depends only on the parameters (q, κ), and not on the side lengths (T, S, N) of the hexagon (as long as the waterfall phase is present, i.e., $N \ll T$), or the macroscopic point of observation around which we consider the local statistics.

This conjecture is supported by high-precision numerical computations with the determinantal kernel of the q-Racah measure on lozenge tilings, as well as by analyzing the results of the perfect sampling algorithm for the measure.

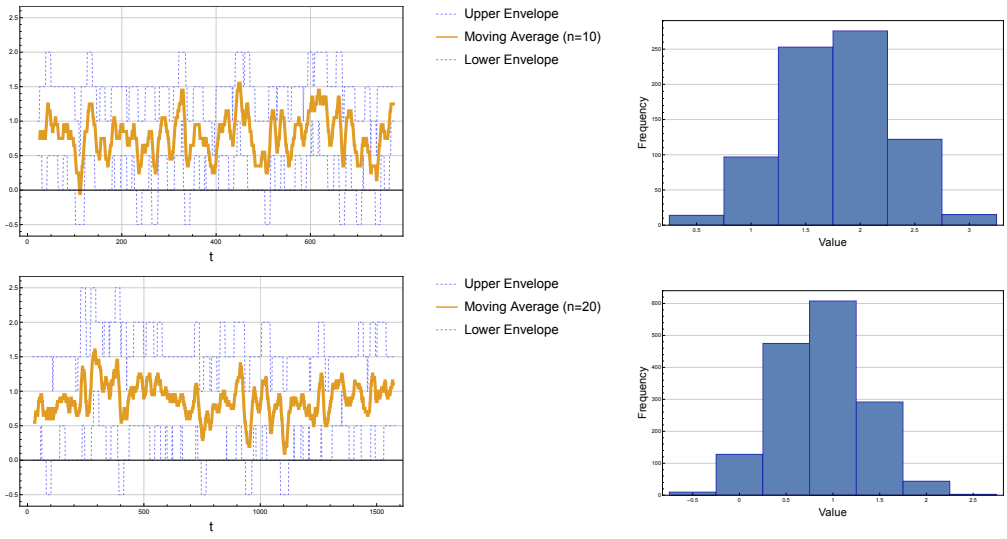

Figure 14: Fluctuations $h(t) - \frac{t}{2}$ of the height function of the barcode process arising in the hexagon with parameters $(T, S, N) = (8L, 4L, 4L)$ for $L = 100$ and 200, where $q = \frac{4}{5}$, $\kappa = 3\mathbf{i}$. The offset is $K = L/10$. On the left, the middle (bold) graph is the moving average, and there are also upper and lower envelopes (dashed lines). On the right, we show the histogram of the fluctuation values.

A Limiting orthogonal functions

In this appendix, we establish several properties of the orthogonal functions $\mathcal{F}_n(x)$ that enter Conjectures 7.2 and 7.7 on the asymptotic behavior of the barcode kernel. This part of the paper is self-contained, its proofs are rigorous, and properties of the functions $\mathcal{F}_n(x)$ may be of independent interest.

A.1 Definition of the functions

We need the Jacobi theta function, its quasi-periodicity, and the triple product identity:

$$\begin{aligned} \theta_q(z) &:= (z;q)_\infty (q/z;q)_\infty, \\ \theta_q\left(q^m z\right) &= (-1)^m q^{-\frac{m(m-1)}{2}} z^{-m} \theta_q(z), \qquad m \in \mathbb{Z}, \\ \theta_q(z) &= \frac{1}{(q;q)_\infty} \sum_{m\in\mathbb{Z}} (-1)^m q^{\frac{m(m-1)}{2}} z^m. \end{aligned} \tag{A.1}$$

Let $\frac{1}{2}\mathbb{Z}$ be the set of all integers and half-integers. We abbreviate $\mathbb{Z}' = \mathbb{Z} + \frac{1}{2}$, so $\frac{1}{2}\mathbb{Z} = \mathbb{Z} \cup \mathbb{Z}'$. If $i - j \in \mathbb{Z}$, we say that i and j have the same *half-parity*.

Define

$$\mathcal{F}_n(x) := \sqrt{1-\kappa^{-2}q^{-2x}} \sum_{i=-n}^{n} \frac{(-1)^{n+i} q^{-i/2}}{(q;q)_{n-i}(q;q)_{n+i}} \frac{1}{\theta_{\sqrt{q}}\left(|\kappa| q^{x+i+\frac{1}{2}}\right)}, \tag{A.2}$$

where $0 < q < 1$ and $\kappa \in \mathbf{i}\mathbb{R}_{>0}$ are the q-Racah parameters, $n, x \in \frac{1}{2}\mathbb{Z}$, and $n \geq 0$. By convention, in (A.2) and throughout this appendix, the sum runs only over those i that have the same half-parity as n. Any sum over all half-integers will be indicated explicitly.

Remark A.1. The functions $\mathcal{F}_n$ can be expressed in a q-hypergeometric form as

$$\mathcal{F}_n(x) = \frac{(-1)^{2n+2x+1} q^{(n-x)^2+x/2} |\kappa|^{2x-2n+1} \sqrt{1-\kappa^{-2}q^{-2x}}}{(q;q)_{2n} \theta_{\sqrt{q}}(|\kappa|)} \, {}_2\phi_0 \left(\begin{matrix} q^{2n}, 0 \\ - \end{matrix} \,\middle|\, q^{-1}; \kappa^2 q^{2(x-n)} \right). \quad \text{(A.3)}$$

The series ${}_2\phi_0$ is terminating, and can be identified with the continuous q-Hermite orthogonal polynomial $H_{2n}(\kappa q^x \mid q^{-1})$, where [KS96, Chapter 3.26]:

$$H_n(\lambda \mid q) = \lambda^{-n} \, {}_2\phi_0 \left(\begin{matrix} q^{-n}, 0 \\ - \end{matrix} \,\middle|\, q; \lambda^2 q^n \right). \quad \text{(A.4)}$$

Since $0 < q < 1$ and the polynomials involve the inverse parameter q^{-1}, they are often referred to as the *continuous q^{-1}-Hermite polynomials*.

The occurrence of the orthogonal polynomial H_{2n}, with the index doubled from n to $2n$, reflects the fact that the parameter n in $\mathcal{F}_n$ may be a (proper) half-integer.

In the remainder of this appendix, we establish the following properties of the functions $\mathcal{F}_n(x)$:

- (Proposition A.2 in Appendix A.2) Three-term relation in x;
- (Proposition A.4 in Appendix A.3) Orthogonality of the functions $\mathcal{F}_n(x)$, $n \in \frac{1}{2}\mathbb{Z}_{\geq 0}$, in each of the three spaces $\ell^2(\mathbb{Z})$, $\ell^2(\mathbb{Z}')$, and $\ell^2(\frac{1}{2}\mathbb{Z})$;
- (Proposition A.5 in Appendix A.4) Explicit expression for ℓ^2-norms of $\mathcal{F}_n$;
- (Proposition A.8 in Appendix A.5) Completeness of the functions in $\ell^2(\mathbb{Z})$ and $\ell^2(\mathbb{Z}')$, and the corresponding representation of the identity operator.

All of these properties, except the last one, are proved directly using the definition (A.2) and the properties of the Jacobi theta function (A.1). To establish completeness, however, we employ the q-hypergeometric representation from Remark A.1, together with the q-Mehler formula (an explicit Poisson kernel) for the continuous q^{-1}-Hermite polynomials obtained in [IM94].

A.2 Three-term relation

Proposition A.2. *We have*

$$\mathfrak{a}(x)\mathcal{F}_n(x-\tfrac{1}{2}) + \mathfrak{a}(x+\tfrac{1}{2})\mathcal{F}_n(x+\tfrac{1}{2}) = -q^n \mathcal{F}_n(x), \qquad n, x \in \tfrac{1}{2}\mathbb{Z}, \quad n \geq 0, \quad \text{(A.5)}$$

where $\mathfrak{a}$ is given by

$$\mathfrak{a}(x) := \left[\frac{-\kappa^2 q^{2x-1}}{(1-\kappa^2 q^{2x})(1-\kappa^2 q^{2x-1})} \right]^{\frac{1}{2}}, \qquad x \in \tfrac{1}{2}\mathbb{Z}.$$

Proof. Using the quasi-periodicity (A.1) and after the necessary simplifications, the three-term relation becomes

$$\sum_{i=-n}^{n} \frac{(-1)^{n+i} q^{-i/2}}{(q;q)_{n-i}(q;q)_{n+i}} \left(\frac{q^{i^2-\frac{1}{2}i} |\kappa|^{2i} q^{2ix}}{\sqrt{1-\kappa^2 q^{2x}}} + \frac{q^{i^2+\frac{3}{2}i} |\kappa|^{2i+2} q^{(2i+2)x}}{\sqrt{1-\kappa^2 q^{2x}}} \right) \frac{1}{\theta_{\sqrt{q}}(|\kappa| q^x)}$$
$$= -q^n \sum_{i=-n}^{n} \sqrt{1-\kappa^{-2} q^{-2x}} \frac{(-1)^{n+i} q^{-i/2}}{(q;q)_{n-i}(q;q)_{n+i}} \frac{-q^{i^2+\frac{1}{2}i} |\kappa|^{2i+1} q^{(2i+1)x}}{\theta_{\sqrt{q}}(|\kappa| q^x)}$$

(up to sign $(-1)^{2i} = \pm 1$ which is the same on both sides). This identity reduces to

$$\sum_{i=-n}^{n} \frac{q^{i^2} \left(z^i q^{-i} - z^{i+1} q^i - z^i q^n + z^{i+1} q^n \right)}{(q;q)_{n-i}(q;q)_{n+i}} = 0, \tag{A.6}$$

where $z = \kappa^2 q^{2x}$. Using the fact that $(q;q)_{n-i}(q;q)_{n+i} = q^{i^2+n^2+n}(q^{-1};q^{-1})_{n-i}(q^{-1};q^{-1})_{n+i}$, we can remove the factor q^{i^2} from the numerator in (A.6) by changing q to $\hat{q} := 1/q$. Moreover, by symmetry, we can replace i by $(-i)$ in the first and the third summands in the numerator in (A.6). Thus, we need to show that

$$\sum_{i=-n}^{n} \frac{z^{-i} \hat{q}^{-i} - z^{i+1} \hat{q}^{-i} - z^{-i} \hat{q}^{-n} + z^{i+1} \hat{q}^{-n}}{(\hat{q};\hat{q})_{n-i}(\hat{q};\hat{q})_{n+i}} = 0. \tag{A.7}$$

Factorizing $z^{-i} \hat{q}^{-i} - z^{i+1} \hat{q}^{-i} - z^{-i} \hat{q}^{-n} + z^{i+1} \hat{q}^{-n} = -(1 - \hat{q}^{n-i}) \hat{q}^{-n} (z^{-i} - z^{i+1})$, we see that (A.7) is equivalent to

$$\sum_{i=-n}^{n-1} \frac{z^{-i} - z^{i+1}}{(\hat{q};\hat{q})_{n-i-1}(\hat{q};\hat{q})_{n+i}} = 0.$$

The latter identity follows directly from the symmetry under $i \mapsto -i-1$. Consequently, we obtain the desired three-term relation (A.5). Moreover, this relation is valid for all x, because the argument reduces to an identity of rational functions in the variable $z = \kappa^2 q^{2x}$. □

Remark A.3. Alternatively, Proposition A.2 can also be derived directly from the difference equation [KS96, (3.26.5)] satisfied by the continuous q^{-1}-Hermite orthogonal polynomials, which are related to $\mathcal{F}_n(x)$ (see Remark A.1).

A.3 Orthogonality

Proposition A.4. *The functions $\mathcal{F}_n(x)$, $n \in \frac{1}{2}\mathbb{Z}_{\geq 0}$, are orthogonal in the variable x in each of the three spaces $\ell^2(\mathbb{Z})$, $\ell^2(\mathbb{Z}')$, and $\ell^2(\frac{1}{2}\mathbb{Z})$.*

Proof. Once we have the three-term relation (Proposition A.2), the orthogonality of $\mathcal{F}_n(x)$ in $\ell^2(\frac{1}{2}\mathbb{Z})$ (as functions of x) readily follows. Indeed, the left-hand side of (A.5) defines a symmetric operator

$$f(x) \mapsto \mathfrak{a}(x) f(x - \tfrac{1}{2}) + \mathfrak{a}(x + \tfrac{1}{2}) f(x + \tfrac{1}{2}) \tag{A.8}$$

in $\ell^2(\frac{1}{2}\mathbb{Z})$. This operator is bounded because its coefficients $\mathfrak{a}(\cdot)$ rapidly decay at $\pm\infty$. Therefore, it is self-adjoint in $\ell^2(\frac{1}{2}\mathbb{Z})$.

The functions $\mathcal{F}_n$ are eigenfunctions of (A.8) with distinct eigenvalues $-q^n$, $n \in \frac{1}{2}\mathbb{Z}_{\geq 0}$, and hence they are orthogonal in $\ell^2(\frac{1}{2}\mathbb{Z})$.

Next, the square of the operator (A.8) is also bounded and self-adjoint, but preserves each of the spaces $\ell^2(\mathbb{Z})$ and $\ell^2(\mathbb{Z}')$. The functions $\mathcal{F}_n$ are eigenfunctions of the square of (A.8) with distinct eigenvalues q^{2n}, and hence they are orthogonal in $\ell^2(\mathbb{Z})$ and $\ell^2(\mathbb{Z}')$. This completes the proof. □

A.4 Norms

Proposition A.5. *For all $n \in \frac{1}{2}\mathbb{Z}_{\geq 0}$, we have*

$$\|\mathcal{F}_n\|^2_{\ell^2(\mathbb{Z})} = \|\mathcal{F}_n\|^2_{\ell^2(\mathbb{Z}')} = \frac{1}{2}\|\mathcal{F}_n\|^2_{\ell^2(\frac{1}{2}\mathbb{Z})} = \frac{(q;q)_\infty(-\kappa^2)\theta_q(\kappa^{-2})}{q^n(q;q)_{2n}\theta_{\sqrt{q}}(|\kappa|)^2}. \tag{A.9}$$

Proof. The functions $\mathcal{F}_n(x)$ are real-valued (as n and i are of the same half-parity), so we can sum their squares to compute the norms. We have

$$(\mathcal{F}_n(x))^2 = \frac{1}{\theta_{\sqrt{q}}(|\kappa|)^2}(1-\kappa^{-2}q^{-2x})\sum_{i,j}\frac{(-1)^{2n+i+j}q^{-(i+j)/2}}{(q;q)_{n-i}(q;q)_{n+i}(q;q)_{n-j}(q;q)_{n+j}} \times |\kappa|^{4x+2+2i+2j}q^{(i+x)(i+x+1/2)+(j+x)(j+x+1/2)}. \tag{A.10}$$

Here the sum is over $-n \leq i,j \leq n$ of the same half-parity as n. Next, let us sum the x-dependent part of (A.10) over $x \in \mathbb{Z}$. We have, using the triple product identity (A.1):

$$\sum_{x\in\mathbb{Z}}(1-\kappa^{-2}q^{-2x})(-\kappa^2)^{2x}q^{2x^2+(2i+2j+1)x} = (q^4;q^4)_\infty\Big[\theta_{q^4}(-\kappa^4q^{2i+2j+3}) - \kappa^{-2}\theta_{q^4}(-\kappa^4q^{2i+2j+1})\Big]. \tag{A.11}$$

We can simplify this expression depending on the parity of $i+j$. If $i+j$ is even, we have

$$(\text{A.11}) = (q^4;q^4)_\infty(-\kappa^{-2})^{i+j}\big[\theta_{q^4}(-\kappa^4q^3)q^{-(i+j)(i+j+1)/2} - \kappa^{-2}\theta_{q^4}(-\kappa^4q)q^{-(i+j)(i+j-1)/2}\big].$$

If $i+j$ is odd, we have

$$(\text{A.11}) = (q^4;q^4)_\infty(-\kappa^{-2})^{i+j-1}\big[\kappa^{-4}\theta_{q^4}(-\kappa^4q)q^{-(i+j)(i+j+1)/2} - \kappa^{-2}\theta_{q^4}(-\kappa^4q^3)q^{-(i+j)(i+j-1)/2}\big].$$

Multiplying this by the remaining terms in (A.10), we have for $i+j$ even:

$$\begin{aligned}&-(-1)^{2n+i+j}\kappa^2q^{(i-j)^2/2}(q^4;q^4)_\infty\big[\theta_{q^4}(-\kappa^4q^3)q^{-(i+j)/2} - \kappa^{-2}\theta_{q^4}(-\kappa^4q)q^{(i+j)/2}\big]\\ &\qquad = (-1)^{2n+i+j}q^{(i-j)^2/2}(q^4;q^4)_\infty\big[\theta_{q^4}(-\kappa^4q)q^{(i+j)/2} - \kappa^2\theta_{q^4}(-\kappa^4q^3)q^{-(i+j)/2}\big],\end{aligned}$$

and for $i+j$ odd:

$$(-1)^{2n+i+j}q^{(i-j)^2/2}(q^4;q^4)_\infty\big[\theta_{q^4}(-\kappa^4q)q^{-(i+j)/2} - \kappa^2\theta_{q^4}(-\kappa^4q^3)q^{(i+j)/2}\big].$$

Utilizing the symmetry of the summation intervals for i,j, we see that the power $q^{-(i+j)/2}$ can always be replaced by $q^{(i+j)/2}$. This eliminates the dependence on the parity of $i+j$, and thus we have:

$$\sum_{x\in\mathbb{Z}}(\mathcal{F}_n(x))^2 = \frac{(q^4;q^4)_\infty\left(\theta_{q^4}(-\kappa^4q) - \kappa^2\theta_{q^4}(-\kappa^4q^3)\right)}{\theta_{\sqrt{q}}(|\kappa|)^2}\sum_{i,j}\frac{(-1)^{2n+i+j}q^{(i-j)^2/2+(i+j)/2}}{(q;q)_{n-i}(q;q)_{n+i}(q;q)_{n-j}(q;q)_{n+j}}.$$

By Lemma A.6 below, the prefactor is equal to $\frac{(-\kappa^2)(q;q)_\infty \theta_q(\kappa^{-2})}{\theta_{\sqrt{q}}(|\kappa|)^2}$. The remaining sum over i,j is simplified to $q^{-n}(q;q)_{2n}^{-1}$ in Lemma A.7 below. Thus, we arrive at the desired norm in $\ell^2(\mathbb{Z})$.

Let us obtain the norm in $\ell^2(\mathbb{Z}')$. The sum in (A.11) over $\mathbb{Z}'$ is equal to

$$\sum_{x\in\mathbb{Z}'}(1-\kappa^{-2}q^{-2x})(-\kappa^2)^{2x}q^{2x^2+(2i+2j+1)x} = \sum_{y\in\mathbb{Z}}(1-\kappa^{-2}q^{-2y-1})(-\kappa^2)^{2y+1}q^{2y^2+(2i+2j+3)y+i+j+1}$$
$$= -\kappa^2 q^{i+j+1}(q^4;q^4)_\infty\big[\theta_{q^4}(-\kappa^4 q^{2i+2j+3}) - \kappa^{-2}q^{-1}\theta_{q^4}(-\kappa^4 q^{2i+2j+1})\big].$$

Summing this expression (together with the remaining factors from (A.10)) over i,j is analogous to the case of $\ell^2(\mathbb{Z})$, and we omit the details. In the end, one can check that the norms in $\ell^2(\mathbb{Z})$ and $\ell^2(\mathbb{Z}')$ are equal to each other. This completes the proof of Proposition A.5 modulo the two lemmas below. □

Lemma A.6. *We have*

$$(q^4;q^4)_\infty\left(\theta_{q^4}(-\kappa^4 q) - \kappa^2\theta_{q^4}(-\kappa^4 q^3)\right) = (-\kappa^2)(q;q)_\infty\theta_q(\kappa^{-2}).$$

Proof. Using the Jacobi triple product identity (A.1), we have

$$(q^4;q^4)_\infty\left(\theta_{q^4}(-\kappa^4 q) - \kappa^2\theta_{q^4}(-\kappa^4 q^3)\right) = \sum_{m\in\mathbb{Z}}(q^4)^{m(m-1)/2}\left(\kappa^{4m}q^m - \kappa^2\kappa^{4m}q^{3m}\right).$$

We aim to show that this sum is equal to $\sum_{j\in\mathbb{Z}}(-1)^{j+1}\kappa^{2-2j}q^{j(j-1)/2}$. Indeed, for $j=2m+1$, the j-th summand is equal to $(q^4)^{(-m)(-m-1)/2}\kappa^{-4m}q^{-m}$, and for $j=2m$, the j-th summand is $-(q^4)^{(-m)(-m-1)/2}\kappa^2\kappa^{-4m}q^{-3m}$. This completes the proof. □

Lemma A.7. *We have for all $n\in\frac{1}{2}\mathbb{Z}_{\geq 0}$:*

$$\sum_{i=-n}^{n}\sum_{j=-n}^{n}\frac{(-1)^{2n+i+j}q^{(i-j)^2/2+(i+j)/2}}{(q;q)_{n-i}(q;q)_{n+i}(q;q)_{n-j}(q;q)_{n+j}} = \frac{1}{q^n(q;q)_{2n}}, \tag{A.12}$$

where the sums are over i,j of the same half-parity as n.

Proof. Let us show that, for a fixed i, the sum over j in (A.12) is zero unless $i=-n$. Indeed,

$$\sum_{j=-n}^{n}\frac{(-1)^{n+j}q^{j(j+1)/2}z^j}{(q;q)_{n-j}(q;q)_{n+j}} = \frac{z^{-n}q^{n(n-1)/2}}{(q;q)_{2n}}\prod_{r=-n+1}^{n}(1-zq^r), \tag{A.13}$$

which is a direct consequence of the q-binomial theorem (it allows one to extract the coefficient of z^j on the right-hand side). The polynomial on the right-hand side of (A.13) vanishes at $z=q^{-i}$ for every i with $-n+1\leq i\leq n$. Therefore, the sum over j in (A.12) is zero unless $i=-n$. When $i=-n$, substituting $z=q^{-n}$ yields the desired result. □

A.5 Representation of the identity and completeness

Proposition A.8. *For all $x, y \in \frac{1}{2}\mathbb{Z}$ with $x - y \in \mathbb{Z}$, we have*

$$\sum_{n \in \frac{1}{2}\mathbb{Z}_{\geq 0}} \frac{\mathcal{F}_n(x)\mathcal{F}_n(y)}{\|\mathcal{F}_n\|^2_{\ell^2(\mathbb{Z})}} = \mathbf{1}_{x=y}. \tag{A.14}$$

This implies that the orthonormal functions $\mathcal{F}_n/\|\mathcal{F}_n\|_{\ell^2(\mathbb{Z})}$, $n \in \frac{1}{2}\mathbb{Z}_{\geq 0}$, are complete in each of the spaces $\ell^2(\mathbb{Z})$ and $\ell^2(\mathbb{Z}')$.

Proof. We need to show that

$$\sum_{n \in \frac{1}{2}\mathbb{Z}_{\geq 0}} q^n (q;q)_{2n} \mathcal{F}_n(x)\mathcal{F}_n(y) = \mathbf{1}_{x=y} \frac{(-\kappa^2)(q;q)_\infty \theta_q(\kappa^{-2})}{\theta_{\sqrt{q}}(|\kappa|)^2}. \tag{A.15}$$

We employ the so-called q-Mehler formula for the continuous q^{-1}-Hermite polynomials H_n (A.4) with $q > 1$, which is available from [IM94, Theorem 2.1]. In our notation, it reads

$$\begin{aligned}\sum_{m=0}^{\infty} \frac{H_m(\lambda \mid q^{-1}) H_m(\mu \mid q^{-1}) q^{m(m-1)/2} z^m}{(q;q)_m} \\ = \frac{(-z\lambda\mu;q)_\infty (-z/(\lambda\mu);q)_\infty (-z\lambda/\mu;q)_\infty (-z\mu/\lambda;q)_\infty}{(z^2/q;q)_\infty}.\end{aligned} \tag{A.16}$$

The summands in the left-hand side of (A.15) are expressed through the continuous q^{-1}-Hermite polynomials as

$$\begin{aligned}q^n (q;q)_{2n} \mathcal{F}_n(x)\mathcal{F}_n(y) = \frac{(-1)^{2x+2y} q^{x^2+y^2+(x+y)/2} |\kappa|^{2(x+y+1)} \sqrt{(1-\kappa^{-2}q^{-2x})(1-\kappa^{-2}q^{-2y})}}{\theta_{\sqrt{q}}(|\kappa|)^2} \\ \times \frac{H_{2n}(\kappa q^x \mid q^{-1}) H_{2n}(\kappa q^y \mid q^{-1}) q^{2n(2n-1)/2} (-q)^{2n}}{(q;q)_{2n}}.\end{aligned}$$

Applying (A.16) with $z = -q$, $\lambda = \kappa q^x$, and $\mu = \kappa q^y$, we see that the sum in the left-hand side of (A.15) becomes

$$\begin{aligned}\frac{(-1)^{2x+2y} q^{x^2+y^2+(x+y)/2} |\kappa|^{2(x+y+1)} \sqrt{(1-\kappa^{-2}q^{-2x})(1-\kappa^{-2}q^{-2y})}}{\theta_{\sqrt{q}}(|\kappa|)^2} \\ \times \frac{(\kappa^2 q^{x+y+1};q)_\infty (\kappa^{-2}q^{1-x-y};q)_\infty (q^{x-y+1};q)_\infty (q^{y-x+1};q)_\infty}{(q;q)_\infty}.\end{aligned} \tag{A.17}$$

Thanks to the factors $(q^{x-y+1};q)_\infty (q^{y-x+1};q)_\infty$, if $x - y \in \mathbb{Z}$, then expression (A.17) vanishes unless $x = y$.

To complete the proof of Proposition A.8, it remains to simplify (A.17) for $y = x$ and match it to the right-hand side of (A.15). We have

$$\begin{aligned}(\text{A.17}) &= \frac{q^{2x^2+x}|\kappa|^{4x+2}(1-\kappa^{-2}q^{-2x})}{\theta_{\sqrt{q}}(|\kappa|)^2}(\kappa^2 q^{2x+1};q)_\infty(\kappa^{-2}q^{1-2x};q)_\infty(q;q)_\infty \\ &= \frac{q^{2x^2+x}|\kappa|^{4x+2}(q;q)_\infty\theta_q(\kappa^{-2}q^{-2x})}{\theta_{\sqrt{q}}(|\kappa|)^2} \\ &= \frac{(-\kappa^2)(q;q)_\infty\theta_q(\kappa^{-2})}{\theta_{\sqrt{q}}(|\kappa|)^2},\end{aligned}$$

where in the last line we used the quasi-periodicity (A.1). □

Remark A.9. When x and y have different half-parities, the product $(q^{x-y+1};q)_\infty(q^{y-x+1};q)_\infty$, and hence the whole expression (A.17), does not vanish. Consequently, the functions $\mathcal{F}_n(x)$ are *not complete* in the larger space $\ell^2(\frac{1}{2}\mathbb{Z})$.

B `Mathematica` code

Here we present the `Mathematica` definitions of the two-dimensional q-Racah kernel $\widetilde{K}$ (6.7), the pre-limit barcode kernel $K^{\text{barcode}}_{(L)}$ (6.17), and the conjectural limit $\mathcal{K}^{\text{barcode}}(s,t)$ (7.11). These code snippets are involved in the numerical verification of Conjectures 7.2, 7.6 and 7.7 which is described in Section 7.4. All `Mathematica` formulas are written only for the first parameter zone in the hexagon (2.15). Note that in code, we refer to N as `NN`.

Listing 1: The orthonormal q-Racah polynomials $f_n^t(x)$ (2.22)

```
w[t_, x_] := (
    (q^(1 - 2 NN - T))^-x (1 - q^(1 - S - t + 2 x) \[Kappa]^2)
    QPochhammer[q^(1 - NN - S), q, x] QPochhammer[q^(1 - NN - t), q, x]
    QPochhammer[q^(1 - S - t) \[Kappa]^2, q, x] QPochhammer[q^(1 - T) \[Kappa]^2, q, x]
) / (
    (1 - q^(1 - S - t) \[Kappa]^2) QPochhammer[q, q, x] QPochhammer[q^(1 - S - t + T), q, x]
    QPochhammer[q^(1 + NN - S) \[Kappa]^2, q, x] QPochhammer[q^(1 + NN - t) \[Kappa]^2, q, x]
)

R[n_, t_, x_] := QHypergeometricPFQ[
    {q^-n, q^(1 + n - 2 NN - T), q^-x, q^(1 - S - t + x) \[Kappa]^2},
    {q^(1 - NN - S), q^(1 - NN - t), q^(1 - T) \[Kappa]^2},
    q, q
]

h[n_, t_] := (
    (1 - q^(1 - 2 NN - T)) (q^(1 - S - t) \[Kappa]^2)^n QPochhammer[q, q, n]
    QPochhammer[q^(2 - 2 NN - T), q, -1 + NN + t] QPochhammer[q^(1 - NN + S - T), q, n]
    QPochhammer[q^(1 - NN + t - T), q, n] QPochhammer[q^(1 - 2 NN) / \[Kappa]^2, q, n]
    QPochhammer[q^(-NN + S) / \[Kappa]^2, q, -1 + NN + t]
) / (
    (1 - q^(1 + 2 n - 2 NN - T)) QPochhammer[q^(1 - NN - S), q, n] QPochhammer[q^(1 - NN - t), q, n]
    QPochhammer[q^(1 - 2 NN - T), q, n] QPochhammer[q^(1 - NN + S - T), q, -1 + NN + t]
    QPochhammer[q^(1 - 2 NN) / \[Kappa]^2, q, -1 + NN + t] QPochhammer[q^(1 - T) \[Kappa]^2, q, n]
)

f[n_, t_, x_] := R[n, t, x] Sqrt[w[t, x] / h[n, t]]
```

Listing 2: The two-dimensional kernel $\widetilde{K}(s,x;t,y)$ (6.7)

```
CTilde[n_, t_] := Sqrt[(q^(n - t - NN) - 1) * (1 - q^(T + NN - t - n - 1))]

Ker[s_, x_, t_, y_] :=
  Which[
    s >= t,
      Sum[
        1/Product[CTilde[n, j], {j, t, s - 1}] * f[n, s, x] * f[n, t, y],
        {n, 0, NN - 1}
      ],
    s < t,
      -Sum[
        Product[CTilde[n, j], {j, s, t - 1}] * f[n, s, x] * f[n, t, y],
        {n, NN, NN + s - 1}
      ]
  ]
```

Listing 3: The inverse Kasteleyn matrix (6.15)

```
wLozenge[j_] := \[Kappa] q^(j - (S + 1)/2) - 1/(\[Kappa] q^(j - (S + 1)/2))

wTilde[t_, x_] := (
    (-1)^(t + S) * q^(x * (2 * NN + T - 1)) * (1 - \[Kappa]^2 * q^(2 * x - t - S + 1))
) / (
    QPochhammer[q, q, x] * QPochhammer[q, q, T - S - t + x] *
    QPochhammer[q^(-1), q^(-1), t + NN - x - 1] *
    QPochhammer[q^(-1), q^(-1), S + NN - x - 1] *
    QPochhammer[\[Kappa]^2 * q^(x - T + 1), q, T + NN - t] *
    QPochhammer[\[Kappa]^2 * q^(x - t - S + 1), q, NN + t]
)

G[t_, x_] := (
    (-1)^(x) * \[Kappa]^(-t) * q^(x * (T + NN - t - 1) + t * (S/2 - 1/2) + t * (t + 1)/4) *
    (1 - \[Kappa]^2 * q^(2 * x - t - S + 1))
) / (
    QPochhammer[q^(-1), q^(-1), S + NN - 1 - x] *
    QPochhammer[q, q, T - S + x - t] *
    QPochhammer[\[Kappa]^2 * q^(x - T + 1), q, T + NN - t]
) / Sqrt[wTilde[t, x]]

KastInv[s_, x_, t_, y_] := G[s, x] / G[t, y] / wLozenge[x - s/2 + 1] *
  (If[x == y && s == t, 1, 0] - Ker[s, x, t, y])
```

Listing 4: The pre-limit barcode kernel $K_{(L)}^{\mathrm{barcode}}(s,t)$ (6.17)

```
T := 8 L; NN := 4 L; S := 4 L;

Kbar[s_, t_] := KastInv[2 L + s, 3 L, 2 L + t - 1, 3 L]
```

Listing 5: The orthogonal functions $\mathcal{F}_n(x)$ (A.2)

```
th[q_, z_] := QPochhammer[z, q] * QPochhammer[q/z, q]

F[n_, x_] := Sqrt[1 - \[Kappa]^(-2) * q^(-2 * x)] * Sum[
    (-1)^(n + i) * q^(-i/2) / QPochhammer[q, q, n - i] /
    QPochhammer[q, q, n + i] / th[Sqrt[q], q^(x + i + 1/2) * \[Kappa]/I],
    {i, -n, n}
]

fsqnorm[n_] := (
    QPochhammer[q, q] * (-\[Kappa]^2) * th[q, \[Kappa]^(-2)] / q^n /
    QPochhammer[q, q, 2 * n] / th[Sqrt[q], \[Kappa]/I]^2
```

```
)
```

Listing 6: The partial sum in the conjectural limiting barcode kernel $\mathcal{K}^{\mathrm{barcode}}(s,t)$ (7.11)

```
prefactorFromG[s_, t_] := (
    -q^(1 - s) * Sqrt[-\[Kappa]^2 / (1 - \[Kappa]^2 * q^(2 - t)) / (1 - \[Kappa]^2 * q^(1 - s))]
)

KLimitBarcodeHalf[s_, t_][M_] := (
    (-1)^(s - t) * q^((M + 1) * (s - t)) * q^((s - 1)/2) * prefactorFromG[s, t] *
    (-Sum[
        (-q^n)^(t - 1 - s) * F[n, -(t - 2)/2] * F[n, -(s - 1)/2] / fsqnorm[n],
        {n, 0, M + 1/2, 1/2}
    ])
)

KLimitingBarcode[s_, t_][M_] := If[s >= t,
    KLimitBarcodeHalf[s, t][M],
    KLimitBarcodeHalf[t, s][M]
]
```

References

[AG22] A. Aggarwal and V. Gorin, *Gaussian unitary ensemble in random lozenge tilings*, Prob. Theory Relat. Fields **184** (2022), no. 4, 1139–1166. arXiv:2106.07589 [math.PR]. ↑1

[Agg23] A. Aggarwal, *Universality for Lozenge Tiling Local Statistics*, Ann. of Math. (2) **198** (2023), no. 3, 881–1012. arXiv:1907.09991 [math.PR]. ↑1, 17

[AH25] A. Aggarwal and J. Huang, *Edge statistics for lozenge tilings of polygons, II: Airy line ensemble*, Forum Math. Pi **13** (2025), e2. arXiv:2108.12874 [math.PR]. ↑1

[ARVP22] A. Ahn, M. Russkikh, and R. Van Peski, *Lozenge Tilings and the Gaussian Free Field on a Cylinder*, Comm. Math. Phys. **396** (2022), 1221–1275. arXiv:2105.00551 [math.PR]. ↑17

[BB23] T. Berggren and A. Borodin, *Geometry of the doubly periodic Aztec dimer model*, arXiv preprint (2023). arXiv:2306.07482 [math.PR]. ↑3

[BG13] A. Borodin and V. Gorin, *Markov processes of infinitely many nonintersecting random walks*, Probab. Theory Relat. Fields **155** (2013), no. 3-4, 935–997. arXiv:1106.1299 [math.PR]. ↑17

[BG18] A. Bufetov and V. Gorin, *Fluctuations of particle systems determined by Schur generating functions*, Adv. Math. **338** (2018), 702–781. arXiv:1604.01110 [math.PR]. ↑1

[BGR10] A. Borodin, V. Gorin, and E. Rains, *q-Distributions on boxed plane partitions*, Selecta Math. **16** (2010), no. 4, 731–789. arXiv:0905.0679 [math-ph]. ↑2, 3, 4, 5, 8, 9, 11, 12, 14, 15, 16, 17, 18, 19, 20, 37, 38, 39, 40, 41, 45, 52

[BKMM07] J. Baik, T. Kriecherbauer, K. T.-R. McLaughlin, and P. D. Miller, *Discrete Orthogonal Polynomials: Asymptotics and Applications*, Annals of Mathematics Studies, Princeton University Press, 2007. arXiv:math/0310278 [math.CA]. ↑1

[BNR24] T. Berggren, M. Nicoletti, and M. Russkikh, *Perfect t-embeddings and Lozenge Tilings*, arXiv preprint (2024). arXiv:2408.05441 [math.PR]. ↑1

[BO07] A. Borodin and G. Olshanski, *Asymptotics of Plancherel-type random partitions*, Journal of Algebra **313** (2007), no. 1, 40–60. arXiv:math/0610240. ↑3, 5, 16

[Bor11] A. Borodin, *Determinantal point processes*, Oxford handbook of random matrix theory, 2011. arXiv:0911.1153 [math.PR]. ↑14, 38

[BPZ25] A. Bufetov, L. Petrov, and P. Zografos, *Domino Tilings of the Aztec Diamond in Random Environment and Schur Generating Functions*, arXiv preprint (2025). arXiv:2507.08560 [math.PR]. ↑4

[Cha20] C. Charlier, *Doubly periodic lozenge tilings of a hexagon and matrix valued orthogonal polynomials*, Stud. Appl. Math. **146** (2020), no. 1, 3–80. arXiv:2001.11095 [math-ph]. ↑2

[CK01] R. Cerf and R. Kenyon, *The low-temperature expansion of the Wulff crystal in the 3D Ising model*, Comm. Math. Phys. **222** (2001), 147–179. ↑17, 20

[CKP01] H. Cohn, R. Kenyon, and J. Propp, *A variational principle for domino tilings*, Jour. AMS **14** (2001), no. 2, 297–346. arXiv:math/0008220 [math.CO]. ↑1

[CLP98] H. Cohn, M. Larsen, and J. Propp, *The shape of a typical boxed plane partition*, New York J. Math **4** (1998), 137–165. arXiv:math/9801059 [math.CO]. ↑17

[DDL24] M. Duits, E. Duse, and W. Liu, *Lozenge Tilings of a Hexagon and q-Racah Ensembles*, J. Phys. A Math. Theor. **57** (2024), no. 40, 405202. arXiv:2311.13407 [math.PR]. ↑3, 17

[DFG19] P. Di Francesco and E. Guitter, *A tangent method derivation of the arctic curve for q-weighted paths with arbitrary starting points*, J. Phys. A **52** (2019), no. 11, 115205. arXiv:1810.07936 [math-ph]. ↑17

[DK19] E. Dimitrov and A. Knizel, *Log-gases on quadratic lattices via discrete loop equations and q-boxed plane partitions*, J. Funct. Anal. **276** (2019), no. 10, 3067–3169. arXiv:1710.01709 [math.PR]. ↑3, 12, 14, 17

[Dys62] F. J. Dyson, *Statistical Theory of the Energy Levels of Complex Systems. III*, J. Math. Phys. **3** (1962), no. 1, 166–175. ↑52

[FS03] P. Ferrari and H. Spohn, *Step fluctuations for a faceted crystal*, J. Stat. Phys **113** (2003), no. 1, 1–46. arXiv:cond-mat/0212456 [cond-mat.stat-mech]. ↑17, 20

[GH24] V. Gorin and J. Huang, *Dynamical loop equation*, Ann. Probab. **52** (2024), no. 5, 1758–1863. arXiv:2205.15785 [math.PR]. ↑3, 17

[Gor08] V. Gorin, *Nonintersecting paths and the Hahn orthogonal polynomial ensemble*, Funct. Anal. Appl. **42** (2008), no. 3, 180–197. arXiv:0708.2349 [math.PR]. ↑1

[Gor21] V. Gorin, *Lectures on random lozenge tilings*, Cambridge Studies in Advanced Mathematics. Cambridge University Press (2021). ↑1, 17

[GP15] V. Gorin and G. Panova, *Asymptotics of symmetric polynomials with applications to statistical mechanics and representation theory*, Ann. Probab. **43** (2015), no. 6, 3052–3132. arXiv:1301.0634 [math.RT]. ↑1

[GR04] G. Gasper and M. Rahman, *Basic hypergeometric series*, Cambridge University Press, 2004. ↑12, 43

[Hua24] J. Huang, *Edge statistics for lozenge tilings of polygons, I: concentration of height function on strip domains*, Prob. Theory Relat. Fields **188** (2024), 337–485. arXiv:2108.12872 [math.PR]. ↑1

[HYZ24] J. Huang, F. Yang, and L. Zhang, *Pearcey universality at cusps of polygonal lozenge tilings*, Comm. Pure Appl. Math. **77** (2024), no. 9, 3708–3784. arXiv:2306.01178 [math.PR]. ↑1

[IM94] M. E. H. Ismail and D. R. Masson, *q-Hermite polynomials, biorthogonal rational functions, and q-beta integrals*, Trans. Amer. Math. Soc. **346** (1994), no. 1, 63–116. ↑7, 56, 60

[Ken08] R. Kenyon, *Height fluctuations in the honeycomb dimer model*, Commun. Math. Phys. **281** (2008), no. 3, 675–709. arXiv:math-ph/0405052. ↑1

[Ken09] R. Kenyon, *Lectures on dimers*, arXiv preprint (2009). arXiv:0910.3129 [math.PR]. ↑4, 15, 17, 41

[KO07] R. Kenyon and A. Okounkov, *Limit shapes and the complex Burgers equation*, Acta Math. **199** (2007), no. 2, 263–302. arXiv:math-ph/0507007. ↑3, 17

[Kön05] W. König, *Orthogonal polynomial ensembles in probability theory*, Probab. Surv. **2** (2005), 385–447. arXiv:math/0403090 [math.PR]. ↑12, 14, 15

[KOS06] R. Kenyon, A. Okounkov, and S. Sheffield, *Dimers and amoebae*, Ann. Math. **163** (2006), 1019–1056. arXiv:math-ph/0311005. ↑1, 17, 52

[KS96] R. Koekoek and R.F. Swarttouw, *The Askey-scheme of hypergeometric orthogonal polynomials and its q-analogue*, Technical report, Delft University of Technology and Free University of Amsterdam (1996). arXiv:math/9602214 [math.CA], report no. OP-SF 20 Feb 1996. Updated version available at https://fa.ewi.tudelft.nl/~koekoek/documents/as98.pdf. ↑2, 7, 12, 26, 56, 57

[Meh04] M.L. Mehta, *Random matrices*, Academic press, 2004. ↑15

[Mkr14] S. Mkrtchyan, *Plane partitions with 2-periodic weights*, Letters in Mathematical Physics **104** (2014), no. 9, 1053–1078. arXiv:1309.4825 [math.PR]. ↑3

[Mkr21] S. Mkrtchyan, *Turning Point Processes in Plane Partitions with Periodic Weights of Arbitrary Period*, Prog. Math. **340** (2021), 497–527. arXiv:1908.01246 [math.PR]. ↑3

[MP17] S. Mkrtchyan and L. Petrov, *GUE corners limit of q-distributed lozenge tilings*, Electron. J. Probab. **22** (2017), no. 101, 24 pp. arXiv:1703.07503 [math.PR]. ↑17

[NHB84] B. Nienhuis, H. J. Hilhorst, and H. W. J. Blöte, *Triangular SOS models and cubic-crystal shapes*, J. Phys. A: Math. Gen. **17** (1984), no. 18, 3559–3581. ↑17

[Ols08] G. Olshanski, *Difference operators and determinantal point processes*, Functional Analysis and Its Applications **42** (2008), no. 4, 317–329. arXiv:0810.3751 [math.PR]. ↑3, 5, 16

[OR03] A. Okounkov and N. Reshetikhin, *Correlation function of Schur process with application to local geometry of a random 3-dimensional Young diagram*, Jour. AMS **16** (2003), no. 3, 581–603. arXiv:math/0107056 [math.CO]. ↑1, 17, 20, 45

[OR06] A. Okounkov and N.Y. Reshetikhin, *The birth of a random matrix*, Mosc. Math. J. **6** (2006), no. 3, 553–566. ↑1

[OR07] A. Okounkov and N. Reshetikhin, *Random skew plane partitions and the Pearcey process*, Commun. Math. Phys. **269** (2007), no. 3, 571–609. arXiv:math/0503508 [math.CO]. ↑1

[Pet14] L. Petrov, *Asymptotics of Random Lozenge Tilings via Gelfand-Tsetlin Schemes*, Probab. Theory Relat. Fields **160** (2014), no. 3, 429–487, available at 1202.3901. arXiv:1202.3901 [math.PR]. ↑1

[Pet15] L. Petrov, *Asymptotics of Uniformly Random Lozenge Tilings of Polygons. Gaussian Free Field*, Ann. Probab. **43** (2015), no. 1, 1–43, available at 1206.5123. arXiv:1206.5123 [math.PR]. ↑1

[Pet25] L. Petrov, *3D q-volume lozenge tilings visualization*, 2025. ↑52

[PT23] L. Petrov and M. Tikhonov, *Asymptotics of noncolliding q-exchangeable random walks*, J. Phys. A: Math. Theor. **56** (2023), no. 36, 365203. arXiv:2303.02380 [math.PR]. ↑17

[RS72] M. Reed and B. Simon, *Methods of Modern Mathematical Physics, Vol. I. Functional Analysis*, Academic Press, New York, 1972. ↑27, 45

[She05] S. Sheffield, *Random surfaces*, Astérisque **304** (2005). arXiv:math/0304049 [math.PR]. ↑1, 17

[Tao12] T. Tao, *Topics in random matrix theory*, Graduate Studies in Mathematics, vol. 132, AMS, 2012. ↑3, 16

[WMTB76] T. T. Wu, B. M. McCoy, C. A. Tracy, and E. Barouch, *Spin-spin correlation functions for the two-dimensional Ising model: Exact theory in the scaling region*, Phys. Rev. B **13** (1976), no. 1, 316–374. ↑4

A. KNIZEL, BARNARD COLLEGE, COLUMBIA UNIVERSITY, NEW YORK, NY, USA
e-mail: aknizel@barnard.edu

L. PETROV, UNIVERSITY OF VIRGINIA, CHARLOTTESVILLE, VA, USA
e-mail: lenia.petrov@gmail.com